Master's thesis

NTNU
Norwegian University of Science and Technology
Faculty of Engineering
Department of Energy and Process Engineering

Erik Eikeng

Power to Ammonia

A Computational Framework for Optimizing Green Ammonia Production from off-grid Wind and Solar Energy

Master's thesis in Energy and Environmental Engineering
Supervisor: Bruno G. Pollet
June 2023

NTNU
Norwegian University of
Science and Technology

Erik Eikeng

Power to Ammonia

A Computational Framework for Optimizing Green Ammonia Production from off-grid Wind and Solar Energy

Master's thesis in Energy and Environmental Engineering
Supervisor: Bruno G. Pollet
June 2023

Norwegian University of Science and Technology
Faculty of Engineering
Department of Energy and Process Engineering

NTNU
Norwegian University of
Science and Technology

Preface

This thesis marks the finalization of the 2-year Master's degree program Energy and Environmental Engineering (MIENERG) at the department of Energy and Process Engineering (EPT), Norwegian University of Science and Technology (NTNU), Trondheim.

I would like to thank my supervisor, Professor Bruno G. Pollet for providing insightful knowledge and guidance along the way. I would also like to give a special thanks to my family and girlfriend for their support. It's good to be done, even though Ligretto is fun.

Erik Eikeng
Trondheim, 11.06.2023

Abstract

As a couple of guys (Eikeng and Rogneby, 2021), who once quoted another guy (Bob Dylan, 1963), wrote, *The times they are a-changin'*. And indeed they are. The world is currently undergoing a major clean up, where decarbonization is on top of the agenda. In that regard, large scale production of green ammonia for replacement of the conventional fossil-fuel based ammonia has gained interest in recent times. Today's ammonia is currently responsible for around 1% of global CO_2 emissions, where almost all of the ammonia is used for fertilizer production. Replacing the fossil-fuel based ammonia with green ammonia, synthesized from air, water, and renewable energy, could lead to substantial reduction of emission. In addition to cleaning up the fertilizer industry, green ammonia also has the potential for system power balancing over time (energy storage) and space (energy transfer), thus may potentially become an important part of the global energy transition from fossil fuels to renewables.

This study investigates the creation of a computational optimization framework, that enables the generation of optimal green ammonia plants solutions for any given location. The framework is based on off-grid wind and/or solar energy, along with battery energy storage systems and hydrogen buffer tanks to ensure reliable production of green ammonia, while being able to handle the intermittent renewable energy supply. To illustrate the applicability of the framework, three different locations and scenarios has been evaluated; Tan-Tan, Morocco (solar-based scenario); Utsira, Norway (wind-based scenario); and Patagonia, Argentina (hybrid scenario). For each location, the optimal plant configuration has been found; that is the optimal sizing of each system component which ensures a reliable green ammonia delivery at the lowest possible price.

The simulations revealed a levelized cost of ammonia (LCOA) at 595 USD/tNH_3 for the solar-based scenario, 599 USD/tNH_3 for the wind-based scenario, and 501 USD/tNH_3 for the hybrid scenario. These results are in the upper ranges of what conventional fossil-fuel based ammonia is valued at, yet not far away from being considered competitive in terms of cost.

The research presented in this study demonstrates the feasibility and potential of designing optimal green ammonia plants powered by renewable energy sources. The computational framework developed in this thesis provides a versatile tool for the design and assessment of green ammonia plants, enabling the generation of optimal solutions for any given location. The findings illustrates the great potential of green ammonia as part of large scale decarbonization.

Sammendrag

Verden er for tiden gjennom et grønn skifte, og avkarbonisering står høyt på agendaen. I den forbindelse har det oppstått økt interesse for produksjon av grønn ammoniakk som erstatning for konvensjonell ammoniakk basert på fossile brensler. Dagens ammoniakkproduksjon står for rundt 1% av verdens totale CO_2-utslipp, og nesten all ammoniakken brukes til produksjon av kunstgjødsel. Ved å erstatte den fossilbasert ammoniakk med grønn ammoniakk, som produseres av luft, vann og fornybar energi, kan en betydelig reduksjon av utslipp oppnås. I tillegg til å avkarbonisere kunstgjødselindustrien, har grønn ammoniakk også potensial til å balansere kraftsystemet over tid (ved energilagring) og rom (som energibærer), og kan dermed potensielt bli en viktig del av overgangen fra fossile brensler til fornybar energi.

Denne studien ser på muligheten for å konstruere et beregningsbasert optimaliseringsrammeverk, der målet er å finne optimale løsninger for grønne ammoniakkfabrikker ved gitte lokasjoner. Rammeverket er basert på off-grid vindenergi og/eller solenergi, samt batterilagringssystemer og hydrogentanker for å håndtere de variable energikildene og dermed sikre pålitelig produksjon av grønn ammoniakk. For å illustrere bruksområddene og anvendeligheten til rammeverket, er tre forskjellige lokasjoner og scenarioer blitt evaluert: Tan-Tan i Marokko (solbasert scenario), Utsira i Norge (vindbasert scenario) og Patagonia i Argentina (hybrid scenario). For hver lokasjon er den optimale fabrikksammensetningen funnet, det vil si optimal dimensjonering av hver enkelt systemkomponent, for å kunne sikre pålitelig produksjon og levering av grønn ammoniakk til lavest mulig pris.

Simuleringene resulterte i en ammoniakkostnad (LCOA) på 595 USD/tNH_3 for det solbaserte scenariet, 599 USD/tNH_3 for det vindbaserte scenariet og 501 USD/tNH_3 for det hybridbaserte scenariet. Sammenliknet med den konvensjonelle fossilbaserte amoniakken ligger den grønne i det øvre spekteret hva gjelder kostnad, men er likevel ikke langt unna å være konkurransedyktig.

Undersøkelsene presentert i denne studien viser at gjennomførbarheten og potensialet til grønne ammoniakkfabrikker, drevet av fornybar energi er tilstede allerede i dag. Det utvikled rammeverket gir et allsidig verktøy for konstruksjon og vurdering av grønne ammoniakkfabrikker, og gjør det mulig å finne optimale fabrikkløsninger for enhver gitt lokasjon.

Contents

List of Abbreviations

Terms	Description
AEMWE	Anion-exchange membrane water electrolyzer
CAPEX	Capital expenditure
CRF	Capital recovery factor
HER	Hydrogen evolution reaction
LCOA	Levelized cost of ammonia
LCOE	Levelized cost of energy
LCOH	Levelized cost of hydrogen
LiB	Lithium-ion battery
MEA	Membrane electrode assembly
MUSD	Million US dollars
NPC	Net present cost
OER	Oxygen evolution reaction
OPEX	Operating expenditure
PEN	Positive-electrode-electrolyte-negative-electrode assembly
PCCEL	Proton conducting ceramic electrolyzer
PGM	Platinum group metals
PTL	Porous transport layers (current collectors)
PSA	Pressure swing adsorption
SOEC	Solid oxide electrolyzer
TAD	Total ammonia deficit

List of Symbols

Symbol	Description	Unit
P_{wt}	Power produced by wind turbines	kW
P_{pv}	Power produced by photovoltaic panels	kW
P_{re}	Total power produced (WT and/or PV)	kW
P_{tot}	Total power after ASU input	kW
C_{H2tank}	State of charge of H2 tank	kg_{H2}
$C_{H2tank,min}$	Maximum state of charge of H2 tank	kg_{H2}
$C_{H2tank,max}$	Minimum state of charge of H2 tank	kg_{H2}
C_{bat}	State of charge of batteries	kWh
$C_{bat,min}$	Maximum state of charge of batteries	kWh
$C_{bat,max}$	Minimum state of charge of batteries	kWh
P_{asu}	Power consumed by ASU	kW
P_{elz}	Power consumed by electrolyzers	kW
$P_{elz,min}$	Maximum power consumed by electrolyzers	kW
$P_{elz,max}$	Minimum power consumed by electrolyzers	kW
P_{bat_in}	Power charged to batteries	kW
P_{bat_out}	Power discharged from batteries	kW
$m_{H2_{elz}}$	H2 produced by electrolyzers	kg_{H2}/h
$m_{H2_{asu}}$	H2 consumed by ASU	kg_{H2}/h
$m_{H_2,def}$	H2 deficit for ASU	kg_{H2}/h
$m_{H2_{tank_in}}$	H2 charged into tanks	kg_{H2}/h
$m_{H2_{tank_out}}$	H2 discharged from tanks	kg_{H2}/h
E_{curt}	Energy curtailed (excess production)	kW
N_{WT}	Installed wind-turbine cap (optimization variable)	kW
N_{PV}	Installed solar PV cap (optimization variable)	kW
N_{elz}	Installed electrolyzer cap (optimization variable)	kW
N_{bat}	Installed battery cap (optimization variable)	kWh
$N_{H_2,tank}$	Installed hydrogen tank cap (optimization variable)	kgH_2

List of Figures

List of Tables

1 Introduction

The global shift towards decarbonization and the implementation of green, renewable energy through all sectors is fully underway. Countries, brought together by the UN, reaffirmed the Paris Agreement during the global climate summit of 2021 (COP26), with the goal of limiting the increase in the global average temperature to well below 2°C above pre-industrial levels (Nations, 2021). By the end of 2022, global renewable generation capacity reached 3,372 GW (IRENA, 2023a), accounting for around 26% of the total worldwide electricity generation of 27,000 TWh (with fossil fuels at 63.2% and nuclear at 10.4%) (IRENA and AEA, 2022). The installed capacity of renewables is expected to increase in line with the anticipated increased power generation as a result of global electrification. Total renewable installed capacity is expected to grow threefold to 10,770 GW in 2030 and eight-fold to 27,800 GW in 2050, supplying 65% of total electricity generation by 2030 and 90% by 2050 (International Renewable Energy Agency, IRENA, 2021). Solar PV and wind energy are expected to be the main contributors, exceeding 5,200 GW and 3,300 GW respectively by 2030, up from 1,053 GW and 899 GW today (IRENA, 2023b)).

With an increasing share of renewables, the intermittent nature of these energy sources presents a significant challenge in terms of energy storage and distribution (MacFarlane et al., 2020). Storage will be needed to aid in the inevitable power supply and demand mismatch throughout the year due to variable weather conditions. Additionally, the ability to transport the energy from areas of the world where wind and solar resources are abundant to the market will be key in enabling the green transition. By using hydrogen and its derivatives (ammonia, methanol etc.) as renewable energy carriers, energy can be store and transported at will (Egerer et al., 2023; Bastien Bonnet-Cantalloube et al., 2023). This enables both direct use of electricity for power, and also indirect use in hard-to-abate sectors such as fertilisers, steel manufacturing, aviation, marine, and heavy-duty road transport, that are typically dominated by coal, oil, and gas (Wang et al., 2023).

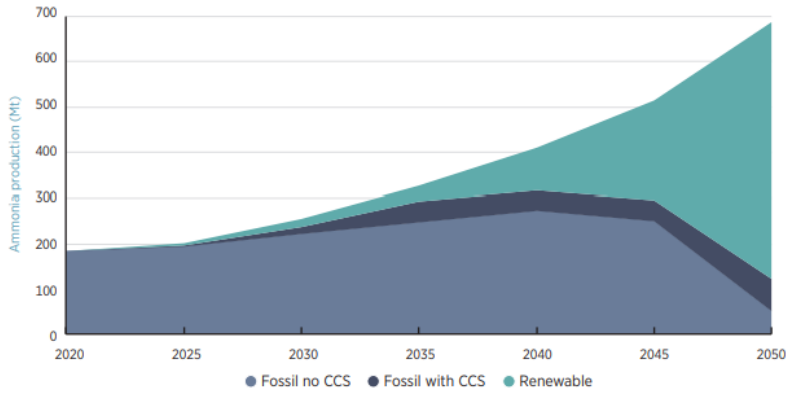

Figure 1.1: Estimated future production of green ammonia IRENA and AEA (2022).

Of the potential energy carriers available, ammonia is considered to be one of the most promising (The royal society, 2021). Compared to other energy carriers such as liquid hydrogen, ammonia has a higher volumetric density (1.5 times higher than liquid hydrogen),

and is easier to liquefy and transport (Wang et al., 2023). Ammonia (NH_3), synthesized from hydrogen and nitrogen using the Haber-Bosch process, liquefies at -33°C, whereas liquid hydrogen requires a temperature of -253°C, making it more challenging to produce and store over longer periods of time or distance (U.S. Department of Energy, 2006). Additionally, ammonia as a product is already produced at an industrial scale, with an annual global production of around 175 million tonnes as shown in figure 1.1.

However, almost all of the produced ammonia comes from fossil fuel based hydrogen, generating around 0.5 Gt of CO_2 emissions each year, which accounts for 1% of global greenhouse gas emissions. The replacement of fossil fuel-based hydrogen feedstock with green hydrogen, produced via water electrolysis powered by renewable energy, provides an opportunity to produce emission-free green ammonia. It does, however, not come without challenges. Historically, ammonia production relied on a continuous supply of fossil-fuel-based hydrogen and power, implying that traditional ammonia synthesis units aren't designed to handle fluctuating energy supplies typical of renewable energy sources. This problem could potentially be addressed by incorporating hydrogen buffer tanks and battery banks to maintain a continuous mass and energy supply. By 2050, the total ammonia production is projected to increase to around 688 Mt (four times that of today), with green ammonia expected to be the primary source, contributing to around 80% of total production (IRENA and AEA, 2022; International Energy Agency, 2021; The royal society, 2021).

Most of the ammonia produced today is used in the production of fertilizers (around 80%) (Nosherwani and Neto, 2021), with a small amount going into explosives, other chemicals and materials. By substituting the traditional fossil-fuel based ammonia with green ammonia, a decarbonization of the fertilizer industry is possible. In addition to the fertilizer industry and the role as an energy/hydrogen carrier, green ammonia is also expected to play an important part as a maritime fuel for international shipping. Ammonia-fuelled vessels are currently being developed and are expected to be available by 2024 (IRENA and AEA, 2022). Another promising area of use is power generation for grid balancing by replacing natural gas in gas turbines, or coal in coal-fired power plants, either partially or (eventually) fully (International Energy Agency, 2021). To summarize, the production of green ammonia has three major roles to play in energy transition; cleaning up the fertilizer industry, system power balancing over time (energy storage) and space (energy transfer) (Ikäheimo et al., 2018) - making the production of green ammonia particularly interesting in the years to come. Understanding how to efficiently and economically deploy green ammonia plants at a global scale is crucial if green ammonia is to become a feasible solution.

1.1 Literature review

There are plenty of techno-economical studies done on the optimization of green hydrogen production, but limited resources available on the optimization of the green ammonia plant. However, as ammonia is a product of hydrogen, the approach of optimizing green hydrogen production is closely related to that of green ammonia. Tebibel (2021, 2022) developed a methodology for optimizing a off-grid wind/battery system for production of green hydrogen at various locations. Al-Buraiki and Al-Sharafi (2022) used a similar approach for green hydrogen production from an off-grid hybrid solar/wind/battery/hydrogen storage system. These papers explored ways of modelling the strategy for controlling power and hydrogen flows, by creating algorithms for controlling flows between each system component, thus being able to control how the variable energy input from the renewables will determine how and when hydrogen is being produced, as well as how the battery bank charges and discharges for optimal operation.

As far as the green ammonia plant modelling goes, Morgan et al. (2014) was one of the first who brought production of green ammonia to the masses in his dissertation on an offshore wind based green ammonia plant. Osman et al. (2020) and Gallardo et al. (2021) performed techno-economic optimizations in areas with high insolation, and solely based the ammonia production on solar PV generated energy, supported by either battery banks or hydrogen tanks, or both, to provide a more continuous operation. Reversely, Morgan et al. (2014) and Bañares et al. (2015) performed case studies and analyzed production of green ammonia entirely supplied by wind energy, with support from hydrogen storage tanks. By combining the two energy sources, Arnaiz del Pozo and Cloete (2022), Fasihi et al. (2021), and Salmon and Bañares-Alcántara (2022) explored a hybrid scenario using both solar and wind in combination with a battery bank and hydrogen storage. Fasihi et al. (2021), Wang et al. (2023), Nayak-Luke et al. (2018), and Armijo and Philibert (2020) took the hybrid scenario one step further, and explored fully flexible production of green ammonia by allowing the ammonia synthesis unit to operate over a range of energy inputs at operational windows ranging between 20-100%, thus being better suited for the variable renewables. The resulting LCOA from the aforementioned studies can be found in Appendix A.

While the studies thus far provide important knowledge into the modeling and optimization of green ammonia production, there are still room for additional input. This thesis aims to create a more general computational framework, that is able to encapsulate a wider array of possible scenarios. By creating a model with adjustable input parameters, one can optimize the green ammonia with a wider operational range. Whether that would be a purely wind-based system without any form of battery or hydrogen storage, or a hybrid system with both hydrogen and battery storage, or purely solar-based system with only battery storage available. Doing this provides flexibility in terms of choosing the right configuration at the right place, and allows for a wider arrange of possible solutions.

1.2 Research question and objectives

This thesis seeks to answer the following research questions; ***RQ1:*** *How can we construct and utilize a computational framework to optimize the production of a green ammonia plant based on off-grid wind and/or solar energy at different geographical locations?* and ***RQ2:*** *Is the production of green ammonia techno-economically feasible?*

To address this question, the following objectives have been set:

1. Perform research on current state of the art green ammonia production to get a complete overview of the production processes, technological capabilities and challenges.
2. Develop a computational model that simulates and optimizes the production of green ammonia from off-grid renewable sources. The model will focus on solar, wind and a hybrid combination of both.
3. Evaluate the model at various locations with different restrictions to see how the model reacts. Perform simulations using only solar PV, only wind, and a hybrid scenario at suitable locations.
4. Identify the optimal parameters and operational conditions that enable the most efficient conversion of renewable energy into green ammonia, while minimizing the related costs. The model will determine the sizing of each system component, making sure the system is able to perform in a reliable way and at the minimum cost.
5. Evaluate the techno-economical feasibility of the green ammonia plant based on output from the simulation. This will involve a comprehensive analysis of the capital and operational expenditures and and overall system performance.

By delving into these objectives, the study aims to contribute a general framework applicable for any green ammonia plant at any location, thereby aiding in the understanding of the green ammonia plant and its increasingly important role in the energy transition.

1.3 Thesis outline

Chapter 2 conducts a literature review, where previous similar work on the optimization of green ammonia plant is being evaluated. In chapter 3, all relevant background theory is presented. This builds the required theoretical foundation and supports the methodology of chapter 4. Here, the development of the computational framework for modelling and optimizing the green ammonia plant is being discussed. Chapter 5 presents the cases that is being studied in the thesis, which is the various geographical locations set for modelling. Chapter 6 presents and explains the outcomes from the case study, with system sizing, energy distribution, system economics, and performance metrics. It also offers a comparison between the different locations and scenarios that has been simulated. Chapter 7 offers a discussion of the results, interpreting them in the context of the research question and objectives, before a summary and conclusion is presented in chapter 8.

2 Background theory

This chapter will introduce some background information needed in order to fully grasp the concepts and provide reasoning behind some of the choices that has been made throughout the paper. Wind energy, solar energy, batteries, energy carriers, production of hydrogen, and production of green ammonia will all be discussed. The background theory sections regarding water electrolysis and electrolyzer technologies are based on the work done by (Erik Eikeng, 2022), in the specialization project leading up to this thesis.

2.1 Renewable energy sources

Theory behind energy extraction from wind and solar will be presented in the following sub-chapter.

2.1.1 Wind energy

Wind energy, which can be defined as the mechanical extraction of kinetic energy from wind, is an important part of renewable energy infrastructure. Wind is essentially movement of air caused by pressure differences in the earths atmosphere, as a result of irregular heating of the surface (Chiras, 2010). By implementing wind turbines, these wind resources can be harnessed for energy production. The most commonly design of wind turbine, is the horizontal axis wind turbine (HAWT), where the axis of rotation is parallel to the ground (J.F Manwell et al., 2009). The main components of an HAWT include the rotor system (blades and hub), drive train (main shaft and gearbox), and an electric generator, as illustrated in Figure 2.1. When wind interacts with the aerodynamically designed turbine blades, it generates a lift force which causes the rotor to rotate. This rotation induces mechanical energy, which is transferred through the main shaft and gearbox to the generator, before being converted into electrical energy (Burton et al., 2011).

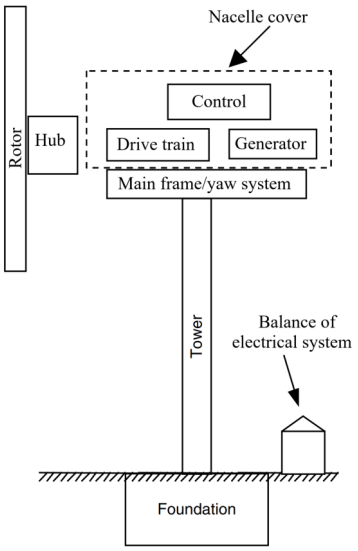

Figure 2.1: Wind turbine components (J.F Manwell et al., 2009).

The amount of energy generated by the wind turbine is governed by equation 2.1, where ρ is the air density, C_p is the power coefficient, A is the rotor swept area, and U is the free stream velocity (Burton et al., 2011). The power coefficient describes the fraction of the power in the wind that may be converted by the turbine into mechanical work. It is by definition limited by Betz law to 59.3%, which is the maximum theoretical amount of energy the wind turbine is able to extract from the available wind energy passing through the swept area of the rotor blades (Jain, 2010). Most commercially available wind turbines today, reach an operational efficiency of about 50% (Jain, 2010).

$$P = \frac{1}{2} C_p \rho A U^3 \tag{2.1}$$

From the equation, it becomes evident that the larger the rotor diameter, the larger the power output. Also, higher wind-speeds will lead to higher power outputs. As a result of this, the commercially available wind turbines has rapidly increased in size over the last decades. Where the largest rotor diameter was 50m with a capacity of 600kW in 1995 (Burton et al., 2011), there are today commercially available wind turbines spanning up to 260m in diameter with a capacity of 18 MW (Blain, 2023).

To correctly model the power output of the turbine, the wind power curve, illustrated by Figure 2.2 is used. The power curve expresses the relationship between the wind speed and the power output by the wind turbine, and each turbine model has its own specific power curve that is provided by the manufacturers.

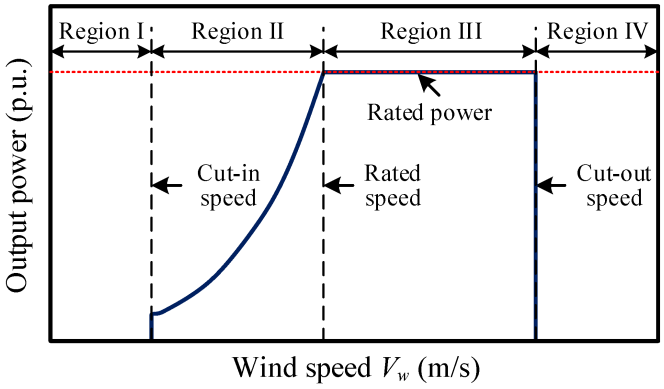

Figure 2.2: Basic wind power curve(Yang et al., 2018).

The curve features three crucial wind speeds: the cut-in wind speed, the rated wind speed, and the cut-out wind speed, where each is defined as follows (Burton et al., 2011):

- **Cut-in Wind Speed**: This is the minimum wind speed at which the turbine begins to generate power. Below this speed, the turbine remains in a standby mode.
- **Rated Wind Speed**: At this wind speed, the turbine produces its maximum, or rated, power output.
- **Cut-out Wind Speed**: This is the maximum wind speed that the turbine can withstand. When wind speeds exceed this limit, the turbine will shut down to avoid potential damage.

By using the power curve, one can obtain the power output of a wind turbine at any given wind speed, thus being able to accurately model the wind turbine power output.

2.1.2 Solar energy

Solar energy comes in the form of electromagnetic radiation emitted by the sun (Wolfe, 2018). The average intensity of the solar energy, or solar irradiance, reaching the top of earths atmosphere is around 1350 W/m^2 (NASA earth observatory, 2009). As the sunlight travels through the atmosphere, only 1/4 of this initial irradiance reaches the surface of the earth. This incoming irradiance is the sum of direct radiation and diffuse radiation. Where the direct radiation is the is the solar radiation that reaches the earths surface straight from the sun, and the diffuse radiation is sunlight that has been reflected or scattered by molecules and particles in the earths atmosphere (PVGIS, 2021).

Through the use of photovoltaic cells (PV), the solar energy received can be converted into electrical energy. The conversion is performed in a solar cell, which are typically made up of semiconductor materials (Silicon (Si) is most commonly used) (Hegedus and Luque, 2011). The process is schematically illustrated in Figure 2.3. The semiconductors has electrons forming covalent bonds between each atom in the crystalline structure. These electrons are stuck in their bonds until enough energy (in the form of sunlight) excites

the electron to a high-energy, free state. The amount of energy required to release the electron from the bound state to the free state is called the band gap energy. A hole is created where the electron was bound.

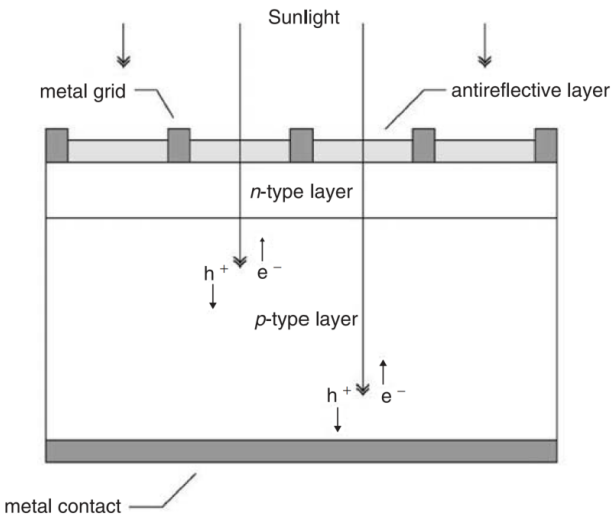

Figure 2.3: Schematics of a conventional solar cell (Hegedus and Luque, 2011).

In order to vary the amount of free electrons and holes in a semiconductor, and to control/change the conductivity of the material, the concept of doping is introduced. This involves the addition of impurities, and creates two types of semiconductors: an n-type semiconductor and a p-type semiconductor. N-type semiconductors are created by doping the silicon with a substance that has more electrons in its outer shell, creating an overall negative charge. Conversely, p-type semiconductors are created by doping the silicon with a material that has fewer electrons in its outer shell, resulting in fewer free electrons, or wholes, creating a positive charge (Mcevoy et al., 2012; Hegedus and Luque, 2011). By bringing the n-type and p-type semiconductors together, a p-n junction is created. At this junction, free electrons from the n-type semiconductor fill the holes in the p-type semiconductor, creating a depletion region where an electric field is formed (Mcevoy et al., 2012; PVGIS, 2021).

When sunlight in the form of photons hits the solar cell, energy can be absorbed by the electrons in the covalent bonds. If the incoming energy is equal to, or greater than the band gap, the electron is excited to a free, high energy state, while an empty hole is left behind - effectively creating an electron-hole pair (PVGIS, 2021). The electric field at the p-n junction separates these pairs, preventing them from recombining. The electrons are then collected at the n-type layer, and the holes at the p-type layer, resulting in a flow of electric current (Hegedus and Luque, 2011; PVGIS, 2021).

Currently, commercially available solar PV cells have an efficiency of about 20%. This means that only 20% of the incoming radiation is converted into electricity, with the remainder being converted into thermal energy that raises the temperature of the solar cell (Skoplaki and Palyvos, 2009). While this conversion rate may appear low, it is important to note that the theoretical maximum efficiency of a solar cell is around 40.7% (Hegedus and Luque, 2011).

2.2 Energy conversion and storage

In order to fully utilize and implement large scale intermittent renewables, it is crucial to have a way of storing and transporting the energy. This makes it possible to manage energy systems by controlling and suppressing the fluctuating renewable energy supply, and by transporting energy from point of generation to point of utilization without having to be grid-connected. Batteries and energy carriers are two prominent solutions, and will be evaluated in the following sections.

2.2.1 Battery storage: lithium-ion batteries

The most commonly used commercialized battery today is the Lithium-ion Battery (LiB). Compared to other battery technologies such as lead-acid, nickel-iron and nickel-metal hydride, the Li-ion battery has the largest potential for industrial use as it has the highest specific and volumetric energy density. Additionally, the Li-ion batteries have fast ion mobility, high charge/discharge efficiencies (around 95%) as well as well as the possibility of diverse electrode designs. (Wu et al., 2020)

Figure 2.4 shows the basic principles and design of a rechargeable Li-ion battery. Two electrodes, one positively charged (cathode) and one negatively charged (anode) is immersed in an ion-conducting electrolyte and separated by a porous separator. The anode is typically graphite made from carbon (C), whereas the cathode is typically a metal oxide, such as Lithium Cobalt Oxide (LiCoO2), Lithium Iron Phosphate (LiFePO4), Lithium Nickel Manganese Cobalt Oxide (LiNiMnCoO2 or NMC), or Lithium Manganese Oxide (LiMn2O4 or LMO). These materials, known as the active material of the electrodes, play a key role in the deposition and storage of migrating Li-ions during the charging and discharging of the battery cell. The active material is coated onto current collectors to close the circuit and allow for current to flow. (Wu et al., 2020; Burheim, 2017; Bryntesen et al., 2021)

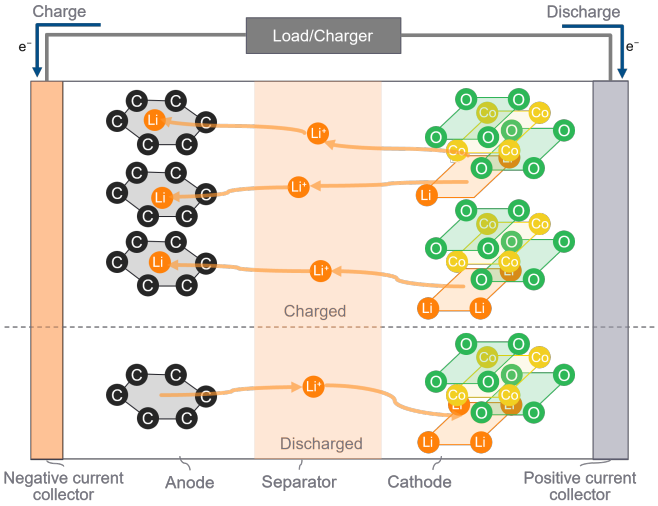

Figure 2.4: Schematics of the charging and discharging state of a lithium-ion battery inspired by Burheim (2017).

During charging, Li-ions are removed from the cathode structure, and transported through the separator to the anode where they reduce to form lithiated graphite (LiC_6) (Reiner Korthauer, 2018). In order not to collapse the atomic structure of the cathode, only around half the Li-ions can be removed (Burheim, 2017). During discharge, the process is reversed, as Li-ions migrate from the anode to the cathode, towards the emptied out metal-oxide framework. As the ions oxidise, electrons are released to the external circuit and power is generated (Reiner Korthauer, 2018).

2.2.2 Energy carriers

Another way of storing the intermittent renewable energy is through energy carriers, which is chemical conversion of energy into fuels. The conversion of energy to hydrogen through water electrolysis is considered an especially promising alternative, and the worldwide demand for hydrogen is rapidly increasing (Chatterjee et al., 2021). However, storage and transportation of hydrogen is difficult. Being the lightest element on earth, the volumetric and specific energy densities are low compared to other conventional fuels such as diesel, gasoline, and LNG, as shown from the Ragone plot in Figure 2.5. As a result, the hydrogen must be compressed (up to 700 bar) or liquefied (boiling point at -253 °C) in order to reach acceptable levels of volumetric energy density. These extreme pressure and temperatures means storing, transporting and production of hydrogen is tricky. Liquefaction can consume up to 40% of the chemical energy stored in hydrogen. (U.S. Department of Energy, 2006; Burheim, 2017)

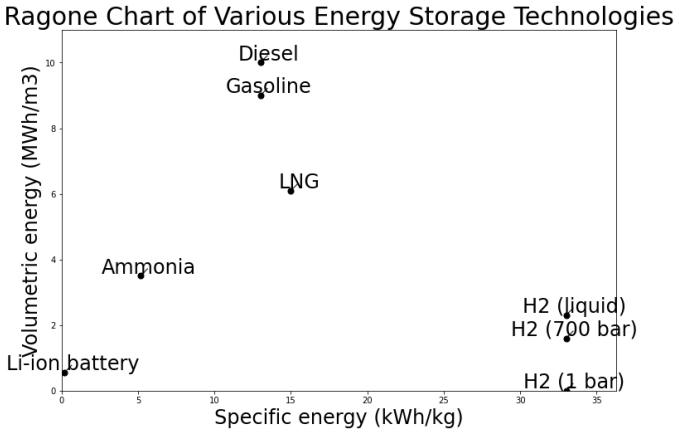

Figure 2.5: Ragone plot showing specific energy and volumetric energy for a various energy storage components (Burheim, 2017).

As an alternative, ammonia has been recognized for its potential as an energy carrier, or more specifically, a hydrogen carrier. Ammonia is already well established with worldwide trading routes, and has great potential as a hydrogen carrier (Chatterjee et al., 2021). Compared to liquid hydrogen, ammonia is liquefied at only -33°C or even at room temperature at an elevated pressure of around 10 bar (Osman et al., 2020). Furthermore, ammonia carries a substantial hydrogen content of 17.65 wt.% and has a volumetric energy content 50% greater than that of liquid hydrogen (Jain et al., 2022). Given these

compelling characteristics, ammonia is increasingly recognized as a viable and promising energy carrier for future transportation and storage of energy (Jain et al., 2022; Osman et al., 2020; Morgan et al., 2017).

2.3 Ammonia production overview

Ammonia has the chemical formula NH_3, and consists of 82.4% nitrogen and 17.6% hydrogen by weight (Morgan et al., 2017). To produce ammonia, nitrogen and hydrogen must be reacted together at correct stoichiometric values, as shown by the chemical reaction equation 2.2. The reaction is non-spontaneous at standard conditions, and requires elevated temperature and pressure to occur. Additionally, the reaction is exothermic, illustrated by the negative enthalpy, and releases about 2.7 GJ or 0.75 MWh per metric tonne of ammonia produced, which is around 8% of the total energy required for ammonia synthesis. (Morgan et al., 2017; IRENA and AEA, 2022; Chatterjee et al., 2021)

$$N_2 + 3H_2 \rightarrow 2NH_3, \qquad \Delta H^\circ = -92.44 \text{kJ/mol} \tag{2.2}$$

Different approaches exist for producing ammonia, yet the fundamental process remains consistent. This involves production of nitrogen and hydrogen gas, combining and compressing these gases into syngas, and converting the syngas into ammonia under certain conditions (typically temperatures of 400-500°C and pressure between 100-400 bar) using a catalyst, often iron-based (Eric R. Morgan, 2013). This process of converting syngas into ammonia, also known as ammonia synthesis, is commonly carried out using the Haber-Bosch synthesis loop, a technology established in the early 1900s. Following synthesis, ammonia is typically condensed and stored as a liquid. (Chatterjee et al., 2021)

Although the aforementioned principles remains the same, there are several possible routes available for producing ammonia, as illustrated in Figure 2.6. The production routes are color coded for simplicity, and the colors are determine by how the hydrogen is produced in the ammonia production supply chain, as well as by the energy supplied to the ammonia synthesis loop itself. Almost all of todays around 150 Mt annual ammonia production comes from fossil-fuel based production (Chatterjee et al., 2021; IRENA and AEA, 2022). Here, the hydrogen is produced from natural gas by steam methane reforming, from coal by coal gasification, or from heavy fuel oil by partial oxidation (IRENA and AEA, 2022). Around 72% of the global ammonia plants uses natural gas as its hydrogen sources today (grey), while around 22% uses coal (black), releasing around 1.8 tonnes and 4 tonnes of CO_2 per tonne ammonia in, respectively (Egerer et al., 2023). By adding a carbon capture storage (blue), emissions can be by reduced 60-85% during steam methane reforming (i.e., production of hydrogen form natural gas). This has the potential to reduce the emissions to around 0.2-0.8 tonnes CO_2 per tonne ammonia, including upstream emissions from extraction of natural gas (Egerer et al., 2023; IRENA and AEA, 2022).

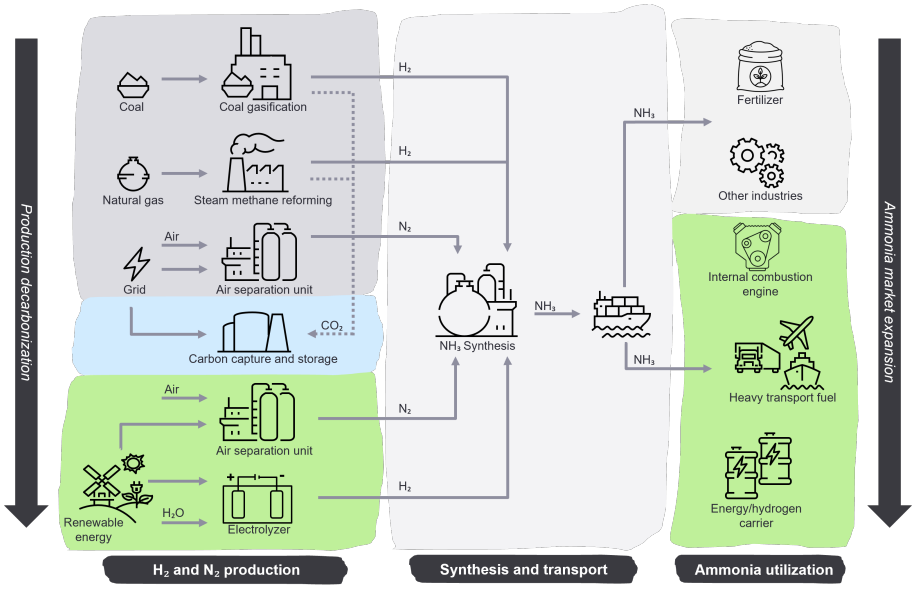

Figure 2.6: Schematic illustration showing different production routes of ammonia as well as its utilization, inspired by Egerer et al. (2023).

The alternative approach for production of ammonia, which forms the basis of the thesis, is the production of green ammonia. Green ammonia is produced in a sustainable manner, by utilizing renewable sources such as solar, wind or hydro power for the production of hydrogen via electrolysis (The royal society, 2021). This approach has the potential to reduce emissions by 98% compared to ammonia produced from natural gas. The green pathway typically emits below 0.1 tonne CO_2 per tonne ammonia, including upstream and downstream emissions (Kleijne et al., 2022; IRENA and AEA, 2022). Today's green ammonia production only constitutes around 0.5% of the global ammonia supply (Morgan et al., 2014). The following subsection will go into detail of all aspects involved in the production of green ammonia.

2.4 Production of green ammonia

To produce green, renewable ammonia, water (H_2O) is split into hydrogen (H_2) and oxygen (O_2) through water electrolysis, while nitrogen (N_2) is purified from air. The hydrogen and nitrogen gases are combined (syngas) and compressed, before being converted to ammonia (NH_3) through the Haber-Bosch ammonia synthesis loop, as shown in Figure 2.7. (IRENA and AEA, 2022; IRENA, 2021a).

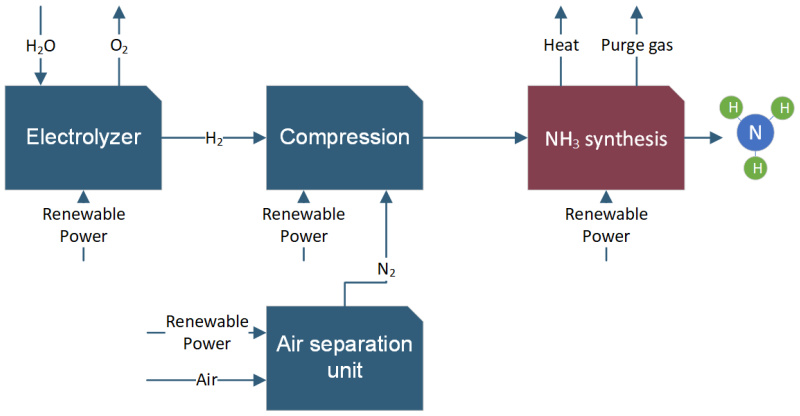

Figure 2.7: Illustration of the green ammonia production sequence (IRENA and AEA, 2022).

There are several ways of producing hydrogen through various electrolyzer technologies. Similarly, there are a few relevant approaches for production/extraction of nitrogen. These methods and technologies, in addition to the ammonia synthesis process itself, will be explained and discussed in the following sections.

2.4.1 Water electrolysis

First comes first, the basic theory of splitting water into hydrogen. There are a wide array of technologies and methods for performing water electrolysis, but despite the technological, physical and electrochemical differences (Taibi et al., 2020), the electrolysis itself is the same; water being split into hydrogen and oxygen by inducing electric current, as shown from equation 2.3 (Burheim, 2017).

$$\text{Overall: } H_2O + \text{electric work} \rightarrow H_2 + \frac{1}{2}O_2 \tag{2.3}$$

The very basic electrochemical cell in which the water splitting reaction occurs is made up of two electrodes - a positively charged anode and a negatively charged cathode, separated by an electrolyte with an external power source. When power is applied, two intertwined reactions are taking place at each electrode, known as redox-reactions. (Ironside, 2022) These redox-reactions are individually expressed by dividing the overall reaction into two

half cell reactions; the hydrogen evolution reaction (HER) and the oxygen evolution reaction (OER) (Wang et al., 2021). At the cathode, H_2 is produced by reduction of water in the HER, and at the anode, O_2 is produced by oxidation of water in the OER. The electrodes are separated by a diaphragm or a separator, and placed in contact with, or immersed in an electrolyte. The purpose of the electrolyte is to increase the conductivity in the solution - which leads to improved ion mobility. The separation between the electrodes is important in order to avoid recombination of the H_2 and O_2 gases that are produced at the electrodes, as well as making sure the electrochemical cell is not short circuited (Ursua et al., 2012). The separator must be permeable to ion transfer in order to allow ions to travel between the electrodes, and at the same time be impermeable the product gases as well as to electron transfer.

2.4.2 Electrolyzer technologies

In the following subsections, relevant electrolyzers technologies will be reviewed. First and foremost the commercially available alkaline electrolyzers and PEM electrolyzers, but also the solid oxide electrolyzers, which is on the brink of commercialization. Additionally, other promising technologies will be mentioned.

2.4.3 Alkaline water electrolysis

The alkaline water electrolyzer (AWE) has been in wide use ever since the beginning of the 20th century, and is considered to be a mature and well established technology (LeRoy, 1983). The basic alkaline water electrolyzer, shown in Figure 2.8, represents the simplest form of an electrochemical system, consisting of two metallic (non-noble material) electrodes, typically based on nickel, iron or cobalt (Gambou et al., 2022), which are separated by a porous diaphragm (often zirfon or polyephenylane sulfide (ZrO_2) (Guo et al., 2019)), and immersed in an alkali electrolyte (Chatenet et al., 2022). The electrolyte is normally a high-concentrate aqueous solution of 25-30 wt.% potassium hydroxide (KOH), which purpose is to improve the ionic conductivity in the cell (Chi and Yu, 2018). The electrochemical cell is enclosed by bipolar end plates. The typical operating temperature of an alkaline electrolyzer is 70-100°C (Chi and Yu, 2018).

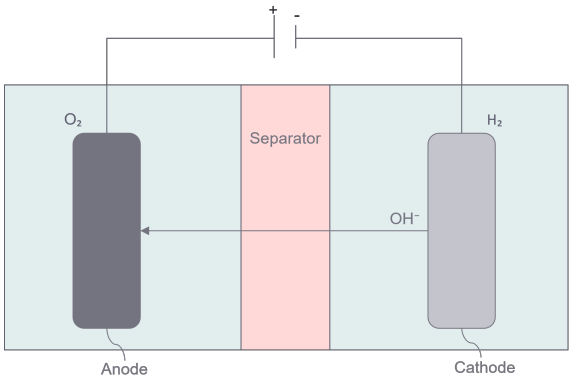

Figure 2.8: Alkaline Water Electrolysis based on illustration from Eikeng and Rogneby (2021).

The half cell reactions occurring at the electrodes are given by equation 2.4 and 2.5, representing the cathodic and anodic reactions, respectively. Water molecules (H_2O) are reduced by electrons (e^-) to form hydrogen and negatively charged hydroxide ions (OH^-) at the cathode (Rashid et al., 2015). The ions are the charge carriers in the AWE, and they migrate through the electrolyte and diaphragm over to the anode side, where they are oxidized to form oxygen and water (Brauns and Turek, 2020).

$$\text{Cathode: } 2H_2O(l) + 2e^- \rightarrow H_2(g) + 2OH^-(aq) \tag{2.4}$$

$$\text{Anode: } 2OH^-(aq) \rightarrow H_2O(l) + \frac{1}{2}O_2(g) + 2e^- \tag{2.5}$$

A key advantages in the alkaline electrolysis cell is the cheap and non-noble materials that makes up the electrode. Additionally, the technology is mature and readily available and durable (Schmidt et al., 2017). There are, however, some drawbacks to the AWE. There are limited current density, j [A/m^2] (current per electrode cross-sectional area), meaning more electrode material is needed to reach the desired current level, resulting in a less compact system. This is due to the high ohmic losses across the electrolyte and diaphragm (Carmo et al., 2013). Additionally, the AWE operates at a low pressure with slower loading response (ramp up and ramp down rate) and a relatively limited dynamic range of operation (Chi and Yu, 2018).

2.4.4 Proton exchange membrane water electrolysis

The proton exchange membrane water electrolyzer, PEMWE, represents the second important electrolyzer technology in todays market. A schematic review of the PEMWE's working principles is found in Figure 2.9. The defining part of the PEM water electrolyzer is the polymer electrolyte membrane (PEM), which is a thin membrane with a thickness of around 0.05mm. The highly acidic (pH $\sim$ 2) membrane is mechanically strong, and is typically a Nafion-membrane (Burheim, 2017; Carmo et al., 2013). The membrane functions both as an electrolyte, as well as a separator of electrodes and product gases (Naimi and Antar, 2018). Only deionized water is fed into the cell, meaning no need for any aqueous electrolytic solutions, unlike that of the AWE. The electrodes are thin porous layers that are attached to both sides of the membrane, effectively forming the membrane electrode assembly, MEA (Burheim, 2017). Catalysts are typically deposited directly onto the membrane surface, with porous transport layers, PTL's (also known as current collectors), pressed against them - combining to form the electrode (Grigoriev et al., 2020). Because of the strong acidic and corrosive environment in the cell, using noble metal catalysts like iridium (Ir) and ruthenium (Ru) at the anode, and platinum (Pt) or Palladium (Pd) at the cathode, is a requirement in order to avoid material degradation (Chi and Yu, 2018; Bessarabov et al., 2016).

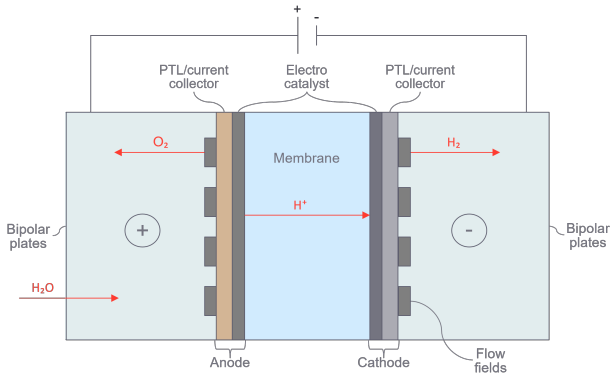

Figure 2.9: PEM water electrolysis, based on illustrations from Grigoriev et al. (2020).

The PTL's are electrically connected to the bipolar plates, which are end plates that encloses the cell, and also provide electrical contact with the external power source (Bessarabov et al., 2016). This enables current to flow between the bipolar plates and the electrodes (Lehner et al., 2014). Additionally, the PTL's and bipolar plates transports liquid water into the anode compartment, and oxygen and hydrogen gas out of the electrolysis cell (Rashid et al., 2015). The bipolar plates allows for several cells to be connected into a stack - thus making it possible to reach the desired production output by increasing the number of cells (Taibi et al., 2020).

As the MEA is immersed in pure water, and a sufficient cell voltage is applied, the OER at the anode, and HER at the cathode is initiated, given by equations 2.7 and 2.6, respectively. At the anode, water is oxidized, and electrons passes through an external circuit as oxygen gas evolves. Protons (H^+), the ionic charge carrier in PEMWE, migrates through the membrane towards the cathode, where they reduce to form hydrogen gas. (Bessarabov et al., 2016)

$$\text{Cathode: } 2H^+(aq) + 2e^- \rightarrow H_2(g) \tag{2.6}$$

$$\text{Anode: } H_2O(l) \rightarrow \frac{1}{2}O_2(g) + 2H^+(aq) + 2e^- \tag{2.7}$$

Some of the advantages of a PEM water electrolyzer is its compact design, the ability to reach high current densities (meaning high power, and subsequently a high H_2 production), high energy efficiency and a flexible operation, as a result of a dynamic load range and the ability to ramp up and down the load at a fast rate (Grigoriev et al., 2020; Chatenet et al., 2022; Kumar and Himabindu, 2019). The major drawback is the need for costly and scarce noble materials, also known as platinum group metals (PGM), in the electrodes, as well as the high capital cost (Ironside, 2022; Kumar and Himabindu, 2019).

2.4.5 Solid oxide electrolysis cell

The solid oxide electrolysis cell (SOEC) is a high temperature electrolyzer. In comparison with AWE and PEMWE, which operates in the temperature ranges of 50-100 °C, the SOEC typically operates in the temperature ranges of 700-1000 °C (Carmo et al., 2013). This mid- to high operational temperature yields improved thermodynamic properties such as low operational voltages of around 1.2-1.3 V, and high electrode kinetics (no need for PGM catalysts), which leads to low overpotentials (Carmo et al., 2013; Lehner et al., 2014). At elevated temperatures, water vaporizes, and gaseous H_2O is fed into the cell, rather than liquid H_2O, as was the case for the AWE and PEM electrolyzers. This significantly reduces the electrical energy demand for the electrolysis processes, since the energy needed for vaporization is provided thermally within the system, rather than electrically (Grigoriev et al., 2020; Lehner et al., 2014).

Where the PEM electrolyzer is based around the MEA, the SOEC is defined by the PEN; the positive electrode-electrolyte-negative electrode assembly (Shi et al., 2017). An oxygen-ion-conducting solid ceramic membrane is used as an electrolyte and separator between the anodic and cathodic compartment. Two thin, porous electrodes are placed on each side of the membrane, and enclosed by cell separators - also known as interconnects. The separators are equipped with flow fields to make sure the water vapor is supplied to the cathode, as well as to control the collection and transportation of product gases (Grigoriev et al., 2020).

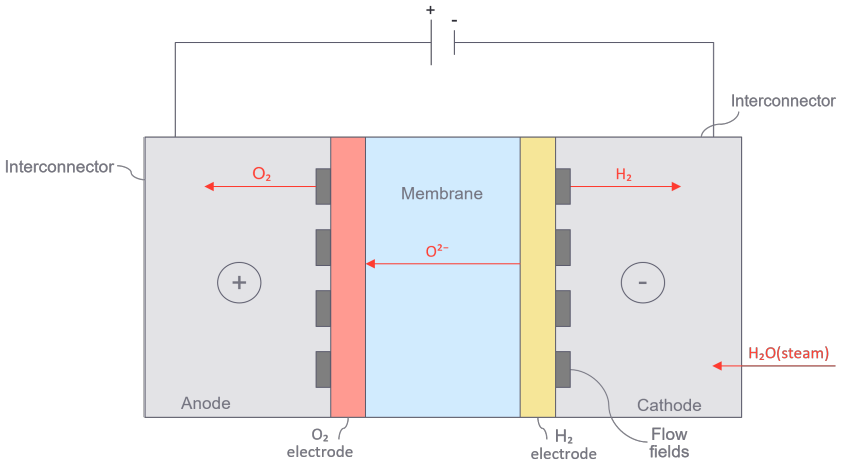

Figure 2.10: Solid Oxide Water Electrolysis inspired by Chatenet et al. (2022).

The basic operating principles of a SOEC is shown by the two half-cell reactions 2.8 and 2.9. Water vapor is fed into the cathode where it is reduced by an external power source to produce hydrogen and oxide (O^{2-}). The oxide ions travels through the solid electrolyte to the anode, where they recombine to form oxygen and release electrons - thus enclosing the circuit. (Ursua et al., 2012)

$$\text{Cathode: } H_2O(g) + 2e^- \rightarrow H_2(g) + O^{2-} \tag{2.8}$$

$$\text{Anode: } O^{2-} \rightarrow \frac{1}{2}O_2(g) + 2e^- \tag{2.9}$$

The SOEC's main advantage is the low operational cell voltages of around 1.2 V, which leads to high operational efficiencies and low electric consumption for production of hydrogen. Because the SOEC's is a high temperature electrolyzer, it needs to be paired with waste excess heat from other forms of production, such as heat from solar concentrators, geothermal energy (Sigurvinsson et al., 2007) or waste heat from power stations/nuclear reactors in order to be considered a feasible solution (Ebbesen et al., 2014). Additionally, recovered heat released during ammonia synthesis may be a promising alternative. However, operation under such elevated temperatures cause problems for the cell components, as they degrade at a fast rate. In theory, the current densities could be at the level of the PEM electrolyzer (1-3 A/cm^2), but are typically kept at lower levels of 0.3-1 A/cm^2 to prevent further material degradation (Ebbesen et al., 2014). The SOEC has shown the ability to operate dynamically, meaning it can be coupled to intermittent renewable energy sources. A dynamic operation means that the electrolysis cell must tolerate to be cycled in temperature, causing additional material strain (Burheim, 2017). (Lehner et al., 2014)

2.4.6 Electrolyzer comparison

Table 2.1 compares the state-of-the art operating parameters for each of the three main electrolyzers; alkaline, PEM and SOEC.

Table 2.1: Comparison of AWE, PEM, and SOEC technologies

Technology	**AWE**	**PEM**	**SOEC**
Status	Mature	Commercial	Demo plants
Operating temperature (°C)	70-100	50-80	700-1,000
Pressure range (bar)	<30	<70	1
Current density (A/cm^2)	0.2-0.8	1-3	0.3-1
Cell voltage (V)	1.4-3	1.4-2.5	1.0-1.5
Load range (%)	15-100	5-120	30-125
Cold start to nominal (min)	<50	<20	<600
System efficiency (LHV)	50-68	50-68	75-85
Electrical efficiency (kWh/kgH_2)	47-66	47-66	35-50
Lifetime stack (hours)	80,000	80,000	<20,000

2.4.7 Other promising technologies

In addition the alkaline, PEM and SOEC electrolyzers, two other technologies are showing potential. The first one is the anion-exchange membrane electrolyzer (AEMWE). This

technology combines the benefits of PEM and alkaline electrolyzer technologies, achieving low-cost and efficient hydrogen production from intermittent, renewable energy sources (Vincent and Bessarabov, 2018). It uses a solid anion exchange membrane for conducting hydroxide ions in an alkaline environment. Some key advantages include the ability to use non-noble transition metal catalysts, a less corrosive environment, a less expensive membrane, and a reduction in size and weight. However, several challenges, like optimizing non-PGM catalysts, decreasing ionic resistance of AEM membrane, and improving the electrolyzer durability, needs to be addressed for it to become a viable option (Henkensmeier et al., 2020; Chatenet et al., 2022).

The proton conducting ceramic electrolyzer (PCCEL), is another emerging high temperature water electrolyzer technology based around a solid ceramic electrolyte (similar to the SOEC), but with a lower operational temperature range of 300-700 °C (Duan et al., 2020). Water vapor is fed into the air electrode, where an externally applied voltage drives the reactions leading to the production of pure, dry hydrogen. PCCEL's benefits include pure H_2 production, higher ionic conductivity for H^+ transportation leading to higher thermodynamic efficiency at lower temperatures, and less material degradation due to mid-range operational temperatures. However, improvements in efficiencies, electrode kinetics, and stability are required for this technology to become viable (Le et al., 2022, 2021; Duan et al., 2019).

2.4.8 Air separation

In addition to hydrogen produced from electrolysis, the green ammonia production is also in need of nitrogen, which is obtained through separation of air. The earths atmosphere contains about 78% nitrogen (20% oxygen, 1% argon, as well as some water vapor, carbon dioxide and other contaminants) which is readily available for extraction (Bañares et al., 2015). There are several ways of performing the air separation, but the cryogenic distillation is the most widely used and accounts for around 80% of total world nitrogen production (Eric R. Morgan, 2013; Ivanova and Lewis, 2012). Pressure swing adsorption (PSA) is also a mature alternative for nitrogen production, while membrane separation is another, less mature option (Rouwenhorst et al., 2019).

Cryogenic distillation

The cryogenic distillation unit utilizes the different boiling points/condensation temperatures of the three main gases present in the atmospheric air (nitrogen, oxygen and argon). The unit is essentially a complex series of chambers, compressors, heat exchangers and adsorbers that allows for step-wise extraction and separation of the gases (Castle, 2002). The process begins with air being compressed and re-cooled for removal of carbon dioxide and water through a sieve adsorbers. Then, the purified air is cooled down through heat exchange to partial liquefaction of the gases. Nitrogen liquefies at 77K (-195°C) and oxygen liquefies at 90K (-183°C). This difference in boiling point, is enough to separate the gases in the distillation chamber. Argon lies in between with a boiling point at 87K (-185°C), and is separated in step-wise columns downstream in the distillation chamber. (The royal society of chemistry, 2023; Castle, 2002; Spelorzi, 2022)

The cryogenic unit are well suited for large scale nitrogen production, and is considered the best alternative for large scale ammonia production with production ranges of 20-2500 tNH_3/d (Osman et al., 2020). The unit requires continuous operation, but has the ability to adjust the load between 60-100%. However, the slow dynamic response (order of hours) means flexibility is limited. (Rouwenhorst et al., 2019)

Pressure swing adsorption

Another method for separation of nitrogen from air is the pressure swing adsorption (PSA). Unlike the cryogenic unit, that achieves separation by liquefaction, the PSA is a non-cryogenic method that uses adsorption and desorption at various pressures (Ivanova and Lewis, 2012).

During operation, compressed air is passed through a combination of filters to remove water, carbon dioxide and minor impurities. The purified air is then passed along to one of two adsorption vessels full of adsorbent sieves. As the compressed air travels through the first vessel, oxygen is adsorbed by the filters. The high pressurized vessel leads to a selective adsorption, allowing nitrogen to pass through at a desired level of purity. At the same time, a second vessel is depressurized to remove the adsorbed gases, releasing it to the atmosphere, thus preparing the for the next cycle. These vessels alternate their operation at high and low pressures, thus increasing the flow of operation. (Ivanova and Lewis, 2012; Bañares et al., 2015; Spelorzi, 2022)

The advantage of PSA is its relative simplicity and its ability to quickly adjust to changes in demand or operational conditions, making it a promising alternative for combination with intermittent renewables. However, it is less energy efficient than cryogenic distillation (around 0.29 kWh/kgN_2 vs 0.1 kWh/kgN_2 (Bañares et al., 2015)) and is better suited for smaller scale operations with production ranges of 5-500 tNH_3/d (Osman et al., 2020). PSA units can also operate intermittently and have the ability to adjust the load between 40-100%, allowing for greater operational flexibility (Rouwenhorst et al., 2019).

Membrane separation

Membrane separation represents another alternative technology for air separation. In this process, compressed air is passed to a membrane unit, which is essentially a tube bundle similar to a shell-and tube heat exchanger, but with smaller tubes with diameter of around 0.2mm. The tubes are completely filled with membrane material, containing thousands of hollow fibers (Castle, 2002). The principle behind the separation is that the gases present in air have different permeability, which determines the gas' ability to diffuse/travel through the membrane wall. Oxygen, carbon dioxide, and water vapor have higher permeability than nitrogen, meaning they pass through the membrane unit at a faster rate. These gases are discarded along the tube bundles, while nitrogen is collected separately at the tube outlet.

Compared to the other technologies, membrane separation typically gives nitrogen of lower purity (95-99.5%), in contrast to the 99.999% purity of cryogenic distillation and the 99.8% purity of pressure swing adsorption (Rouwenhorst et al., 2019). Additionally, the membrane separation is only viable for smaller scale production with a production rate of 1-500 tNH_3/d. Its energy consumption is estimated to be around 0.4 kWh/kgN_2, higher

than that of cryogenic distillation and pressure swing adsorption (Rouwenhorst, 2018; Osman et al., 2020)

2.4.9 Ammonia synthesis

Once hydrogen and nitrogen have been procured through electrolysis and air separation respectively, the next step in the process of producing ammonia, is ammonia synthesis. The synthesis loops for almost all ammonia plants are based on Haber–Bosch process, which was developed nearly one hundred years ago. Regardless of the hydrogen and nitrogen origin, the Haber-Bosch synthesis loop remains largely the same (small variations in plant design based on industry for the specific plant), meaning both green and grey/black ammonia production employ this approach. The specifics of the Haber-Bosch operation will be discussed subsequently (Morgan et al., 2014).

Haber-Bosch synthesis loop

A simplified schematic illustration of the Haber-Bosch synthesis loop is given in Figure 2.11.

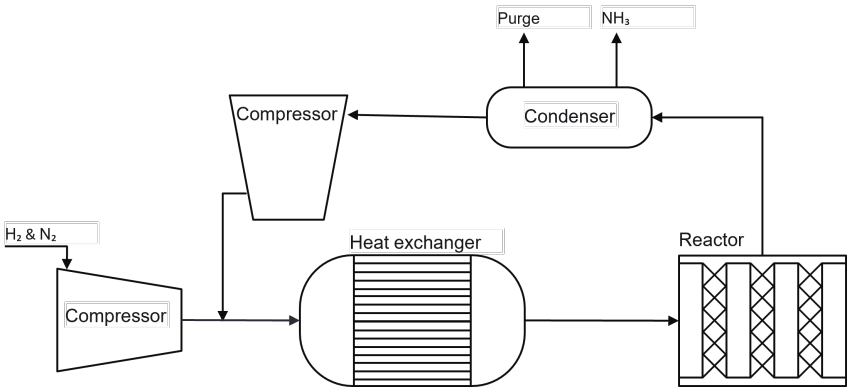

Figure 2.11: Schematic illustration of the Haber-Bosch synthesis loop based on illustrations from Morgan et al. (2014); Bañares et al. (2015).

The initial stage involves the combination and compression of the syngas (hydrogen and nitrogen at a 1:3 ratio) at the inlet, typically to pressures between 100-400 bar. The compressed syngas is then fed into the synthesis loop, where it is heated to the required reactor temperature of between 400-600 °C (Bañares et al., 2015; Eric R. Morgan, 2013). These high temperatures and pressures are required in order to separate nitrogen from its strong triple bond, and to allow for synthesis to occur in the reactor chamber in presence of a catalyst (usually iron (Fe) based) (Rouwenhorst, 2018).

After synthesis in the reactor, the gases are transferred to the condenser, where liquid ammonia is separated from the hydrogen and nitrogen gas that has not yet been synthesized in the reactor. Only about 15-25% of the feed gas is actually being synthesized during the first pass (Bañares et al., 2015; Osman et al., 2020). The remaining unreacted gases are recycled through several additional passes, eventually reaching an overall conversion rate of around 97-99% (Osman et al., 2020; Fasihi et al., 2021).

To compensate for a pressure drop through the loop of about 6%, a recycle compressor is used to restore the syngas to the pressure levels required by the reactor. The gas must also be reheated (Bañares et al., 2015). To avoid build up of inert gases such as argon and carbon dioxide that has not been purified in the air separation process, the loop utilizes a periodic purge to discard these gases from the loop, and to avoid a lowered conversion efficiency in the process (Nosherwani and Neto, 2021).

While the Haber-Bosch process is efficient, it lacks flexibility, and is designed for stable and continuous operation. As a result of this, continuous feed of hydrogen, nitrogen and electricity is required. Deviations will lead to changes in temperature and pressures, which and turn may damage the catalyst and lower the conversion rate. (Osman et al., 2020; Morgan et al., 2017). This is a particularly bad feature when combined with intermittent renewable energy sources such as wind as solar. Implementation of hydrogen buffer tanks and battery banks to provide a more continuous flow of both hydrogen and electricity (for air separation as well as ammonia synthesis) is a promising alternative that helps to mitigate the need for flexibility. Additionally, new research suggests that new Haber-Bosch design solutions may enable operation with a turn-down ratio of 90% (load range of 10-100%) (Haldor Topsøe and Alfa Laval, 2020) and ramp-up rates of 20% per hour (Wang et al., 2023). This increased flexibility is suggested to be obtained by adjusting the operation parameters such as reducing the purge rate and increasing the fraction of inert gases in the reactor. Additionally, varying the fraction of the H_2/N_2 ratio may aid in reducing the load of the H-B plant (Cesaro et al., 2021).

A normal-sized Haber-Bosch plant produces 1000-1500 tonnes ammonia per day and has an energy requirement of around 0.6 kWh/kgNH_3 (Fasihi et al., 2021; Bañares et al., 2015). Some larger plants are also operative at a production of 3000-4000 tonnes per day (Morgan et al., 2017; Bañares et al., 2015).

3 Methodology

In this chapter the methodology of the thesis will be discussed. Each step that has been taken during the construction of the computational optimization framework for production of green ammonia will be methodically presented.

3.1 System description

The off-grid green ammonia power plant is schematically illustrated in figure 3.1. The system consists of (i) power suppliers (wind and/or solar), (ii) power demanders (PEM electrolyzers, cryogenic air separation unit (ASU), syngas compressor and Haber-Bosch unit), (iii) mass flow suppliers (PEM electrolyzer and cryogenic ASU) and mass flow demander (Haber-Bosch unit). Additionally, batteries and hydrogen buffer tanks are added to the supply chain for load management by storing energy and hydrogen in times of excess resources, and supplying in times of deficit.

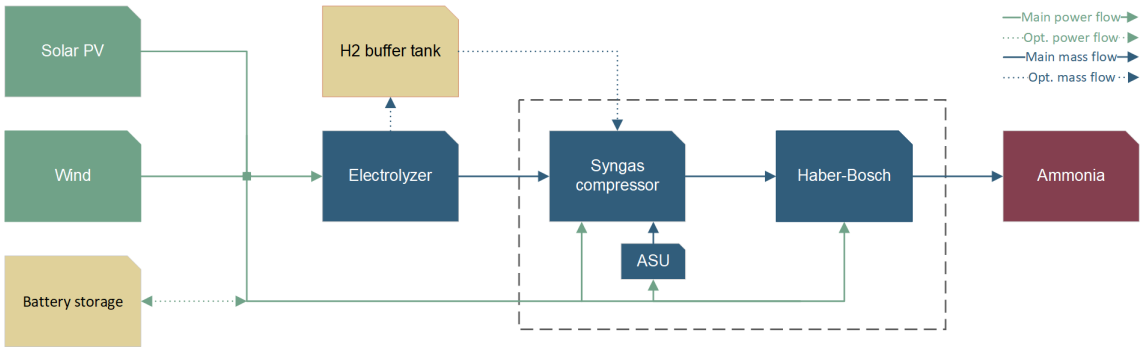

Figure 3.1: Illustrative flowchart for a green ammonia plant including all system components and mass- and energy flows.

3.2 System operation

The production of green ammonia is a complex process involving several system components - all of which are in need of consideration if the plant is to be operated at optimum conditions. The system behaviour is inconsistent and unpredictable due to the ever changing climate. Variable wind speed, solar irradiation, temperature and humidity makes the energy production from renewable energy-based systems fluctuating. A hybrid system comprised of both solar PV and wind turbines will smooth out the energy production, but the system will still be in need of additional balancing units such as battery banks and hydrogen tanks. These balancing units are especially important in a green ammonia production plant, which is typically considered to be a non-flexible plant in need of continous and even input of both power and mass flow (hydrogen and nitrogen) in order to operate (Haber-Bosch unit and the air separation is the bottleneck for flexible operation).

During system operation, power is generated from the renewables (wind and/or solar) and delivered to the downstream power demanding components. The electrolyzers produces hydrogen through water electrolysis, and the air separation unit extracts nitrogen from the surrounding air. Both elements are compressed in the syngas compressor before they are being fed into the Haber-Bosch unit for production off ammonia, thus ending the (simplified) green ammonia production chain. However, to optimize functionality and utilization of each system component, battery banks and hydrogen buffer tanks have been added to the chain. While the electrolyzers are considered flexible, with the ability to ramp up and down in load at a fast rate, and tolerate frequent start up/shut downs, the Haber-Bosch unit is not, as it must consistently be operated at 100% of its installed capacity. As a result, the battery bank is to function as an additional energy source for the Haber-Bosch unit at times of energy deficiency from the renewables, thus increasing the reliability of the system. Additionally, the hydrogen buffer tank is included to function as a secondary hydrogen provider at times of power deficiency (i.e., at times when the electrolyzers are unable to produce enough hydrogen to cover the Haber-Bosch demand).

3.3 Optimization approach

As stated in the introduction, the main goal of this study is to optimize the production of green ammonia in an off-grid energy system. Specifically, this involves identifying the optimal system configuration, which includes determining the appropriate sizing of each component in terms of installed capacity. The aim is to meet production requirements reliably, ensuring a controlled output with minimal non-production days, all while minimizing costs. To accomplish these objectives, an optimization approach, or a system optimization model, has been developed. Figure 3.2 provides an overview of the various steps involved in this approach. These steps serve as the foundation for the optimization model and establish the framework for the subsequent sections and the entire thesis.

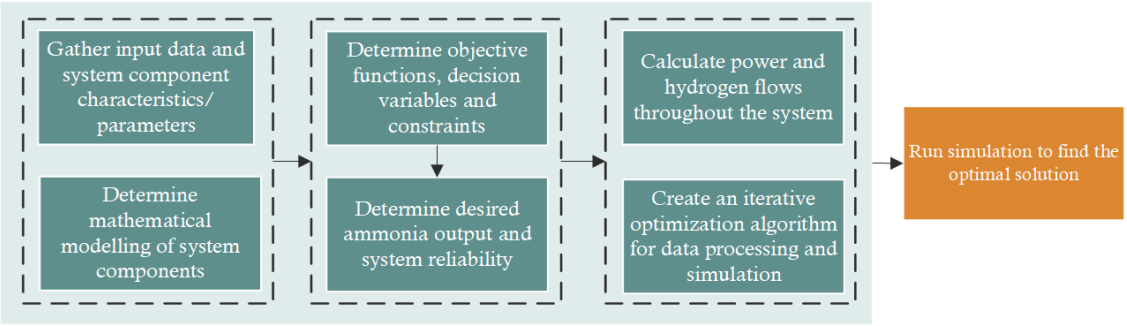

Figure 3.2: Presentation of the design strategy applied for the creation of the simulation framework for the optimization of a green ammonia plant.

The first step of the optimal sizing approach is to gather input data necessary for performing accurate simulations in order to duplicate the functionality and dynamics of a fully functional green ammonia plant. This includes meteorological data of wind speed and solar irradiation, economical data (CAPEX and OPEX), and technical data (specifications and characteristics) of each system component. Additionally, each system component (e.g., PV, wind turbine, battery, hydrogen tank, air separation and Haber-Bosch unit) must be mathematically expressed in order to simulate its functionality and performance during operation. This is done by using mathematical expressions and equations with the purpose of mimicking real-time behaviour.

The second step is to determine objective functions, decision variables and constraints. Objective functions can be thought of as the goal of the optimization, depending on what the desired end result is; whether that will be to minimize cost or maximize system reliability. The decision variables are the variables in the optimization problem in which the decision-maker has control over. These variables allows the optimization model to simulate through a number of possible solutions in the search of the best one. Decision variables can represent the installed capacities of the system components (e.g., the ability to search through a number of different installed capacities of for example PV and wind turbines, in order to find the best combination of the two relative to the desired output). Additionally, a target ammonia output and level of system reliability must be set in order for the simulation to have a starting point to perform the optimization.

By incorporating technical and economical data, developing mathematical modelling of each system component, determining the objective functions, decision variable, and constraints, and setting the desired outputs, the stage is set for the third step to be included. Here, the hydrogen and power flow requirements is calculated, before an optimization algorithm is created to process all data input and to perform the simulation. By using a programming language to run the simulation, an optimal solution is to be found, thus completing the optimization process. All these steps will be discussed in the following sections.

3.3.1 System flexibility

The energy available from the renewables are variable due to the intermittent nature of the wind turbines and solar PVs. Adding batteries and hydrogen tanks will help minimize these fluctuations in energy supply, but there is still necessary to have a certain flexibility in the various system components if the production of green ammonia is to be fully optimized. The electrolyzers, and especially the PEM electrolyzers, allows for flexible load management and has the ability to be ramped up and down at a fast pace at times of energy deficiency - thus being able to function well when paired with renewables. The alkaline electrolyzer is generally less expensive than the PEM, but does not offer the operational flexibility to the same extent, even though some dynamic operation is possible (slower ramp up and ramp down potential as well as less flexible load management).

The bottleneck for the green ammonia production flexibility, however, lies in the ammonia synthesis unit, which in the optimization framework is considered to be the ASU, syngas compressor and H-B lumped together. The air separation unit (pressure swing adsorp-

tion) itself is typically rather flexible and can be operated down to 30% load (slow ramp up dynamics, typically over several hours) (Eric R. Morgan, 2013), whereas the syngas compressor typically have a load range of 55–115% (Bañares et al., 2015). Even though these components allows for some flexibility, the real challenges lies within the ammonia synthesis loop occurring in the Haber-Bosch unit. The environment in which the reactions are taking place within the loop, requires nearly continous feed of the reactive components (hydrogen and nitrogen) as well as electricity input in order not to damage catalysts present in the reactor and lower conversion efficiency (Wang et al., 2023; Eric R. Morgan, 2013). Recent studies show that the ammonia synthesis loop has the ability to operate operate with a turn-down ratio of 40% (i.e., minimum load operation at 60%) as demonstrated by (Armijo and Philibert, 2020), and studies done by (Haldor Topsøe and Alfa Laval, 2020) suggests that an even larger turn-down ratio of 90% is feasible at a design stage. Nevertheless, for the purpose of this paper, a non-flexible Haber-Bosch unit, and therefor also a non-flexible ammonia synthesis unit altogether (combination of H-B, ASU, and syngas compressor) has been chosen for further work. This means that the ammonia synthesis unit will require constant power and hydrogen input in order to operate, or else it must shut down, i.e., full production or no production at all. This lack of flexibility means that the implementation of a battery bank and hydrogen buffer tank is critical if the continous demands for hydrogen and energy is to be met to avoid system shut-down.

3.3.2 Assumptions

In order simulate the operation of the complex green ammonia plant, certain assumptions and simplifications had to be made. Making these necessary adjustments along the production chain, helped facilitate the implementation of the optimization algorithm. The adjustments were as followed:

(1) The electrolyzers has the ability to instantaneously shut down/start up operation, (2) the Haber-Bosch unit, syngas compressor, and air separation unit is lumped together and considered to be one single unit (referred to as the ammonia synthesis unit) Nayak-Luke et al. (2018), (3) even though ammonia synthesis unit requires constant load and continous operation throughout the year, we provide some slack in the form of a predetermined number of days of shut down, later refereed to as total ammonia deficit (TAD), (4) the ammonia synthesis unit can shut down/start up instantaneously, (5) assume constant electrolyzer efficiency through various load ranges, (6) wind turbines, solar PV, electrolyzers, ammonia synthesis unit, batteries and hydrogen tanks are modelled as continuous variables (in real-world project these components typically have a standardized modular unit size), (7) no need for hydrogen compression before the surplus hydrogen is stored in the buffer tanks, as the hydrogen output from the PEM electrolyzers are already compressed to 30 bar, (8) assume fully charged batteries and H2 tank at the beginning of the simulation, and (9) assume no stack replacement is required for the electrolyzers.

3.4 Mathematical modelling of the system components

To accurately depict and optimize the systems behaviour, it is essential to define and incorporate mathematical models of the main components. These models allows us to predict the systems behaviour under various conditions. Four mathematically expressed models is included in the following section, one for each main component; wind turbine, solar PV, battery and hydrogen tank. The electrolyzers and the ammonia synthesis and unit itself is not mathematically modelled, but rather expressed in terms of power and mass flow demands, which will be introduced in a later section.

3.4.1 Wind turbine system model

To accurately calculate the hourly output of a wind turbine, the turbines power curve is typically used (Mokheimer et al., 2015). Each turbine has their own unique power curve based on design parameters. However, a more simplified method to describe a generalized power curve can be implemented when performing computations. Equation 3.1 approximately models the power output of the wind turbine for various wind speeds at a given time t. Where $P_{wt}(t)$ is the wind turbine power output, P_r is the rated wind turbine power (kW), $v(t)$ is the hourly measured wind speed (m/s), v_r is the rated wind speed (m/s), v_{cut-in} is the cut-in wind speed (m/s), and $v_{cut-out}$ is the cut-out wind speed (m/s). Here, v_{cut-in}, refers to the minimum wind speed required in order for the turbine to start rotating, and v_{cut-in} gives the maximum allowable wind speed before conditions goes beyond what the turbine is designed to handle, and the it must shut down. (Das et al., 2021; Nguyen et al., 2021; Smaoui et al., 2015; Shi et al., 2020)

$$P_{wt}(t) = \begin{cases} 0, & \text{if } v(t) \leq v_{cut-in} \text{ or } v(t) \geq v_{cut-out} \\ P_r \left(\frac{v^3(t) - v_{cut-in}^3}{v_r^3 - v_{cut-in}^3} \right), & \text{if } v_{cut-in} < v(t) < v_r \\ P_r, & v_r \leq v(t) < v_{cut-out} \end{cases} \tag{3.1}$$

When calculating wind power output, it's important to convert the hourly wind speed values obtained at measuring point to the hub height. The most commonly used formula is the power law, as expressed by equation 3.2.

$$v(t) = v_{ref}(t) \times \left(\frac{h}{h_{ref}} \right)^{\alpha} \tag{3.2}$$

Here, $v(t)$ is the calculated wind speed at hub height h (m), v_{ref} is the measured wind speed at height h_{ref} (m), and α is the ground surface friction coefficient. For low roughness surfaces and well exposed sites (which is typically locations in which installation of wind turbines is considered feasible), the value of $\alpha = 1/7$ is normally used.

3.4.2 Solar photovoltaic system model

The simplified mathematical model used to determine power generated by the solar PV is based on the physical variables of the PV cell material, the temperature of the solar cell, and the solar irradiation. By using hourly data for solar irradiance and ambient temperature, the model can estimate the hourly power production of the solar PV system. The power output of a PV generator can be computed using equation 3.3. (Samy et al., 2020; Kaabeche et al., 2011; Diaf et al., 2008a; Maleki and Pourfayaz, 2015)

$$P_{pv}(t) = (P_{rated} D_f) \left(\frac{G_t}{G_{ref}} \right) \left(1 + K_T \left(T_{amb}(t) + G_t \left(\frac{\text{NOCT} - 20}{0.8} \right) - T_{ref} \right) \right) \quad (3.3)$$

To compensate for losses caused by various external factors such as difference in temperature and humidity, dust layers on the solar panels etc, a derating factor, D_f, has been introduced. This is set to 0.9, thus minimizing the solar PV output by 10%. The PV modules has been set on an inclined, tilted angle equal to the latitude of the place of simulation. This has proven to be a precise generalization of the optimal placement angle for solar PV over various locations (Samy et al., 2020). The temperature coefficient of efficiency, $K_T = -3.7 \times 10^{-3}$ $(1/^{\circ}C)$ for mono and poly-crystalline Silicon, adjusts the efficiency of the PV based on the temperature (Kord and Rouhani, 2009). T_{amb} is the ambient air temperature of the surroundings, NOCT is the nominal operating temperature, which denotes the PV module surface temperature at standard conditions (with irradiance G = 800 W/m^2, T = 20°C, and wind speed at 1 m/s), P_{pv} is the power output of the PV module (W), P_{rated} is the rated module production (W), G_t is the radiation received (irradiation) on the tilted solar panel (W/m^2), and G_{ref} is the incident radiation (irradiation, combination of direct and diffuse) at standard conditions $(1000W/m^2)$ (Samy et al., 2020; Maleki and Askarzadeh, 2014; Diaf et al., 2008b).

3.4.3 Battery storage system model

The surplus energy produced by the PV and wind turbines can be used to charge the batteries (if the batteries are not fully charged already), whereas the stored energy can be discharged whenever there is a shortage in power generation. The batteries are present to supply energy to the ammonia synthesis unit and air separation unit (not to the electrolyzers) when energy generated from the renewables are not adequate. Subsequently, the discrepancy between total energy generated from the renewables and the energy required by the load, represented by the electrolyzers, air separation unit and ammonia synthesis unit, determines whether the batteries are in a state of charging or discharging. To determine the available capacity of the battery bank at time t, equation 3.4 is used. Here, $C_{bat}(t)$ and $C_{bat}(t-1)$ represents the battery capacity (kWh) at time t and t-1 (i.e., the previous timestamp), respectively, and σ, denotes the self-discharge rate (%) of the battery as provided by the manufacturer. $\eta_{battery}$, also provided by the manufacturer, refers to the battery charging efficiency (%). (Mokheimer et al., 2015; Al-Sharafi et al., 2017; Diaf et al., 2008b; Al-Buraiki and Al-Sharafi, 2022; Diaf et al., 2007; Kaabeche et al., 2011)

$$C_{bat}(t) = C_{bat}(t-1) \times (1-\sigma) + (P_{bat,in}(t) - P_{bat,out}(t))\,\Delta t \times \eta_{battery} \tag{3.4}$$

$P_{bat,in}(t)$ represents the energy put into the battery at a charging state (kWh), whereas $P_{bat,out}(t)$ gives the energy drawn out of the battery during discharge (kWh), for the given time-step Δt, (h). These are input and output values that are determined by the system operation, i.e., the amount of renewables generated, power demands throughout the system from the electrolyzers, air separation unit and ammonia synthesis unit, and the synergies between them - all of which are determined by the strategy for controlling power and hydrogen flows, which is implemented in the optimization algorithm (will be discussed in a section 3.7). (Diaf et al., 2008b)

3.4.4 Hydrogen buffer storage model

Analogously to the battery bank, a hydrogen buffer tank is incorporated to provide additional hydrogen reliability to the system. The hydrogen buffer tank supplies hydrogen to the ammonia synthesis unit at times of production shortage from the electrolyzers, and stores hydrogen at times of production surplus from the electrolyzers. The amount of hydrogen stored in the buffer tank at time t can be expressed by equation 3.5.

$$C_{H_2,tank}(t) = C_{H_2,tank}(t-1) + (m_{H_2,prod}(t) - m_{H_2,cons}(t)) \tag{3.5}$$

Here, $C_{H_2,tank}(t)$ and $C_{H_2,tank}(t-1)$ refers to the hydrogen tanks state of charge, or the amount of hydrogen stored in the buffer tank (t_{H_2}) at time t and t-1, respectively (Nguyen et al., 2021). $m_{H_2,prod}(t)$ is the amount of hydrogen produced hourly from the electrolyzers (t/h), and $m_{H_2,cons}(t)$ is the hourly demand for hydrogen from the system (i.e., hydrogen demanded from the ammonia synthesis unit). (Tebibel, 2021). Accordingly, the amount of hydrogen in the tank at time t, is whatever the amount of hydrogen stored in the tank was at the previous time-step plus the difference in demand/supply at that time.

3.5 Energy consumption and mass flow in a green ammonia system

To perform computations and be able to optimize the green ammonia plant, the energy consumption and mass flow throughout the system must be determined. These flows must be optimized if the system is to function properly. As illustrated in chapter 3.1 the green ammonia plant is an elaborate system consisting of several interconnected components. If one component shuts down due to lack of mass or energy supply, the entire system may shut down. Thus, controlling the flow is an integral part of the system design.

3.5.1 Energy consumption

The total energy demand in the system is the sum of all the energy-demanding components individual consumption; the electrolyzers (for H_2 production), the air separation unit (for N_2 production), and the ammonia synthesis unit (for NH_3 production), which as defined

in chapter 3.3.2, is the combination of H-B and syngas compressor. The estimated energy consumption for the green ammonia plant is listed in table 3.1.

Table 3.1: Energy consumption from the components in the green ammonia plant.

Description	**Energy Consumption** ($kWh/kgNH_3$)	**Fraction** (%)
H_2 **production**	**8.35 - 9.06**[a-c]	**89.1 - 92.5**
N_2 **production**	**0.12 - 0.50**[a,d-f]	**1.3 - 5.1**
NH_3 **production**	**0.53 - 0.64**[a,d,g]	**5.7 - 6.9**
(Syngas compression)	(0.11 - 0.16)	(20.8 - 25.0)
(Haber-Bosch)	(0.42 - 0.51)	(75.0 - 79.2)
Total production	**9.00 - 10.2**	100

[a](Eric R. Morgan, 2013), [b](Taibi et al., 2020), [c](Nel Hydrogen Electrolysers, 2021), [d](Cesaro et al., 2021), [e](Rouwenhorst et al., 2019), [f](Spelorzi, 2022), [g](Salmon and Bañares-Alcántara, 2022), [h](Gallardo et al., 2021)

Here, the energy consumption is expressed in terms of $kWh/kgNH_3$, i.e., energy required per kg of ammonia produced. This is a way of comparing the amount of energy each component draws per kg NH_3, with the electrolyzer consuming around 90% of the total energy for its production of hydrogen, the air separation unit drawing around 4% and the ammonia synthesis loop around 6%.

Electrolyzer power and mass flow

Since the air separation unit and ammonia synthesis loop are combined and treated as a single unit, it is practical to represent the energy requirement per kg of NH_3. Conversely, for electrolyzers, expressing the energy demand in kWh/kgH_2 is more beneficial, as it enables the direct calculation of hydrogen production relative to the energy input, rather than determining the electrolyzers energy demand based on the ammonia plant's output. From chapter 2.4.1, we know that the lower heating value (LHV) of hydrogen is equal to 33.3 kWh/kgH_2. By combining this with the electrolyzer efficiency, η_{elz} (%), and the instantaneous power input, P_{elz} (MW), the hydrogen production, $\dot{m}_{H_2,elz}$ (kgH_2), can be obtained by equation 3.6 (Al-Buraiki and Al-Sharafi, 2022; Tebibel, 2022; Gallardo et al., 2021; Nel Hydrogen Electrolysers, 2021).

$$\dot{m}_{H_2,elz} = \frac{P_{elz}}{\mathrm{LHV}_{\mathrm{H_2}} \times \eta_{\mathrm{elz}}} \tag{3.6}$$

Electrolyzers can operate at variable loads, which means they can adjust their power input based on the current demand for hydrogen. From 2.4.4, we know that the PEM electrolyzer are able to operate under operational ranges of 20-120%, thus allowing for increased operational flexibility as the electrolyzer are able to run under a wide range of energy input from intermittent renewables.

3.5.2 Mass flow

To estimate the mass flow rates for each component in the green ammonia plant, we need to consider the stoichiometric values of the production components, as shown in Table 3.2. By using these values, the mass flow rates of nitrogen, hydrogen, water, and ammonia can be determined at each stage of the process. In order to produce 1 kg of Ammonia, 0.82 kg of Nitrogen and 0.18 kg of Hydrogen is required, with an additional 1.80 kg of water (H_2O) is required through electrolysis.

Table 3.2: Stoichiometric values of production components.

Product	**Symbol**	**Stoichiometric Ratio**
Nitrogen	N_2	0.82
Hydrogen	H_2	0.18
Water	H_2O	1.80
Ammonia	NH_3	1.00

By adjusting these values relative to the desired plant capacity (i.e., output of tonnes of Ammonia per day), one can calculate the required mass flows throughout the system.

3.5.3 Round-trip efficiency

A suitable method for assessing the efficiency of the green ammonia system is by evaluating its round-trip efficiency. This is defined as the ratio of the energy required for production to the energy content of the ammonia that has been produced. By utilizing the round-trip efficiency approach - an assessment of the overall performance of the green ammonia system can be made, and potential areas for improvement can be discovered. Moreover, by comparing the system's efficiency with other energy storage technologies, a better understanding of it's relative performance and the true potential of green ammonia as an energy storage medium can be obtained.

The round-trip efficiency is the ratio of the energy required for production of ammonia - to the ammonia output energy content. This value can be calculated by dividing the total energy stored in the produced ammonia by the total energy input to the system. The round-trip efficiency provides an indication of the system's effectiveness in converting input energy into ammonia.

To calculate the round-trip efficiency, it is first necessary to determine the energy content of the produced ammonia. The specific energy density, or the lower heating value of ammonia is approximately 5.2 kWh/kg (U.S. Department of Energy, 2006; Morgan et al., 2014; Lhuillier et al., 2019). By multiplying the LHV with the mass flow rate of ammonia, the energy content of the ammonia produced can be estimated. The total energy input to the system is obtained by summation of all the power consumed by the components in the green ammonia plant, as illustrated before in table 3.1. The round-trip efficiency

can be calculated from the ratio between input energy from renewables, and the potential output energy from ammonia (measured by the energy stored in the produced ammonia), as shown in equation 3.7. (Morgan et al., 2014)

$$\text{Round} - \text{trip Efficiency} = \frac{\text{Energy Content of Produced Ammonia}}{\text{Total Energy Input to the System}} \times 100 \tag{3.7}$$

3.6 Formulation of the optimization framework

In the following section, the formulation of the optimization framework will be discussed. This can be thought of as the building blocks behind the operation, as shown in figure 3.3. These fundamental criteria helps setting the scene for the optimization algorithm, and provide the necessary input data and guidance required to run the optimization and simulate the green ammonia plant. Each building block will be discussed subsequently.

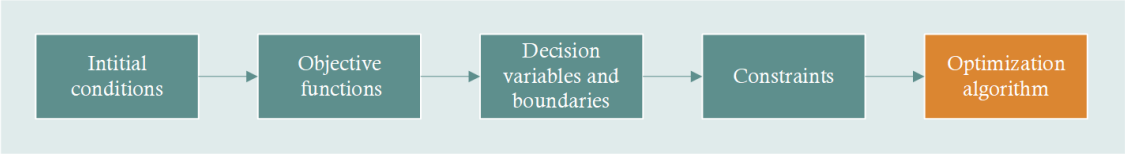

Figure 3.3: Illustration of the fundamental building blocks formulating the optimization framework.

3.6.1 Initial conditions

The initial condition functions as a starting point in which all system sizing is determined by. For the purpose of this project, a desired output rate of 1500 tonnes of ammonia per day (tpd) is set as the initial condition. This allows the rest of the optimization to be modelled and optimized with purpose of achieving the desired output.

3.6.2 Decision variables and boundaries

In order to achieve the desired production of tonnes of ammonia per day, the system components must be scaled properly; meaning that the wind turbine, solar PV, electrolyzer, battery bank, and hydrogen tank all must be sized to the correct installed capacity to be able to delivered the desired output. The reason behind this optimization in the first place, is that we do not yet know what this "correct installed capacity", or the optimum system configuration really is, which is why the system components must act as decision variables with the ability to adjust the installed capacity up and down to find the proper sizing of the system.

The decision variables effectively makes up the search area of the optimization algorithm. In order to decrease simulation time, and shrink down the search area (decrease number of

iterations necessary to locate the optimized system configuration), component boundaries are introduced. By deciding a minimum and maximum installed capacity of each system component, we limit the search to relevant areas, and disregard areas that are considered out of bounds. These upper and lower bounds are expressed as follows (Samy et al., 2020; Bukar and Tan, 2019):

$$N_{WT,min} \leq N_{WT} \leq N_{WT,max} \tag{3.8}$$

$$N_{PV,min} \leq N_{PV} \leq N_{PV,max} \tag{3.9}$$

$$N_{elz,min} \leq N_{elz} \leq N_{elz,max} \tag{3.10}$$

$$N_{bat,min} \leq N_{bat} \leq N_{bat,max} \tag{3.11}$$

$$N_{H_2tank,min} \leq N_{H_2tank} \leq N_{H_2tank,max} \tag{3.12}$$

Even though the components are typically modular, and comes in pre-determined unit sizes (e.g., PEM electrolyzers delivered as 20 MW units (Nel Hydrogen Electrolysers, 2021), or solar PV as a 635 W module (HUASUN, 2022)), the components are for the purpose of this project considered to be continuous variables, with the ability to adjust up and down in size on demand. Thus, N, represents the components' installed capacity (kW, kWh or kgH_2), while the sub-scripted abbreviations represents the component considered (WT = wind turbine, PV = solar PV, elz = electrolyzers, bat = battery, and H_2tank = hydrogen tank).

3.6.3 Objective function

Any optimization method needs an objective function. This a mathematical expression that represents the main goal of the optimization. Typically, this would be minimize or maximize some environmental, technical or economical aspect (Bukar and Tan, 2019). The objective function for this work is to minimize the levelized cost of ammonia (LCOA).

$$\text{Objective function} : \text{min. LCOA}(N_{WT}, N_{PV}, N_{elz}, N_{bat}, N_{H_2tank}) \tag{3.13}$$

The LCOA represents the cost per unit of ammonia produced, and is expressed in USD per tonne of ammonia (USD/tN_{H3}). It takes into account the capital and operational expenditure of all system components over the course of the system's lifetime as well as the total produced ammonia over the same time-period, and is a function of the installed capacities of all system components. By minimizing the LCOA, the optimization algorithm aims to find the most cost-effective system configuration, thus establishing the purpose of the thesis. (Akhavan Shams and Ahmadi, 2021)

Determining system cost analysis

To calculate the levelized cost of ammonia (LCOA) for the optimized, hybrid plant, the net present value of the capital costs (CAPEX) and operations and maintenance costs (OPEX) over the lifetime of the system is summed and then divided by the total ammonia production (Osman et al., 2020), as shown by:

$$\text{LCOA} = \frac{\textit{cost of production over lifetime}}{\textit{mass of ammonia produced over lifetime}} \tag{3.14}$$

$$\text{LCOA} = \frac{\text{NPC} \times \text{CRF}}{\sum_{t=1}^{T} \dot{m}_{NH_3}(t)} \tag{3.15}$$

where the terms net present cost (NPC), and capital recovery factor (CRF), refer to the sum of the current value of all system components' actual cost and the capital recovery factor, respectively (Al-Sharafi et al., 2017). These are represented mathematically as:

$$\text{CRF} = \frac{i(1+i)^n}{(1+i)^n - 1} \tag{3.16}$$

$$\text{NPC} = \text{CAPEX} + \sum_{t=1}^{T} \text{OPEX(t)} \tag{3.17}$$

here, i, is the real interest rate and n is the project lifetime in years. By using the total net present cost (NPC) concept, the cost of the system can be calculated. The NPC takes into consideration the initial capital cost of the system (CAPEX) as well as the annual operational and maintenance cost (OPEX) evaluated throughout the lifetime of the project, starting from t=1 year to the end of the lifetime, T. (Al-Buraiki and Al-Sharafi, 2022; Abdin and Mérida, 2019; Osman et al., 2020).

3.6.4 Constraints

The hybrid energy system is at all times subject to a number of constraints. These constraints allow the system modelling to stay within the boundaries of the system components, thus allowing for realistic simulations based of off real life scenarios. These constraints must at all times be satisfied if the green ammonia plant is to operate. Both reliability constraints and component constraint is considered, and presented in the following part.

Reliability constraint: total ammonia deficit (TAD)

Because the wind energy and solar PV is of an intermittent nature, there is no guarantee for constant energy supply in a green ammonia plant solely reliant upon these off-grid energy sources. For this reason, a reliability measure must be introduced to the system, which for the purpose of this thesis was chosen to be total ammonia deficiency (TAD). This parameter represents the total ammonia demand unmet by the ammonia supply during a specified period, and is calculated on an hourly basis. (Tebibel, 2021)

$$\text{TAD} = \frac{\sum_{n=1}^{T} (\text{m}_{\text{a,d}} - \text{m}_{\text{a,s}})}{\sum_{n=1}^{T} \text{m}_{\text{a,d}}} \tag{3.18}$$

where $m_{a,s}$ is the amount of ammonia supplied (i.e., ammonia produced by the green ammonia plant) to the demand $m_{a,d}$ (i.e., the pre-determined ammonia production re-

quirements). TAD is given as a decimal point from 0-1, with 1 representing 100% deficit, i.e., complete system shutdown. As has been explained in the chapter 3.3.1, the ammonia synthesis must be operated at rated capacity or shut down. Meaning, that for the purpose of this thesis, TAD is either equal to 0 - meaning the ammonia synthesis unit is producing ammonia at rated capacity, or equal to 1 - meaning the ammonia synthesis unit is shut down. TAD is calculated on an hourly basis, where TAD = 1 simply means that the system is completely shut down at this hour, and a TAD = 0 at hour t, means that the system is in operation.

Battery constraint

The amount of charge in the battery bank at any given time t is governed by the following two constraints Maleki and Askarzadeh (2014); Osman et al. (2020); Tebibel (2022):

$$C_{bat,min} \leq C_{bat}(t) \leq C_{bat,max} \tag{3.19}$$

With the maximum capacity at any time t, $C_{bat,max}$, is given by the rated, or nominal capacity of the battery, $C_{bat,rated}$:

$$C_{bat,max} = C_{bat,rated} \tag{3.20}$$

And the minimum capacity of the battery at any time t, $C_{bat,min}$, is given by the depth of discharge, DOD (%), which represents maximum allowable depth of discharge of the battery, determined by the battery manufacturer Akhavan Shams and Ahmadi (2021); Maleki and Pourfayaz (2015):

$$C_{bat,min} = \text{DOD} \times C_{bat,rated} \tag{3.21}$$

Hydrogen buffer tank constraint

Similarly to the battery bank, the hydrogen buffer tank is also subject to constraints. The H_2 tank must at all times be at a state of storage determined by equation 3.22.

$$C_{H_2,tank,min} \leq C_{H_2,tank}(t) \leq C_{H_2,tank,max} \tag{3.22}$$

Here, the minimum and maximum capacity simply refers to an empty (no ammonia stored in the tank) and a full buffer tank (completely filled up with ammonia, i.e., at rated storage capacity).

Electrolyzers constraint

As previously stated (ref chapter 2.4.2), the electrolyzers typically have an operational window that allows them to operate at variable power input. This can be expressed by equation 3.23 Tebibel (2022).

$$P_{elz,min} \leq P_{elz}(t) \leq P_{elz,max} \tag{3.23}$$

Depending on the electrolyzers technology, this can typically range from 20% - 120% of nominal power Tebibel (2022); Nel Hydrogen Electrolysers (2021); Eric R. Morgan (2013). So, the operational window in which the electrolyzer is powered, and in production of hydrogen, is governed by the range set by the minimum input, $P_{elz,min}$, and the maximum allowable input, $P_{elz,max}$.

3.7 Strategy for controlling power and hydrogen flows

In order to effectively operate and control the hybrid off-grid energy system for production of green ammonia, it is important to incorporate a strategy for controlling power and hydrogen flows (SCPH) that is able to deal with allocating and controlling mass and energy flows of the system at all times. As the energy generated from the renewables are of an intermittent and uncontrollable nature, the strategy for controlling power and hydrogen flows must be able to deal with these fluctuations in order to correctly and efficiently supply the downstream system components.

Considering that the electrolyzers is able to operate at a variable load (20-120%), that the ammonia synthesis unit must be continuously operated at full capacity, and that the battery bank and hydrogen buffer tanks are installed to help support power and hydrogen flow at times of either excess power or at power deficit - one can understand that there is a certain complexity to the system that must be handled in order to fully optimize functionality and utilization of all system components. The SCPH provides a description of the hybrid off grid energy system's behavior at every hour over one year, as well as providing a recipe of its response to different levels of available power, battery charge, and hydrogen tank capacity.

The design of the strategy for controlling power and hydrogen flows in this study is modelled to satisfy the constraints of the system (i.e., the electrolyzer and ammonia synthesis load ranges, the battery bank and hydrogen tank states of charge) relative to the decision variables (i.e., the energy generated by the renewables, and the desired system output of daily ammonia production). As a result of the variable energy generation of the system, four different cases are assessed within the SCPH in order to cover all possible operational scenarios. The ammonia synthesis unit requires continous and steady energy supply at all times. This forms the foundation of the SCPH, and the energy available for the rest of the system components is determined by the ammonia synthesis' energy requirements. $P_{tot}(t)$ denotes the power available after the continuously running ammonia synthesis unit has claimed its share (i.e., energy available for electrolysis or battery charging), as shown in the equation below. This, and all other relevant arrays used in the simulation is shown in shown in the list of symbols.

$$P_{tot}(t) = P_{re}(t) - P_{asu}(t) \tag{3.24}$$

The four different cases evaluated in the SCPH is; (i) case 1; when there is not enough power to fully power the ammonia synthesis unit (nor the electrolyzer), (ii) case 2; when there is enough excess power for hydrogen production by the electrolyzer, but enough to fully power the ammonia synthesis unit, (iii) case 3; when there is enough power to operate

the the ammonia synthesis unit (H-B and ASU) and also to run the electrolyzers (not at full load), but not enough to charge the battery, and (iv) case 4; when there is surplus power that exceeds the electrolyzer and ammonia synthesis unit (H-B and ASU) demands, and the batteries may be charged (if not already fully charged). The SCPH strategy is evaluated at an hourly interval over one full year of operation.

Case 1: *When $P_{tot}(t) < 0$; (there is no available power for hydrogen production nor ammonia synthesis, the battery bank and hydrogen tank must address the deficits).*

(a) Calculate power and hydrogen deficits ($P_{def}(t)$ and $m_{H_2,def}(t)$).

(b) Check if the battery bank and hydrogen tank have enough charge to supply and cover the deficit (($C_{bat}(t-1) \geq P_{def}(t) \times dt$) and ($C_{H_2tank}(t-1) \geq m_{H_2,def}(t) \times dt$)):

(i) If yes, the battery supplies power to the ammonia synthesis unit (H-B + ASU) to cover the renewable deficit, and the hydrogen tank supplies hydrogen for ammonia synthesis.

(ii) If no, the system shuts down as there isn't enough battery charge and/or hydrogen in the tank to support demands of the ammonia synthesis unit (H-B and ASU).

(d) Calculate TAD for the current hour (ratio of ammonia not supplied to meet the demand - to the total demand).

(e) Update the state of charge for the battery and hydrogen tank based on the current inputs and outputs.

Case 2: *When $0 \leq P_{tot}(t) < P_{elz,min}$; (Not enough excess power, $P_{tot}(t)$, for hydrogen production, but enough to fully power ammonia synthesis unit (H-B and ASU), and to charge the batteries (i.e., the provided hydrogen must be supplied from the H_2 tanks or the system must shut down. The excess power (whats left after the ammonia synthesis unit has claimed its share) will charge the batteries as long as they are not at max capacity. Any remaining excess power will be curtailed)).*

(a) Calculate the power available for the battery to charge and the hydrogen deficit ($P_{avail}(t)$ and $m_{H_2,def}(t)$).

(b) Check if the hydrogen tank has enough capacity to cover the deficit ($C_{H_2tank(t-1)} \geq m_{H_2,def}(t) \times dt$):

(i) If yes, the hydrogen tank supplies the ammonia demand, and excess power is used to charge the batteries. Calculate energy curtailment if any.

(ii) If no, the system shuts down due to insufficient hydrogen tank capacity.

(d) Calculate TAD for the current hour (ratio of ammonia not supplied to meet the demand to the total demand).

(e) Update the state of charge for the battery and hydrogen tank based on the current inputs and outputs.

Case 3: *When $P_{elz,min} \leq P_{tot}(t) \leq P_{elz,max}$; (Enough power available to fully power the ammonia synthesis unit (H-B and ASU) and enough power for the electrolyzers to be operated within their operational range for production of hydrogen, but not any excess power left to charge the batteries, i.e., all excess power, $P_{tot}(t)$ is allocated to the electrolyzers. Should the electrolyzer produce more hydrogen than is demanded by the ammonia synthesis unit (H-B and ASU), and more than the there is space for in the hydrogen tanks, the electrolyzer production will be adjusted (to produce just enough to meet demands), and surplus power will be curtailed).*

(a) Calculate the power available for the battery to charge and the hydrogen deficit ($P_{avail}(t)$ and $m_{H_2,def}(t)$).

(b) Calculate the available space in the H_2 tank ($m_{H_2tank,avail}(t)$).

(c) Evaluate the following scenarios to determine system behavior:

(i) If the electrolyzer produces less hydrogen than required for the ammonia synthesis unit (H-B and ASU), but the H_2 tank has enough hydrogen stored to cover the deficit, then the electrolyzers and H_2 tank combine to fully supply hydrogen to the ammonia synthesis unit (H-B and ASU).

(ii) If the electrolyzers produces less hydrogen than required for the ammonia synthesis unit (H-B and ASU) and the H_2 tank doesn't have enough H_2 stored to cover the deficit, then the system shuts down due to insufficient hydrogen supply.

(iii) If the hydrogen produced from the electrolyzers exactly meets the hydrogen demand from the ammonia synthesis unit (H-B and ASU), then the demand is supplied entirely by the electrolyzers. No need for hydrogen supply from the H_2 tank.

(iv) If the hydrogen production from the electrolyzers exceeds the hourly demand from the ammonia synthesis unit (H-B and ASU) and the H_2 tanks has available space, store the excess hydrogen production in the H_2 tanks. If the hydrogen tank is full and the ammonia synthesis unit (H-B and ASU) is fully supplied, regulate the electrolyzers to avoid producing excess hydrogen and instead curtail the surplus energy.

(d) Calculate TAD for the current hour (ratio of ammonia not supplied to meet the demand to the total demand).

(e) Update the state of charge for the battery and hydrogen tank based on the current inputs and outputs.

Case 4: *When $P_{tot}(t) \geq P_{elz,max}$; (There is surplus power available that exceeds both the electrolyzer and ammonia synthesis unit (H-B and ASU) demands, thus allowing the batteries to charge if needed. If the batteries are fully charged, any excess power will be curtailed. Should the H_2 production from the electrolyzers surpass the demand from ammonia synthesis unit (H-B and ASU), the H_2 tanks will be filled. If the H_2 tanks are at maximum capacity, the electrolyzer production will be adjusted to only produce H_2 to cover ammonia synthesis unit (H-B and ASU) demand, and the surplus energy will be curtailed).*

(a) Calculate the power available for the battery to charge and the hydrogen deficit ($P_{avail}(t)$ and $m_{H_2,def}(t)$).

(b) Calculate the available space in the H_2 tank ($m_{H_2tank,avail}(t)$).

(c) Evaluate all the same scenarios ((i), (ii), (iii), and (iv)) found in case 3 to determine system behavior.

(d) Calculate TAD for the current hour (ratio of ammonia not supplied to meet the demand to the total demand).

(e) Update the state of charge for the battery and hydrogen tank based on the current inputs and outputs.

3.8 Implementation of the optimal design sizing algorithm

Everything that has been methodically explained in the previous subsections, can be thought of as building blocks leading up to the actual simulation of the working system, and the optimization procedure itself. In this section, all the fundamental parts of system modelling previously discussed is combined with the strategy for controlling power and hydrogen flows for the implementation of the optimal sizing algorithm with the aim of obtaining a functional simulation of the green ammonia plant. The implementation of the optimal sizing algorithm can be explained by three steps (A, B, and C), and is discussed below. Steps A and B can can be thought of as one large block of input parameters that is pushed through to the simulation environment for optimization, as illustrated in Figure 3.4. The algorithm is an iterative optimization script that is implemented in a programming language (python) to run the simulation of the green ammonia plant. The python code used for calculating the hourly energy output from a 1 kW wind-turbine and solar PV is found in Appendix D. These values are scaled up to the desired installed capacities (which are adjustable variables in the optimization code) as they form the foundation of the optimization framework. The iterative optimization code used for finding the point of optimum is given in Appendix E.

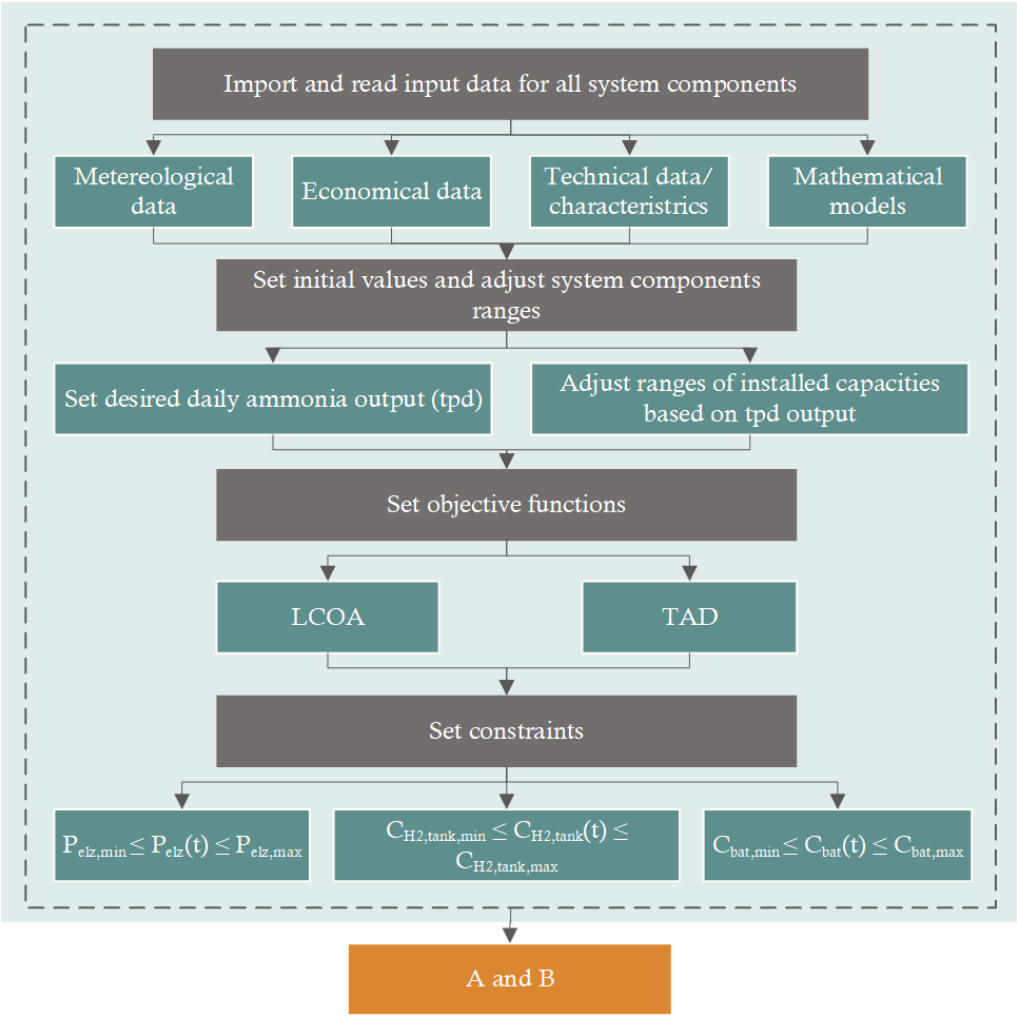

Figure 3.4: Key input parameters that are fundamental to the optimization algorithm.

Step A: read input data

In step A, all building blocks that has been thoroughly discussed in the previous chapter is read, and implemented into the script. That includes (i) meteorological data; hourly wind speed, solar irradiation, and temperature for one year, (ii) economical data; CAPEX and OPEX values for each system component, (iii) technical data; parameters and and describing features for all system components, and (iv) mathematical models; equations that mathematically describes each system components real-world behaviour.

Step B: define initial values, decision variables, and constraints

In Step B, similar to Step A, the fundamental properties described in previous sections are implemented into the script. This involves (i) setting the initial value of desired daily ammonia production (tpd), (ii) identifying the decision variables, which include the installed capacities of wind turbines, PV modules, electrolyzers, battery banks, and hydrogen buffer tanks, (iii) determining and adjusting the bounds of the decision variables to a range that allows limiting the search area while ensuring the optimal solution is within reach, (iv) defining the objective function as the minimization of LCOA, and (v) establishing system constraints to ensure the various system components operate within their respective limits at all times.

Step C: run the optimization simulation

The final step, where the simulation takes place, can be broken down into several smaller, interconnected steps, where each of them are shown in Figure 3.5. First, the search is defined, and the iterative script starts to loop through possible system configurations (i.e., installed capacities of the various system components), with the search area limited by the boundaries set in Step B. Next, the total energy generation is calculated using the mathematical models of wind turbines and PV modules, along with the hourly meteorological data input. The system is then simulated, with its behavior controlled by the strategy for controlling power and hydrogen flows.

For each system configuration, the reliability is evaluated. If the current configuration under simulation is able to stay within the reliability measure (i.e., the TAD threshold), it is saved for further evaluation; otherwise, it is discarded. For all saved configurations, the LCOA is calculated. This process is repeated until all possible system configurations is explored through the iterative loop. Once the loop is completed, the system configuration that achieves the lowest LCOA is considered the point of optimum, thus concluding the simulation and providing the output of the optimized green ammonia plant.

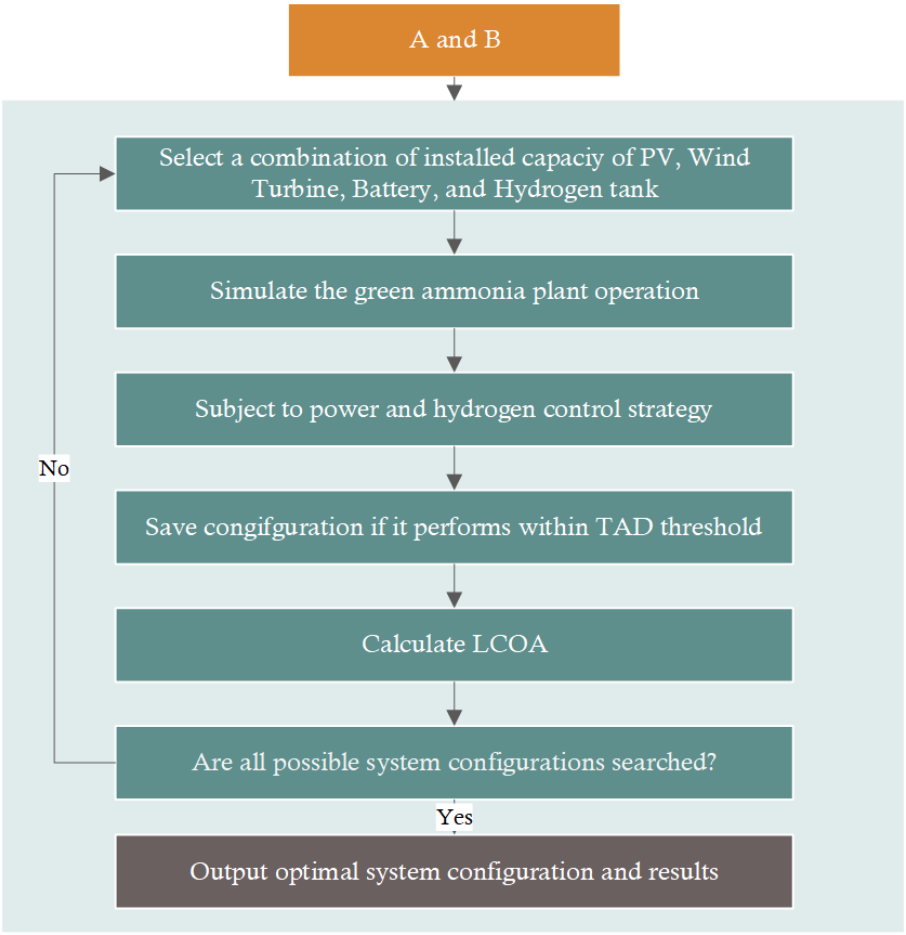

Figure 3.5: Implementation of the optimization framework and simulation of the green ammonia plant.

4 Case study

This chapter will go through the case studied in the thesis. The potential locations that has been investigated for deployment of a green ammonia plant is introduced, along with relevant input data, technical parameters, and additional information required to run the simulation.

4.1 Location

The optimization of the green ammonia plant has been performed at different locations with the purpose of investigating how various renewable resources affects the cost and viability of production. Three various locations have been investigated; one with high solar irradiation, one with high wind speed resources, and one hybrid case where both wind and solar resources are abundant. These locations will have a solar-based (only solar PV installation), wind-based (only wind turbine installation), and a hybrid solution (solar PV and wind turbine installation), respectively, when performing the simulations.

Solar-based system

North Africa has abundant solar resources. IRENA and AfDB suggests that the area has a potential installable capacity of 2,792 gigawatts of solar power - enough to generate more than twice of Europe's 2021 energy output, with Morocco being one of the most prominent countries in terms of solar potential and employment (Alami, 2021). The country is investing 5.2 billion USD in solar energy, and wants 80% of its electricity to come from renewables within 2050 (Anouar, 2022), twice the amount of today. Additionally, there is currently an underwater electric cable spanning 16 kilometers connecting morocco to Spain with potential to supply renewable energy to Spain, Portugal, the UK etc (Birnbaum, 2023; Anouar, 2022).

All these factors put together makes Morocco an interesting prospect and location for investigating the possible production of green ammonia. More specifically, the city Tan-Tan (28.4278°N, 11.1020°W) has been chosen for simulation. Here, the simulation will run a system based purely on solar PV, i.e., no wind turbines will be installed - thus making it a solar-based system.

Wind-based system

For the wind-based system, Utsira in Norway (59.3102°N, 4.8815°E), has been chosen for simulation. Currently, a 1.2 MW onshore wind farm is installed at Utsira, with plans of increasing it to 1.5 GW by 2030 (Energidepartementet, 2023). With high wind resources and a capacity factor above 50%, Utsira is considered a suitable choice for simulation of a green ammonia plant (NVE, 2023). As a result, this area will serve as the base location and technology (onshore wind) for calculations. Additionally, the Norwegian government has identified areas along the Norwegian cost with a combined potential of 30 GW of off-shore wind turbines. These sites are currently being allocated to market participants, with the purpose of having installations completed within 2040, thus demonstrates Norway's commitment and potential in wind-renewable energy for the future (Energidepartementet,

2022).

Hybrid wind- and solar based system

For the hybrid wind- and solar based system, a location with abundant wind speed resources as well as high solar irradiation was needed. Patagonia in the Santa Cruz Province in Argentina (44.9901 °S, 70.6734 °W), was after consideration chosen as location for the hybrid simulation. Argentina as a country has high potential as a future power-to-X contributor, given the countries abundant solar and wind resources, land availability, and access to freshwater (Elisabeth Kriegsmann, 2021).

There are especially high amounts of wind resources in Patagonia (covering a significant part of the country spanning from the south to mid-west), while the north and west of Argentina receives high solar irradiation (Germán Bersalli and Natalia Realpe Carrillo, 2021). The estimated potential for installed wind capacity is around 300 GW, with 2.62 GW already installed in 2021 (Elisabeth Kriegsmann, 2021; Erico Spinadel, 2021).

However, one of the main issues with developing and expanding the renewable production in Argentina is grid connectivity and grid capacity. The transmission lines are already at point of saturation, and the areas of potential power generation are typically situated far from rural areas, and are completely off-grid (Germán Bersalli and Natalia Realpe Carrillo, 2021). As a result, off-grid utilization such as production of green hydrogen or green ammonia sails up as an interesting option - making the location an even more interesting site for simulation of the green ammonia plant.

4.2 Production and mass flow

In each simulation scenario (Wind-based, PV-based, and Hybrid), the baseline ammonia production is set to *1500 tonnes per day*. From the stoichiometric relationships between the mass flow components involved in production of green ammonia (see section 3.5.2), the mass flow required to operate a 1500 tpd green ammonia plant is given in Table 4.1. To meet these mass flow production requirements, the system components must be appropriately sized, thus setting the scene for system optimization.

Table 4.1: Production and mass flow requirements.

Technology	**Product**	**Amount (tonnes/day)**	**Amount (tonnes/hour)**
Air separation	N_2	1,234	51.4
Water supply	H_2O	2,666*	111*
Electrolyzer	H_2	266	11.1
Ammonia output	NH_3	1,500	62.5

* Water supply expressed in liters/day and liters/hour.

4.3 Reliability

In terms of the reliability measurement, the total ammonia deficit (TAD) is set to *120 hours, or 5 days*. This means that during 1 year of operation (8760 hours), the ammonia synthesis unit is allowed to be shut down for 120 hours. This allows the system components (battery bank and hydrogen buffer tank in particular) not to be oversized in order to supply the necessary power and hydrogen flows at times when there are particularly small resources available. In other words, this prevents excess investments in components that would only provide input during extreme hours, when energy generation is low, and battery banks and hydrogen tanks are depleted.

4.4 Meteorological data

For each of the locations selected for optimization, hourly weather data over 1 year has been extracted from the open-source interactive web-page, Renewables Ninja, created by (Pfenninger and Staffell, 2022). Renewables Ninja primarily utilizes data based off the MERRA (Rienecker et al., 2011) and SARAH datasets (Müller et al., 2015). MERRA, provided by NASA, supplies the required hourly wind-speed data, whereas SARAH provides irradiation and temperature data.

Daily mean irradiation for the solar-based location

For the solar based location, the daily mean irradiation is depicted in Figure 4.1. The average hourly irradiation is 0.27 kW/m^2, or 2356 kWh/m^2 per year.

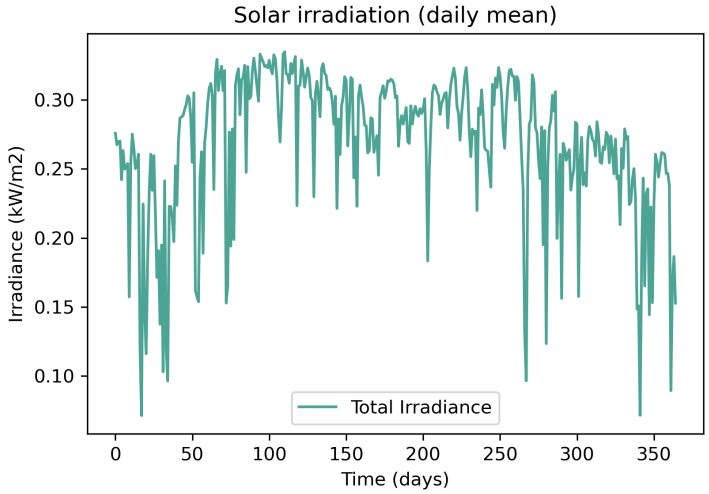

Figure 4.1: Daily mean solar irradiation in Tan-Tan, Morocco.

Daily mean wind speed for the wind-based location

The daily mean wind speeds over 1 year, at Utsira is illustrated in Figure 4.2. The average hourly wind speed is 8.64 m/s.

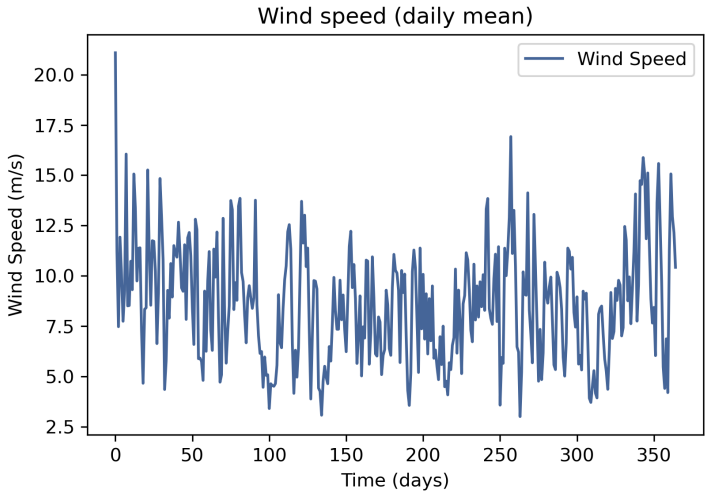

Figure 4.2: Daily mean wind speed Utsira, Norway.

Daily mean wind speed and irradiation for the hybrid location

The daily mean wind speed and solar irradiation is presented for Patagonia in Figure 4.4 and Figure 4.3, respectively. The average hourly wind speed is 9.8 m/s and the average hourly irradiation is 0.23 kW/m^2, or around 2000 kWh/m^2 per year.

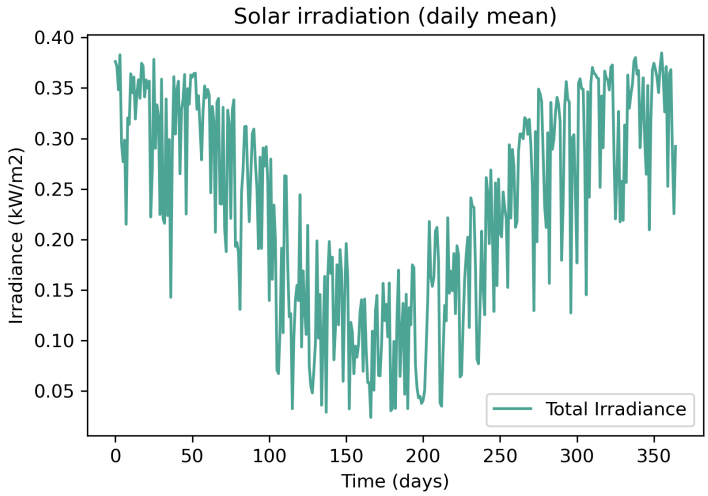

Figure 4.3: Daily mean solar irradiation in Patagonia, Argentina (Santa Cruz Province).

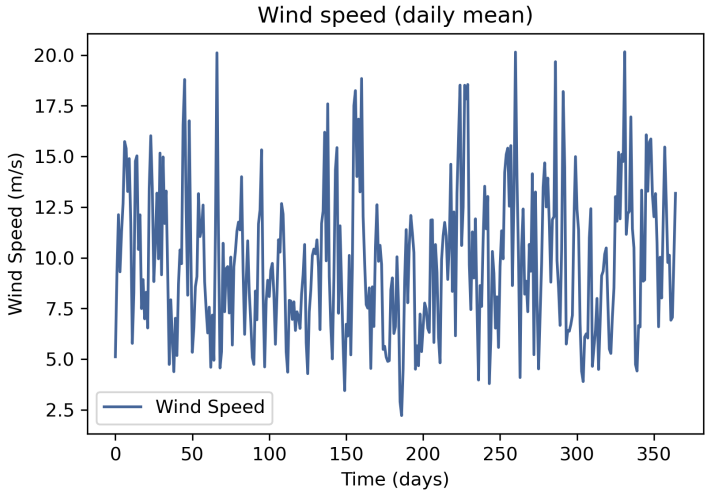

Figure 4.4: Daily mean wind speed in Patagonia, Argentina (Santa Cruz Province).

4.5 Input parameters

In order to simulate and optimize the operation and cost of the green ammonia plant, input parameters are required. Both technical parameters that are determining the system component characteristics, as well as economical parameters that determines the cost of the components.

4.5.1 Technical characteristics

The technical characteristics of each component in the green ammonia plant are listed in Table 4.2. These are input values that are needed for the mathematical modelling, and are key figures in the simulation process. The values are gathered from various sources, and averaged for implementation into this work.

Table 4.2: Parameters for the components in the green ammonia plant.

Component	**Value**	**Units**
Solar PV[1,10]		
Nominal operating cell temperature (NOCT)	44	°C
Reference temperature	25	°C
Module efficiency at standard conditions	22.3	%
Land use	25	m^2/kW
Wind turbine[5,7,10]		
Cut-in wind speed	3	m/s
Rated wind speed	11	m/s
Cut-out wind speed	25	m/s
Hub height	105	m
Land use	181	m^2/kW
PEM electrolyzer[2,3,4]		
System efficiency (LHV)	68	%
Electrical efficiency (LHV)	49	kWh/kgH_2
Operational range	20-115	%
Land use	0.027	m^2/kW
Battery bank[7,8,9]		
Depth of discharge (DOD)	80	%
Self discharge rate	0.005	%
Battery charging/discharging efficiency	99	%

[1](HUASUN, 2022), [2](Taibi et al., 2020), [3](Al-Buraiki and Al-Sharafi, 2022), [4](Nel Hydrogen Electrolysers, 2021), [5](Vestas, 2023), [7](Fasihi et al., 2021), [8](Osman et al., 2020), [9](Cesaro et al., 2021), [10](NREL, 2016),

4.5.2 Economic data

The economical data, representing the specific CAPEX and OPEX values of each system component is given in Table 4.3. The values are averages based on a number of different sources, all referenced in the Table. For calculation of LCOA, the interest rate was set at 7.5%, and the project lifetime estimated to be 30 years.

Table 4.3: Energy consumption from the components in the green ammonia plant.

Component	**CAPEX(USD/kW)**	**OPEX(% of CAPEX)**
Solar PV[1,4,5]	475	2
Wind turbine[4-7]	1150	2
PEM electrolyzer[3,9]	610	3
Battery bank[2,4,8]	250*	1
Hydrogen tank[1,3,6]	400**	0
Ammonia synthesis unit[1-4]	2837	5
Air separation unit[1-4]	3490	2

* CAPEX units for Battery bank are USD/kWh. ** CAPEX units for Hydrogen tank are USD/kgH_2. [1](Eric R. Morgan, 2013), [2](Ikäheimo et al., 2018), [3](Gallardo et al., 2021), [4](Cesaro et al., 2021), [5](Fasihi et al., 2021), [6](Arnaiz del Pozo and Cloete, 2022), [7](IRENA, 2021a), [8](Kaabeche et al., 2011), [9](Taibi et al., 2020), [10](TRACTEBEL ENGIE and HINICIO, 2017), [11](Armijo and Philibert, 2020), [12](Tebibel, 2021), [13](Salmon and Bañares-Alcántara, 2022),

5 Results

The following section presents the key findings from the optimization of the green ammonia plant. Results from simulation at the three different locations specified in the case study (see chapter 4.1) are presented in table format for easy side-by-side comparison. Additionally, plots illustrating the levelized cost of ammonia (LCOA) is given. These plots shows the contributing cost factors, the overall cost, as well as a means to compare the system costs for the different scenarios. Lastly, plots showing the system behaviours through one year of production at the various locations are given. These graphs depict energy distribution and mass flow within the system, offering a visual understanding of the dynamics and synergies at play.

5.1 System sizing and energy distribution

This subsection presents the optimal system sizing and energy distribution for the green ammonia plant, obtained as outputs from the iterative simulation. Table 5.1 givens an overview of the results and a comparison of the "Solar", "Wind", and "Hybrid" scenarios. These labels correspond to the respective locations and system configurations considered in the study.

Table 5.1: Case specific system sizing and energy distribution.

Description	**Technology**	**Value (Unit)**		
		Solar	**Wind**	**Hybrid**
Installed Capacity	Solar PV (GW)	3.25	-	0.39
	Wind Turbine (GW)	-	1.47	1.13
	Electrolyzer (GW)	1.44	0.84	0.76
	Battery Bank (GWh)	1.34	0.38	0.38
	Hydrogen Tank (kt_{H2})	0.34	1.87	1.07
	Air Separation Unit (MW)	6.1	6.1	6.1
	Ammonia Synthesis Unit (MW)	47.5	47.5	47.5
Energy Produced	Solar PV (TWh)	6.37	-	0.67
	Wind Turbine (TWh)	-	6.66	5.89
	Total (TWh)	6.37	6.66	6.56
Energy Consumed	Ammonia Synthesis Unit (TWh)	0.40	0.40	0.40
	Air Separation Unit (TWh)	0.06	0.06	0.06
	Electrolyzer (TWh)	4.70	4.70	4.70
	Total (TWh)	5.16	5.16	5.16
Energy Curtailed	**Total (TWh)**	1.21	1.46	1.38

The table presents the installed capacities of each system component as well as the energy produced, energy consumed and energy curtailed through one year of operation for the solar PV, wind, and hybrid scenarios. For the solar PV-based green ammonia system, located at a place of high insolation (Tan-Tan, Morocco), all the produced energy comes from an installed capacity of 3.25 GW solar PV, supported by an electrolyzer capacity of 1.44 GW for hydrogen production, as well as a battery bank size of 1.34 GWh for energy storage and a hydrogen tank of 0.34 $ktNH_3$ for hydrogen storage. The wind scenario, in contrast has its energy entirely supplied by 1.47 GW wind turbines, with an electrolyzer capacity of 0.84 GW, a smaller battery bank of 0.38 GWh and a larger hydrogen tank of 1.87 $ktNH_3$. The hybrid scenario combines the strengths of both solar and wind energy. It has a lower installed capacity for both solar PV (0.39 GW) and wind turbines (1.13 GW) but maintains a similar electrolyzer capacity (0.76 GW) and battery bank size (0.38 GWh) when compared to the wind scenario. The hybrid scenario also has medium large hydrogen tank of 1.07 $ktNH_3$ (sized between that of the wind-based and solar-based scenarios).

In total, the energy produced is similar for all three scenarios ranging from 6.37 TWh to 6.66 TWh. This is due to the system's production target being set at a constant 1500 tonnes per day (tpd) of ammonia, as outlined in section 4.2. Consequently, the energy consumption for all scenarios is the same. The ammonia synthesis unit, air separation unit, and electrolyzers requires 0.40, 0.06, and 4.70 TWh of energy, respectively, in order to satisfy the mass flow requirements set by a 1500 tpd green ammonia plant.

The energy curtailment is 1.21, 1.46 and 1.38 TWh for the solar-based, wind-based and hybrid scenario. This corresponds to an energy curtailment of 19%, 22%, and 21% relative to total energy produced, respectively.

5.2 System economics

The system economics for each scenario (solar-based, wind-based and hybrid) is presented in table 5.2. The table presents CAPEX and OPEX for each system component in every scenario, and the costs are directly linked with the installed capacities of the various components, as presented in the previous subsection.

Table 5.2: Case specific capital expenditure (CAPEX) and operational expenditure (OPEX).

Description	**Technology**	**Value (MUSD)**		
		Solar	**Wind**	**Hybrid**
CAPEX	Solar PV	1544	-	187
	Wind Turbine	-	1691	1299
	Electrolyzer	876	511	464
	Battery bank	335	93.8	93.8
	Hydrogen tank	133	746	426
	Ammonia Synthesis Unit	135	135	135
	Air Separation Unit	21.3	21.3	21.3
	Total CAPEX	3,044	3,198	2,626
OPEX	Solar PV	30.9	-	3.75
	Wind Turbine	-	33.8	26.0
	Electrolyzer	26.3	15.3	13.9
	Battery bank	3.35	0.94	0.94
	Hydrogen tank	0.00	0.00	0.00
	Ammonia Synthesis Unit	6.74	6.74	6.74
	Air Separation Unit	0.43	0.43	0.43
	Total OPEX	67.7	57.2	51.8

The total CAPEX for the solar, wind, and hybrid scenarios are 3044 MUSD, 3198 MUSD, and 2626 MUSD, respectively. The most expensive component in each scenario is the energy generating components. For the solar-based scenario, that means solar PV (51% of the total CAPEX), for the wind-based system, the wind turbines dominates the cost (53% of total CAPEX), and for the hybrid system, the combination of solar PV and wind turbines makes up 57% (heavily dominated by wind turbines at a 9 to 1 ratio vs solar PV) of the total cost. The OPEX, or the annual operational expenses, is found as a percentage of the CAPEX, and makes up a fraction of the initial investment expenses (CAPEX).

5.3 Performance metrics

Some of the key performance metrics for each optimized scenario is presented in table 5.3. The capacity factor of solar PV is 22.4% in the solar-based scenario and 19.5% in the hybrid scenario (no solar PV installed in the wind-based scenario). The wind turbine capacity factor is actually higher for the hybrid scenario (59.5%), than for the pure wind-based scenario (51.7%), suggesting better wind speed conditions in Patagonia compared to Utsira (see chapter 4.1 for case study location description). The air separation unit and ammonia synthesis unit (Haber-Bosh + syngas compressor) shows steady operation through all scenarios. Additionally, the total production of hydrogen (97 kilo-tonne), nitrogen (449 kilo-tonne), and ammonia (547 kilo-tonne) is consistent throughout each scenario. Annual water consumption is 970 kL (kilo liters), consumed by the electrolyzers for hydrogen production. The round-trip efficiency for the green ammonia plant is 54.5%, meaning per kilowatt input to the system, one gets 0.545 kilowatt output in the form of energy stored in the produced ammonia.

Table 5.3: Case specific performance metrics.

Description	**Technology**	**Value**		
		Solar	**Wind**	**Hybrid**
Capacity Factor (%)	Solar PV	22.4	-	19.5
	Wind Turbine	-	51.7	59.5
	Electrolyzer	37.3	64.0	70.4
	Air separation unit	98.6	98.6	98.6
	Ammonia synthesis unit	98.6	98.6	98.6
Total production (kt)	Hydrogen (H_2)	97	97	97
	Nitrogen (N_2)	449	449	449
	Ammonia (NH_3)	546	546	546
Total consumption (ML)	Water (H_2O)	970	970	970
Round-trip efficiency (%)	Green ammonia plant	54.5	54.5	54.5
LCOE (USD/MWh)	Solar PV	42.7	-	49.1
	Wind Turbine	-	44.8	38.9
	Average	42.7	44.8	39.9
LCOH (USD/kgH_2)	-	3.14	2.80	2.51
LCOA (USD/tNH_3)	-	595	599	501

The levelized cost of electricity (LCOE) in USD/MWh, is 42.7 for in the solar-based sce-

nario and 44.8 in the wind-based scenario. In the hybrid scenario, the electricity generated from wind turbines achieves a LCOE of 38.9 USD/MWh, while the solar PV generated energy comes at a LCOE at 49.1. The combined LCOE in the hybrid scenario is the relative contribution of these two sources, and is equal to 41.4 USD/MWh. The levelized cost of hydrogen (LCOH) decreases from 3.14 USD/kg in the solar scenario to 2.80 USD/kg in the wind scenario, and further down to 2.51 USD/kg in the hybrid scenario.

The levelized cost of ammonia (LCOA) is lowest in the hybrid scenario with 501 USD/tonne, compared to 595 USD/tonne in the solar scenario and 599 USD/tonne in the wind scenario. To accompany the aforementioned values, figure 5.1 has been included for a visual representation of the LCOA. The total height of each bar represents the LCOA for each scenario, where the stacked bars presents all cost contributing components to the overall cost.

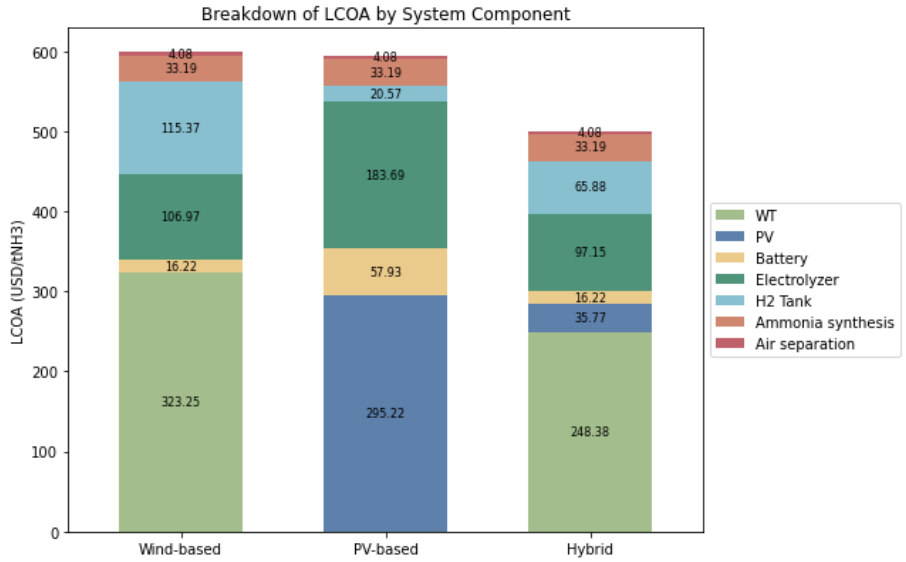

Figure 5.1: LCOA breakdown of all system components for each of the locations.

From the chart, it becomes that clear that the largest contributors to LCOA in the wind-based scenario is the wind turbines, accounting for over half the cost with an LCOA of 303 USD/tNH_3, followed by electrolyzers (105 USD/tNH_3) and the hydrogen tank (115 USD/tNH_3), which constitutes around 17% and 19% of the total LCOA, respectively. The largest LCOA contributors for the PV-based scenario is the solar PV, with 295 USD/tNH_3 - almost half the total LCOA. Additionally, the electrolyzers makes up 183 USD/tNH_3 (about 31%), and the battery bank 57 USD/tNH_3 (around 10%) of the total LCOA. The hybrid scenario has has its energy sources (solar PV and wind turbine), accounting for 284 USD/tNH_3, with a 1-9 ratio between the two components. Other major cost contributors for the hybrid scenario are the electrolyzers (97 USD/tNH_3) and the hydrogen tank (65 USD/tNH_3), which makes up 19% and 13% of the total LCOA, respectively.

In all scenarios, it's noteworthy that the batteries, ammonia synthesis unit, and air separation unit make minor cost contributions. The ammonia synthesis unit and air separation unit together contribute only 37 USD/tNH_3 in any scenario (around 6% of the overall system cost), underscoring their relatively minor role in the overall cost.

5.4 Solar based system

The following figures is meant to give a visual overview of how the green ammonia plant behaves during operation in the solar-based scenario. They provide insights into daily mean and hourly variables, which illustrate how the various system components interact and behave during the operation of the green ammonia plant. The system dynamics and synergies are governed by the strategy for controlling power and hydrogen flows implemented as part of the optimization algorithm, as described in chapter 3.7.

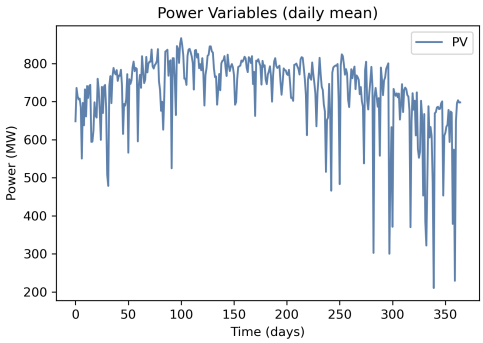

Figure 5.2: Daily mean power production from solar PV (solar-based scenario).

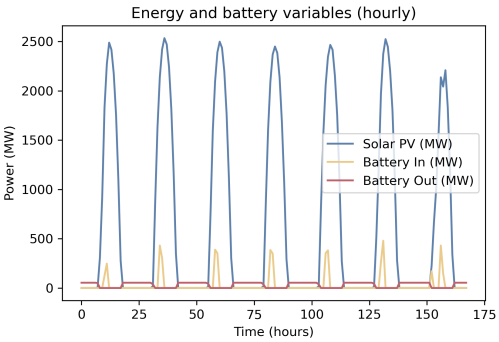

Figure 5.3: Hourly power production, battery input, and battery output over one week (solar-based scenario).

Figure 5.2 presents the daily mean power production from the solar PV, while Figure 5.3 shows the hourly power production, battery input, and battery output over a one-week period.

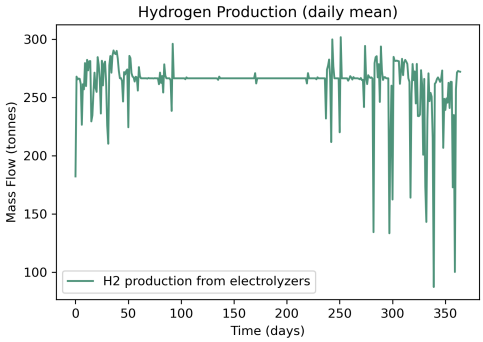

Figure 5.4: Daily mean hydrogen production from the electrolyzers (solar-based scenario).

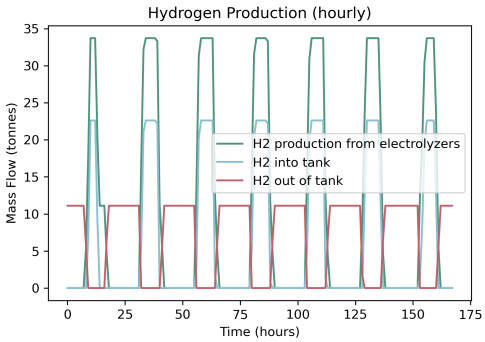

Figure 5.5: Hourly hydrogen production, hydrogen into tank, and hydrogen out of tank over one week over one week (solar-based scenario).

Figure 5.4 and Figure 5.5 outline the daily mean and hourly hydrogen production, as well as hydrogen storage activities over a week, respectively.

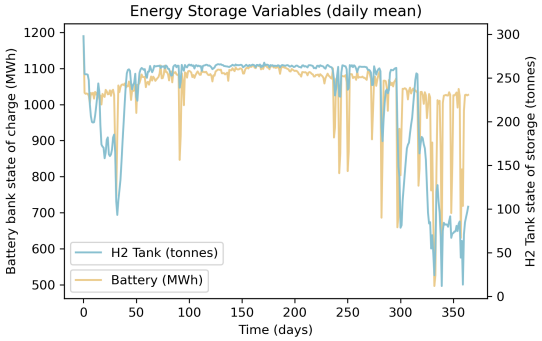

Figure 5.6: Daily mean state of charge of the battery bank and state of storage of the hydrogen tank (solar-based scenario).

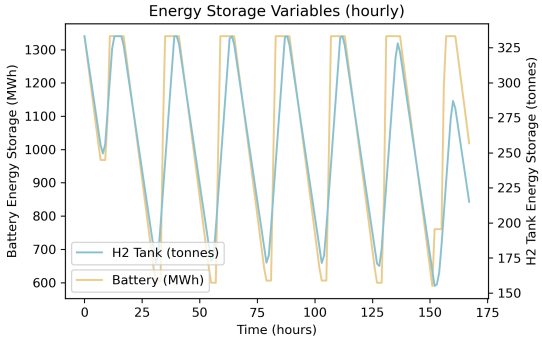

Figure 5.7: Hourly state of charge of battery bank and state of storage of hydrogen tank over one week (solar-based scenario).

Lastly, Figure 5.6 and Figure 5.7 provide a daily mean and hourly view of the energy storage states of the battery bank and the hydrogen tank over a one-week duration. This illustrates how the battery bank and hydrogen tank is continuously charged/discharged in order to balance the energy and hydrogen mass flows throughout the year.

5.5 Wind based system

The figures in this subsection provide a visual guide to the system behavior and dynamics of the green ammonia plant operating under a wind-based scenario. By presenting both daily mean and hourly variables, these figures illustrate the interplay between various system components and their behavior during the plant's operation.

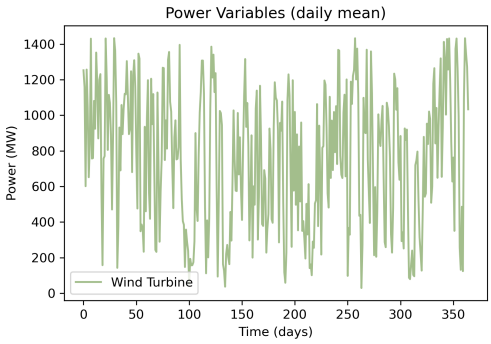

Figure 5.8: Daily mean power production from wind turbines (wind-based scenario).

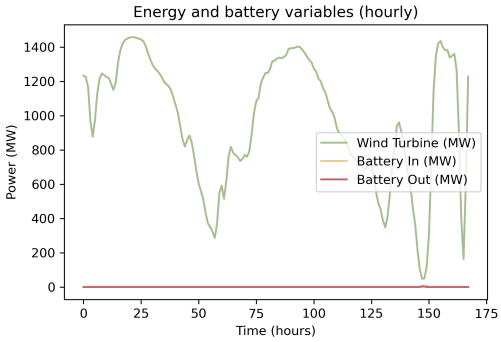

Figure 5.9: Hourly power production, battery input, and battery output over one week (wind-based scenario).

Figure 5.8 displays the daily mean power production from wind turbines, while Figure 5.9 provides an hourly view of power production, battery input, and battery output over a one-week period.

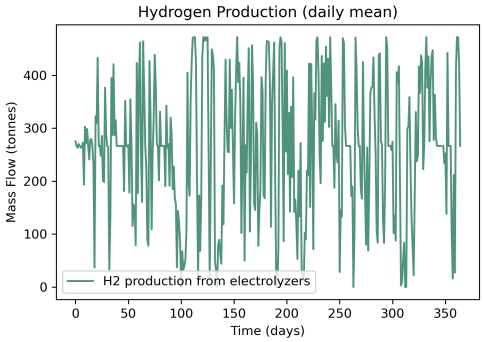

Figure 5.10: Daily mean hydrogen production from the electrolyzers (wind-based scenario).

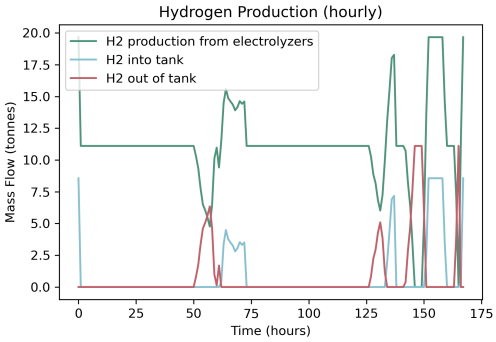

Figure 5.11: Hourly hydrogen production, hydrogen into tank, and hydrogen out of tank over one week (wind-based scenario).

Figure 5.10 shows the daily mean hydrogen production from the electrolyzers, and Figure 5.11 showcases the hourly hydrogen production, along with the amounts of hydrogen input and output from the hydrogen tank over a week.

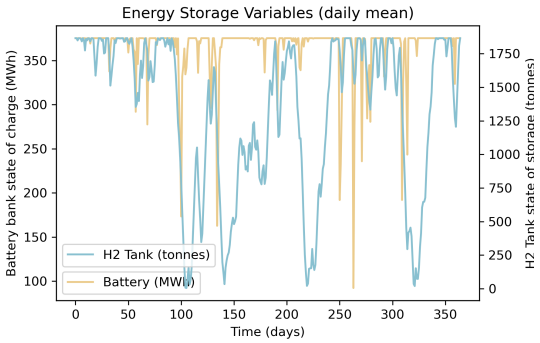

Figure 5.12: Daily mean state of charge of the battery bank and state of storage of the hydrogen tank (wind-based scenario).

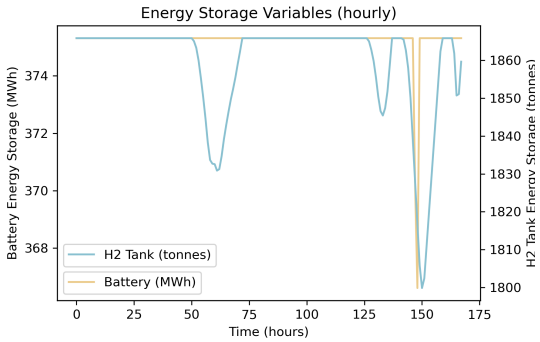

Figure 5.13: Hourly state of charge of battery bank and state of storage of hydrogen tank over one week (wind-based scenario).

Finally, Figure 5.12 and Figure 5.13 illustrate the daily mean and hourly state of charge of the battery bank and the state of storage of the hydrogen tank, respectively, over a one-week period. This illustrates how the battery bank and hydrogen tank is continuously charged/discharged in order to balance the energy and hydrogen mass flows throughout the year.

5.6 Hybrid solar- and wind-based system

This section presents the behavior of the green ammonia plant in the hybrid scenario, considering energy production from both solar PV and wind turbines. The following figures displays daily mean and hourly variables to visually illustrate the operational dynamics and the interplay among different components of the system.

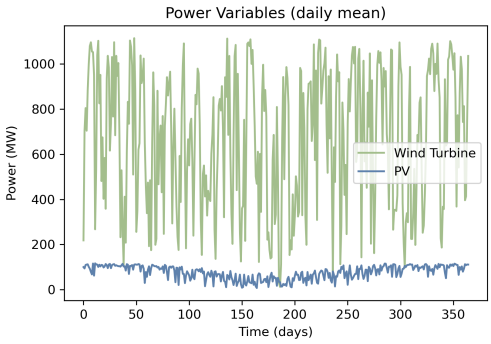

Figure 5.14: Daily mean power production from solar PV and wind turbine (Hybrid scenario).

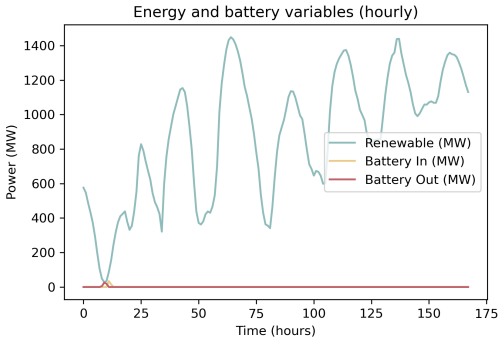

Figure 5.15: Hourly renewable power production (combination of solar PV and wind turbines), battery input, and battery output over one week (Hybrid scenario).

Figure 5.14 presents the daily mean power production from the solar PV and wind turbine, while Figure 5.15 showcases the hourly renewable power production from the wind turbines and solar PV combined, as well as battery input, and battery output over a one-week period.

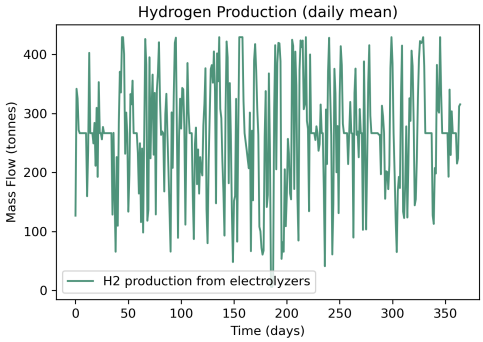

Figure 5.16: Daily mean hydrogen production from the electrolyzers (Hybrid scenario).

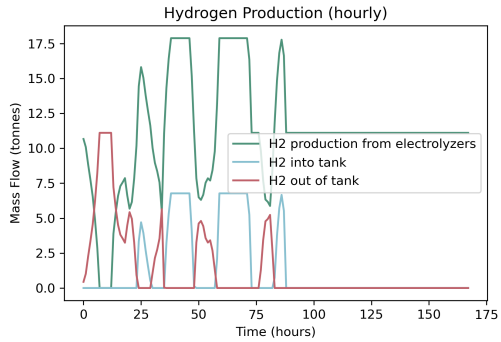

Figure 5.17: Hourly hydrogen production, hydrogen into tank, and hydrogen out of tank over one week over one week (Hybrid scenario).

Figure 5.16 and Figure 5.17 display the daily mean (over one year) and hourly hydrogen production, as well as hydrogen storage activities over a week, respectively.

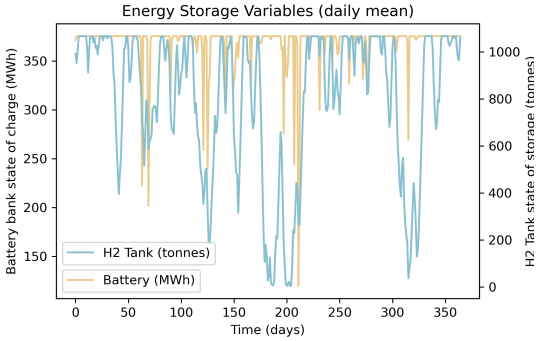

Figure 5.18: Daily mean state of charge of the battery bank and state of storage of the hydrogen tank (Hybrid scenario).

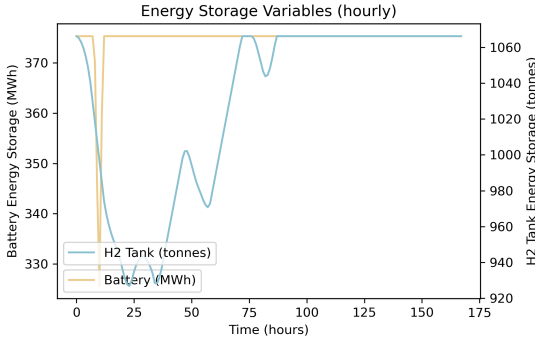

Figure 5.19: Hourly state of charge of battery bank and state of storage of hydrogen tank over one week (Hybrid scenario).

Lastly, Figure 5.18 and Figure 5.19 provide a daily mean and hourly view of the energy storage states of the battery bank and the hydrogen tank over a one-week duration in the hybrid scenario. This illustrates how the battery bank and hydrogen tank is continuously charged/discharged in order to balance the energy and hydrogen mass flows throughout the year.

6 Discussion

The subsequent section will engage in a discussion where the methodology and results are assessed in relation to relevant theory. This evaluation aims to improve the understanding of the conducted work by providing an overview of what has been done and by trying to connect it all together.

6.1 Evaluation of the optimization framework

A natural way of initiating the discussion chapter would be to reiterate the first of two research question attempted to be answered in this thesis.

RQ1: *How can we construct and utilize a computational framework to optimize the production of a green ammonia plant based on off-grid wind and/or solar energy at different geographical locations?*

There are, as one may imagine, several possible ways of doing this, but the general idea is roughly the same; (i) find a way to mathematically represent each system component, (ii) create an algorithm that accurately depicts the system behaviour for a wide range of scenarios, (iii) determine the objective of the optimization and its constraints, and (iv) implement it all into a programming language to run the simulation. These are the basics of many optimization models, including the ones given by Tebibel (2021) and Al-Buraiki and Al-Sharafi (2022), as mentioned in chapter 1.1.

The same approach was used for the creation of the optimization framework in this thesis; mathematical models were determined, and a strategy for controlling power and hydrogen flows was created as a control strategy for simulation of the green ammonia plant to be able to adjust to and handle the fluctuating energy input by the renewables. Additionally, objective functions and constraints were determined according to the desired output. Typically, the objective function is of economical, environmental or technical nature. If the green ammonia plant is to become competitive and feasible for large scale industrial implementation, its economics must be taken into consideration. As a result, the model was set to achieve its point of optimum where the production cost is at its lowest, i.e., to minimize the LCOA subject to various constraints (reliability of production, component operational window constraints etc.)

In order to go from modelling to simulating and performing the actual optimization, an optimization technique needed to be implemented. Out of the reviewed relevant literature, Salmon and Bañares-Alcántara (2022) used linear programming to run the simulation and optimize for the point of minimum LCOA. Samy et al. (2020) used a non-linear heuristic optimization approach, Osman et al. (2020) used a heuristic optimization approach, while Arnaiz del Pozo and Cloete (2022) used an integrated modelling tool (SEA tool) in their search for the optimal plant configuration. In this thesis, however, an iterative optimization approach was used. Each of the aforementioned approaches serve the same purpose, but have their different means of reaching the end goal.

The iterative approach can be thought of as a brute force-approach, where every solution

is evaluated one-by-one in an iterative manner until the optimal solution is obtained. On the other hand, the linear and non-linear approach aims to find the optimal solution in an efficient manner by implementing a well-defined mathematical model for computation. Meanwhile, the heuristic optimization employs educated guesses to minimize the search area, thus decreasing the simulation run time by looking for "good enough" solutions rather than the optimal solution. The primary reasons behind our selection of the iterative approach were its straightforwardness and ease of implementation.

The main drawback, however, and also the biggest drawback of the computational framework, is its time consumption. While the iterative approach is able to handle a large variety of scenarios, and is relatively easy to implement, the actual simulation/run time is long. Depending on the scenario being simulated, the time needed to obtain the optimal solution was be anywhere from 6-72 hours. For the purpose of this thesis, where the main focus was to be able to create a flexible and precise optimization framework, time consumption was not really an issue, and the iterative approach was deemed sufficient. However, if time consumption per simulation would have been decreased, the amount of simulations that could have been performed would have increased as well. Although the results would have been the same, a decreased run time would facilitate the exploration of a wider range of scenarios, where sensitivity analysis of how various parameters impact the point of optimum could have been undertaken. This provides a potential area of improvement, and a possibility of further work.

Constraints

In addition to the objective function, which is the goal of the optimization, the constraints determine the boundaries, or the feasible region where the optimal solution must be found. Having one without the other makes no sense, and their relationship can be compared to a car driving on a road from Trondheim to Oslo. The objective function represents the goal (reaching Oslo), and the constraints are represented by the road. Without following the constraints (the road), not only could one end up taking an inefficient route, but one might also face potential dangers.

One crucial constraint in this study is the total ammonia deficit (TAD). By using this reliability measurement, we are able to quantify the operational window in which the optimization algorithm must to adhere to. As explained in chapter 3.6.4, the TAD represents hours of non-production during a year of operation. Having a total TAD = 0 over the course of the year, would mean that the green ammonia plant would produce at rated capacity every hour of the year. Not only would it be unrealistic, because of the intermittent and unpredictable renewables, but also because the system components require shut down due to maintenance at some point during the year. In fact, the Haber-Bosch synthesis unit has an average yearly down-time of 30 days (Goswami and Goyal, 2012). For the purpose of this thesis, however, the total ammonia deficit constraint was sat to 120 hours, or 5 days.

The reason for the large discrepancy between our determined TAD and the averaged real-life value, is to counteract the potential illusion of high accuracy caused by the likely widespread distribution of down-time hours. Ideally, the 120 hours would be spread across 5 whole days. In reality, however, the system behaviour is completely different. Because of

the unreliable and intermittent nature of the renewables, the 120 hours could potentially be dispersed across 120 different days - with one hour of down-time each day, and not over 5 consecutive days as desired. If ramping times is included, the system components (especially the H-B and ASU) would need time to recover from being shut down, thus the initial one hour of shut down could potentially mean that the system would be shut down the entire day, depending on the ramping times of the components. This worst-case scenario could potentially mean that the ammonia plant is shut down for 120 days, and not 5 days as which was the initially idea when setting the TAD equal to 5 days.

From the simulations, however, we see that this is not the case. The individual hours of non-production (represented by an ammonia deficit = 1 at each hour) is spread across far less days than the worst-case scenario of 120 days for all the cases investigated in this thesis, as illustrated in Appendix B. The hybrid scenario has its off-hours spread across a total of 15 days, the solar-based scenario yielded 30 days, while the wind-based scenario had its off-hours distributed across 16 days. These days correspond to periods of low energy input over consecutive days, where the renewables could not supply energy for electrolysis and ammonia synthesis, and the battery bank or hydrogen tank could not maintain the system's operation as they were drained, thus resulting in shut down. So, despite the potential error and caused by neglecting ramp-up times, the TAD is still kept within reasonable boundaries (compared to the average annual down time of 30 days) by setting the initial TAD constraint to 120 hours, or 5 days. This means that by setting the TAD equal to 5 days, we are able to spread out our days affected by down-time close to the real-life average to 30 off-days per year, despite the the neglected ramping times. This would not have been the case if we had sat the TAD to 30 days, as the would have been the natural constraint. Doing this would have increased the widespread distribution of down-time hours, potentially spanning over a large number of days. Thus making the simulation less real-life like.

Flexibility

During the creation of the framework, there were several defining moments, and the determination of the flexibility of the ammonia plant was one of them. As explained in the introduction section, and also in chapter 3.3.1, the Haber-Bosch is historically a non-flexible unit dependant on constant mass and power input. However, as (Fasihi et al., 2021), (Wang et al., 2023), and (Armijo and Philibert, 2020) suggests in their respective research, it is possible to implement a flexible Haber-Bosch unit, capable of adjusting its operation according to the available energy input from the intermittent renewables. Despite this, our project decided not to take it into account, and formed the optimization framework based upon a non-flexible ammonia synthesis unit. This is in contrast to the electrolyzers, who in fact are considered to be flexible units capable of producing hydrogen at a wide range of input energy (20-120% operational range).

There are a few reasons as to why the electrolyzers were chosen to be flexible, and the Haber-Bosch unit was not. In terms of implementation into the framework, there is not much difference in incorporating the flexible electrolyzer and the flexible Haber-Bosch unit. This could have been done by including an additional constraint determining the operational range of the unit and by doing some modifications to the strategy for controlling power and hydrogen flows (SCPH) in terms of how the system behaviour reacts to various

energy input scenarios, much of the same way the flexible electrolyzer was handled. The algorithm would have been a bit more complex, and the run time would have increased, but implementing a flexible H-B would have been possible by minor adjustments of the existing framework. However, seeing as the flexible H-B is more of a theoretically possible unit, rather than a commercially available industrial scale unit, it was decided not to implement it.

Additionally, if future green ammonia production is to fully replace and exceed todays conventional fossil-fuel based ammonia production, as discussed in the introduction chapter, some (all) of todays existing plants must be modified to run on green hydrogen as opposed to grey, black, or blue. By introducing a non-flexible ammonia plant-based framework, we can utilize the framework to accurately model scenarios in which green ammonia production can replace already existing conventional ammonia plants. By replacing the grey/black hydrogen production and electricity chain with renewable based hydrogen produced from electrolysis, the ammonia synthesis units (H-B and ASU) can be reused for the purpose of producing green ammonia. In fact, this is exactly what (YARA, 2021, 2022) is currently doing at their location in Porsgrunn, Norway. By adding 450MW electrolyzer capacity, the 500kt annual fossil-based ammonia production could be replaced by green ammonia. As per 2023, 24MW is expected to be installed, thus initiating the transfer from gray to green, and manifesting the possibility of fully replacing existing conventional ammonia with green ammonia on site.

Potential sources of error

Even though the model and framework provide valuable insights in the production of green ammonia (as will be discussed in the interpretation of the results section), it's important to acknowledge potential sources of errors, with the first one being the neglected ramp-up and ramp-down times. In our framework, the electrolyzers and ammonia synthesis unit (H-B and ASU) is assumed to have instantaneous ramp-up and ramp-down time, meaning that the electrolyzers and ammonia synthesis is able to completely shut down at times of low/no energy input, and vice versa during times of sufficient supply of energy (and hydrogen in the case of the ammonia synthesis unit). In practise, however, this is not the case. The PEM electrolyzer, being the most dynamic of the three (compared to the alkaline and SOEC), has a fast dynamic response and is able to go from complete shut down to nominal load in lest than 20 minutes, as per table 2.1. The Haber-Bosch unit on the other hand, has a slow dynamic response, and current technologies is limited to a ramp up of 20%/h, thus requiring five hour to reach full capacity after having been shut down (Verleysen et al., 2022). The Air separation unit is even slower, and is limited to a ramp up time of 10%/h, or 10 hours to reach full capacity after shut down (Cheng et al., 2022).

By neglecting these ramp-up/down times, we overestimate the actual production, and reach higher efficiencies and productional values than what would be the case in a real-life scenario. The electrolyzers are dynamic of nature, and would not lead to big fluctuations in the results obtained from our simulations vs real-life. The ammonia synthesis unit (H-B and ASU), on the other hand, might lead to potential errors in the results, meaning the point of optimum obtained from simulations is shifted from its true point of optimum. However, as discussed in the TAD section above, the number of days where the ammonia

synthesis plant is shut down ranges from 15 to 30 days. Thus, the implications of not including ramp-up and ramp-down times in the framework are considered non-critical, even though the real life scenario would then have 15-30 days of non-production, as opposed to 5. Thus overestimating the actual production of ammonia.

Another potential source of error is caused by not including stack replacement costs in our framework. Over time, the electrolyzer stacks degrade and requires replacement. For the AWE and PEM electrolyzers, this is required after 80,000 hours of operation as given in table 2.1, or around 10 years of continous operation. With a plant lifetime of 30 years, that would mean the electrolyzers would have to replace stacks two times throughout its lifetime. However, as the results from the simulation shows, the electrolyzers does not operate continuously throughout the year. Depending on the scenario evaluated (solar-based, wind-based or hybrid), the electrolyzer capacity factor (CF) is between 37% and 70%. For the CF=37% scenario, obtained from the solar-based scenario, the stacks would need replacement after 27 years, thus being able to operate for almost the entire lifespan of the green ammonia plant without having to be replaced. For the hybrid scenario with an electrolyzer capacity factor of 70%, it would need stack replacements after 13 years, or around one time during the lifetime of the green ammonia plant. The wind-based scenario has a capacity factor of 64%, meaning stack replacement would potentially be needed after 14.5 years, also around one time during the plant lifetime.

How would the inclusion of stack replacement cost affect the overall green ammonia plant system cost? Well, stack replacement can be considered as a an additional capital expenditure, and makes up around 40% of the initial electrolyzer cost Taibi et al. (2020). If we take a look at the hybrid scenario, where stack replacement is relevant (as opposed to the solar-based scenario where stack replacement is considered not needed), the pre-stack replacement cost scenario has an electrolyzer cost contribution of 18% of the overall CAPEX. Including the stack replacement cost would have this increased to 23%, and yield an increase in the total CAPEX for the entire green ammonia plant of around 7% (around 6% for the wind-based scenario). So, to summarize; stack replacement cost is only relevant for the wind-based and hybrid scenarios. However, because the electrolyzers are not the dominant CAPEX contributor, the cost of including stack replacement would only increase the overall costs with 6-7% for the wind-based and hybrid scenarios. Although not a substantial amount, it is still a source of error and a potential field for improvement.

6.2 Interpreting the results

To test the ability of the optimization framework, it was decided to conduct a case study where three scenarios would be investigated and compared. The specific locations themselves were not the primary focus, rather it was important to choose three widespread locations with inherently different weather resources at hand. By doing this, the frameworks flexibility and capability would be tested. Additionally, we wanted to see how the green ammonia plant system configuration changes with variable resources and restrictions. As a result, three different locations were chosen; a high solar irradiation case (Tan-Tan in Morocco), a high wind speed case (Utsira in Norway), and a hybrid case (Patagonia, Santa Cruz province in Argentina) with abundant both solar and wind resources. These locations enabled us to evaluate different operational scenarios for green

ammonia production: one powered solely by solar energy, one only by wind energy, and one hybrid plant powered by both solar and wind energy. By assessing these scenarios, we were not only able to evaluate the versatility of our optimization framework across a range of conditions, but also able to gain valuable insights into the dynamics of green ammonia production under varying renewable energy scenarios. Thus allowing us to evaluate the second research question of the thesis; ***RQ2:*** *Is the production of green ammonia techno-economical feasible?* This will be discussed subsequently.

6.2.1 System behaviour, sizing, and performance

The productional target for the green ammonia plants investigated was to produce 1500 tonnes per day of green ammonia for a total for 360 days per year, equal to 540,000 tonnes annually. In order to do so, the various plant scenarios had to be sized correctly. Before delving into the system sizing results themselves, it can be useful to look into how the system behaves during operation to better understand why the systems are sized the way they are. The system behaviour is governed by the strategy for controlling power and hydrogen flows, which is the heart of the optimization, as discussed in the framework evaluation. Each scenario and the their related system behaviour will be discussed subsequently.

Solar-based system behaviour

The system behaviour during operation for the solar-based green ammonia plant is illustrated in the figures presented in chapter 5.4. To understand how the solar-based green ammonia plant behaves during operation, we must first understand how the solar weather resources behaves. Figure 5.3 show how the solar energy is of a cyclic nature as it the sun rises and sets each day. During sunlight hours, energy is generated and used to convert water into hydrogen through electrolysis as well as to power the ammonia synthesis. Additionally, during peak sunlight hours, the battery is charged, also shown in the aforementioned figure. Conversely, during night time, when the sun is set and there is no energy generated from the solar PV, the battery is drained in order to supply energy to the ammonia synthesis to keep it going through the night and avoid shut down. The same cyclic routine applies for the electrolyzers, as shown in Figure 5.5. During peak sunlight hours where production is high, the electrolyzers produce enough hydrogen to supply directly towards ammonia synthesis and at the same time fill up the hydrogen tanks. The tanks work together with the battery to supply hydrogen and energy for synthesis during nighttime when the solar PV production is zero.

The cyclic nature of the sun is also affected by seasonality. For Tan-Tan, during winter time (November-February), the solar PV production suffers from a decline in available solar resources (around 19% capacity factor from October-January and around 24% the rest of the year). As a result, the additional strain is put on the energy storage components (battery and hydrogen tank) to keep the ammonia synthesis running. However, if the energy supplied from solar is insufficient for longer periods of time, there will be a mismatch in energy/hydrogen into battery and tank during daytime and out of battery and hydrogen tank during nighttime, and the energy storage components ends up drained. Thus, the system must shut down. This interplay is visualized in first in Figure 5.2, showing how the energy produced from solar PV declines during the end of the year, before Figure

5.6 shows how the energy storage variables are drained during the same time-period, and lastly Figure B.1 in Appendix B, illustrates when the system shuts down, shown by total ammonia deficit, also during the same time-period.

To handle this complex and dynamic interplay as a result of the rising and setting of the sun, a robust energy storage system is needed to maintain operation during nighttime. This becomes increasingly important if the system is to be able to operate for 360 days throughout the year, as restricted by the system constraints.

Wind-based system behaviour

Similarly to the solar-based system, the wind-based system behaviour is depicted in the figures presented in chapter 5.5. In contrast to the cyclic nature of the sunlight, wind energy is of intermittent nature, with fluctuations over time. Although the wind energy can vary greatly throughout the day, it has the ability to produce energy throughout the entire day, in contrast to the solar energy which is only available at daylight hours. As a result, the battery, which is used to supply energy to the ammonia synthesis unit (Haber-Bosch and ASU) when the wind energy is insufficient, is not activated in the same way as for the solar-based scenario. Figure 5.9 shows how the energy supplied from the wind turbines are intermittent, but not cyclic. More often than not, there is enough energy generated by the wind turbines to supply the ammonia synthesis unit, which is far less energy demanding than the electrolyzers (around 1/9th of the electrolyzer demand as seen from Table 3.1 as well as in Appendix C). This means the need for battery to supply the ammonia synthesis is not as prominent as what was the case for the cyclic solar-based scenario. In fact, the battery capacity needed in the solar-based system is around 4 times the installed battery capacity needed for the wind-based system.

For the hydrogen storage tanks, however, the story is quite different. Even though the wind generated energy is often enough to power the ammonia synthesis unit, its time-variable energy supply shown by Figure 5.8 means that the wind turbines does not always produce enough energy to surpass the electrolyzer minimum energy requirement threshold (electrolyzer is able to operate down to 15% of the installed capacity), which for the wind-based system is around 3 times higher (see Table 5.1) than the energy demanded by the ammonia synthesis unit (H-B + ASU). The intermittent nature of wind energy means the electrolyzers may go several hours (days) without the energy supplied being able to overcome the electrolyzers threshold. Conversely, there are periods of hours or days with extremely good wind conditions meaning the wind turbines operates at full or near full capacity. During these hours, the electrolyzers will operate at full capacity. To cope with these extremes, the hydrogen tanks must be large enough to be able to store the surplus hydrogen during longer periods of good production and also supply hydrogen during longer periods of non- or limited production. As a result, the hydrogen tanks are around 6 times larger for the wind-based scenario than that of the solar-based scenario.

Although there are seasonal variations in the wind resource availability at Utsira, they are not as prominent as the ones experienced in Tan-Tan, and periods of low/no wind generation is spread a bit more evenly than what was the case for the solar-based Tan-Tan scenario. April and November were the worst months in terms of overall wind turbine capacity factor, with averages of around 40% as opposed to the annual average of around

52%, while January and December had averaged capacity factors of around 68%. The periods around late spring and early autumn were particularly demanding for the energy storage system. During these times, the energy storage variables had to compensate more heavily for the lower energy production to ensure continuous plant operation. Figure 5.12 visually demonstrates these periods, illustrating an increased reliance on the energy storage components to cope with lower wind energy production. Especially the hydrogen tanks were depleted, leading to an increased amount of hours with non-production/system shut down as shown in Figure B.2.

While wind energy can potentially generate energy throughout the entire day, its intermittent nature creates challenges that need to be addressed to ensure the uninterrupted operation of a wind-based green ammonia plant. A large hydrogen storage system is especially important for the wind-based scenario, able to store excess hydrogen during high production periods and to supply hydrogen during periods of non- or limited production.

Hybrid system behaviour

The hybrid system displays the best of both worlds, combining the strengths of solar- and wind-based systems. By utilizing these synergistic benefits, the hybrid system achieves a more stable continous flow and as a result also a higher reliability. The baseline energy generation is determined by the wind generated energy, and the peaks are provided by the solar PV. As for the wind-based scenario discussed above, the wind energy is time variable, but with an average daily wind speed of 9.8 m/s, it exceeds the cut-in speed of 3 m/s. More often than not, the ammonia synthesis unit is entirely supplied by the wind turbine at wind speeds equal to 3.7 m/s (this wind speed allows the turbine to generate enough power to run the ammonia synthesis unit). The electrolyzers starts their hydrogen production when the wind energy generation is equal to the minimum energy requirement threshold (i.e., 15% of rated capacity). This occurs at wind speeds above 4.7 m/s, which is enough to power the ammonia synthesis and at the same time operate the electrolyzers at minimum load range.

As we can see based on the average wind-speed of 9.8 m/s, the wind turbine is typically able to provide a continous base-line energy production that is able to provide energy for the ammonia synthesis throughout the day, and also provide for the electrolyzers for hydrogen production, although not at full capacity. The steady energy supply means the need for batteries to act as energy buffers is not as prominent as for the solar-based scenario, but more similar to the wind-based scenario. By adding solar energy to the mix to complement the more steady, yet also time-variable wind-based energy, the total energy supply becomes a mix of time-variable, but with a steady baseline provided from wind energy, combined with cyclic peaks supplied by the added solar energy, as seen in Figure 5.15.

The cyclic peaks are used for max production of hydrogen from the elctrolyzers, which are partially used to supply the ammonia synthesis unit, but also for storage in the hydrogen tanks. From Figure 5.17, we can see this process in motion. The cyclic peaks and valleys caused by the addition of solar PV, means the hydrogen tanks are filled up during daytime, and are depleted during nighttime to provide enough hydrogen flow to the ammonia synthesis. The baseline energy supply is provided by the more stable nature

of wind energy, but at times of higher wind speeds, wind energy also contribute to run the electrolyzers at full capacity, adding to the already large requirement of hydrogen storage.

This baseline-wind-energy and cyclic-peak-solar-energy synergy determines the operational reliability of the green ammonia plant. Where the wind speed is relatively even throughout the year, the solar irradiation shows seasonal variations as seen from Figure 4.3 and 4.4. Especially during the summer months June and July displays limited solar irradiance with average capacity factors around 9%, which is far lower than the annual average of around 20%. This means the cyclic peaks are no longer there to provide hydrogen generation to supply both ammonia synthesis and tank. As a result, the tanks are drained at a faster rate than they are filled as shown in Figure 5.18, leading to system shut down and loss of ammonia supply as shown in Figure B.3 in these particular summer months. It is during these summer months, the reliability of the system is truly tested, and the need of correctly sized components becomes clear.

System sizing, energy distribution and performance comparison

To understand the implications of the different behaviour each scenario displays, we must take a look at the system sizing and performance results from the optimization, presented in Table 5.1 and Table 5.3. Each scenario is designed to meet the production demand of 1500 tonnes ammonia per day. This results in equally large installed capacities across all the scenarios for the air separation unit and ammonia synthesis unit (Haber-Bosch + syngas compressor), with installed capacities of 6.1 MW and 47.5 MW, respectively. Additionally, the energy consumed is constant through all scenarios. This must be true if the production demand of 1500 tpd ammonia is to be met. The total energy consumption is 5.16 TWh across all scenarios, distributed between the ammonia synthesis unit (0.40 TWh), the air separation unit (0.06 TWh) and the electrolyzers (4.70 TWh).

In order to meet these energy demands, the energy generators (solar, wind or both) are sized appropriately through the optimization framework. As described in the solar-based system behaviour section above, all the energy and hydrogen needed for ammonia synthesis in the solar-based scenario must be produced during the day (at sunlight hours), leading to over-sizing of the Solar PV (3.25 GW) to ensure it can meet the demands. This also results in a higher capacity for the electrolyzers (1.44 GW) to be able to handle the large power peaks during daytime (2500 GW at peak sunlight hour), albeit at a low capacity factor of only 37.3. The battery bank (1.34 GWh) is sized to be able to run the ammonia plant for 30 hours of operation, while the hydrogen tank (0.34 ktH_2) is sized to provide an equivalent of 36 hours of coverage for hydrogen supply to the ammonia synthesis unit when the solar energy is non-existent.

The wind- and hybrid based scenarios are a bit different. As discussed in the system behaviour sections above, these scenarios are able to provide energy generation throughout the whole day as the wind turbines operate at higher capacity factors, at 51.7% and 59.5%, respectively. This results in less installed capacity for the wind turbines at 1.47 GW for the wind-based scenario and 1.13 GW for the hybrid scenario, which are supported by an additional 0.39 GW of solar PV. There are other requirements to the battery bank and hydrogen tank for the wind-based- and hybrid scenarios compared to the solar-based. As discussed in the last section, the wind-based and hybrid scenarios has stable baseline

energy generation which supplies the ammonia synthesis at a reliable level. This allows installed battery capacity of only 0.38 GW, which is almost 4 times less than for the solar-based scenario. The 0.38 GW capacity is enough to provide energy enough to run the ammonia plant for 6 hours, which according to the optimization algorithm is large enough to ensure a reliable operation. The hydrogen tanks on the other hand, requires large capacities for the wind-based and hybrid scenario, with a total installed capacity of 1.87 ktH_2 and 1.07 ktH_2, respectively. This would be enough to supply hydrogen to the ammonia synthesis unit for a total of 7 days and 4 days, respectively, at times when the wind turbines and solar PV were entirely non-productive.

So, the solar-based scenario, due to its dependence on cyclic sunlight, requires significantly larger system sizes (both in terms of energy production and storage) to be able to meet the downstream energy and hydrogen demands. On the other hand, the wind-based and hybrid scenarios, as a result of their more continuous energy generation profiles, require smaller energy production capacities but larger hydrogen storage capacities to manage the longer periods of low or zero renewable energy generation.

The hybrid scenario appears to offer the best balance between system size, energy distribution, and resilience. This is illustrated by the high electrolyzer capacity factor of 70.4% as opposed to 64% for the wind-based system and 37.4% for the solar-based. It combines the benefits of continuous wind energy generation and peak solar power, leading to lower installed capacities for both energy production and storage units, compared to the solar- and wind-only scenarios. Additionally, having two energy sources increases the reliability of the system, making it less vulnerable to periods of non-productive solar or wind conditions.

Furthermore, the optimization algorithm also takes into consideration the issue of energy curtailment. The curtailment occurs when the produced energy exceeds the system's instantaneous demand and the excess cannot be stored due to the limitations in storage capacity. The solar scenario resulted in a total of 1.21 TWh (19% of overall energy generation) of energy curtailed, the wind-based scenario curtailed 1.46 TWh (22%), while the hybrid scenario curtailed 1.38 TWh (21%). The more energy curtailed, the less efficient the system will be. Energy curtailed is effectively money lost, and a high percentage of energy curtailment leads to substantial economical losses, and will increase the overall LCOA. Ideally, the curtailed energy would be either minimized or sold. However, selling it would require grid connectivity and availability, which is not considered in this thesis. Not only is it not always available, as is the case for Patagonia (ref 4.1), but it is also an additional expense that needs to be taken into consideration during the optimization.

In conclusion, the sizing of the system components, their energy distribution, as well as the energy curtailment present a trade-off scenario in the design of renewable energy-powered ammonia plants. All of these factors are taken into considerations as the framework optimizes for energy efficiency and reliability, while minimizing energy curtailment in order to limit the cost of production.

6.2.2 System Economics

Another key factor of the results, and also directly linked with the system behaviour, sizing, and performance, is the economical results. Going back to the objective function; to minimize LCOA, we understand that the aforementioned parameters are indeed optimized to give the lowest possible cost of ammonia (as well as keeping within the reliability constraint amongst others, as previously mentioned). So, what is the capital investment required to fund the off-grid green ammonia plant able to produce 1500 tonnes of ammonia per day (540,000 tonnes annually)? For the solar-based scenario it is 3044 MUSD, for the wind-based scenario it is 3198 MUSD, and for the hybrid scenario it is 2626 MUSD, as shown in Table 5.2. These are extreme numbers, and because they are so case-specific, they do not tell us a whole lot other than the fact that there's a lot of zeros involved and that the hybrid scenario is the least expensive one, which is cohesive with what was discussed in the previous section. In order to better understand and compare the costs, evaluating the levelized cost of ammonia (LCOA) is a better alternative, as this gives us the overall cost (CAPEX + OPEX) per tonne ammonia produced, i.e., a generalized cost presentation.

Levelized cost evaluation

From the levelized cost breakdown presented in Figure 5.1, we see that the LCOA for the three scenarios are as follows; solar-based scenario with LCOA of 595 USD/tNH_3, wind-based scenario with LCOA of 599 USD/tNH_3, and the hybrid scenario with LCOA of 501 USD/tNH_3.

Almost half the cost contributor for the LCOA in the solar-based system comes from solar PV, while 30% comes from the large electrolyzer installation. This is in line with the analysis of the system behaviour previously discussed, where it was found that the solar-based system is largely dependant on a high installed capacity of solar PV and electrolyzers to counteract the cyclic behaviour of the sunlight, and be able to produce hydrogen during daytime to also meet demands at night. Despite having a large battery bank (1.24 GWh), its overall cost contribution is only about 10% due to the lower cost of lithium-ion batteries.

For the wind-based system, with an LCOA of 595 USD/tNH_3, half the cost comes from investments and operational expenditure for the wind turbines, similar to what was the case for solar PV relative cost contribution in the solar-based scenario. Additionally, around 17% of the cost comes from the electrolyzers and 19% from the hydrogen tanks. This is in agreement with what was discussed in the previous section, as energy is generated throughout the whole day and the need for over-sizing the electrolyzers is not as prominent as for the solar-based scenario. There is, however, a greater demand for a substantial hydrogen storage tank meaning the relative cost contribution for the tank is greater than for the solar-based scenario.

The hybrid scenario demonstrates its advantages when compared to the single-source scenarios. The hybrid system makes use of the strengths of both solar and wind energy sources, thereby reducing the periods of low energy production that are inevitable for the single-source scenarios. This merge of solar and wind power gives a more constant energy

supply, reducing the need for installed capacity of energy generators (wind turbines and solar PV), as well as hydrogen buffer tank capacity. From a cost perspective, the hybrid scenario is similar to the wind-based scenario in terms of relative cost contribution; around 50% of the cost comes from energy generation (90% from wind and 10% from solar), 19% from electrolyzers, and 13% from hydrogen tanks. However, due to the synergistic benefits between solar and wind energy, there's a decrease in capacity installations for all of the above-mentioned components, giving a lower capital expenditures, and, consequently, a lower LCOA of 501 USD/tNH_3.

When comparing the solar-based scenario to the wind-based scenario, the LCOAs are relatively similar, despite the energy sources and energy storage requirements being quite different. This is due to the cost structure of each scenario. It is worth noting that although the installed capacity of solar PV in the solar-based scenario is more than twice that of the installed wind turbine capacity in the wind-based scenario (3.25 GW installed solar PV vs 1.47 GW installed wind turbine capacity in the solar-based and wind-based scenarios, respectively), the cost of energy generation is about the same. This is due to the fact that solar PV cost is only 475 USD/kW while the wind turbine is at 1150 USD/kW, thus allowing for much more solar PV installation than wind turbine installation at the end cost, as per Table 4.3.

Another interesting remark, is the fact that the ammonia synthesis unit itself (air separation, syngas compressor and Haber-Bosch unit) only makes up around 6% of the cost contribution to the overall LCOA for all the scenarios, as well as only 8% of the overall energy demand. Conversely, the electrolyzers makes up 17% - 30% of the cost contribution to the LCOA, depending on the scenario, as well as a total of 90% of the overall energy consumption for the entire green ammonia plant, as seen from Figure C.1. In other words, the hydrogen production is the defining cost parameter for the green ammonia plant. Reducing the cost of hydrogen, both the electrolyzer CAPEX and OPEX as well as the power requirements, one directly reduce the overall cost of the green ammonia production. How to reduce these cost will be discussed in a later part.

Comparing LCOE, LCOH and LCOA

In addition to the levelized cost of ammonia (LCOA), the levelized cost of electricity (LCOE), and the levelized cost of hydrogen (LCOH), has also been calculated for the green ammonia plant, all found in Table 5.3. As we already know, the power generation and hydrogen production are the key components of the green ammonia plant. By analysing the LCOE and LCOH, and providing some real-life context, it allows for better understanding of the green ammonia plants cost in its entirety.

The LCOE reflects the costs associated with the generation of electricity through the renewable sources, while the LCOH represents the subsequent cost of production of hydrogen through electrolysis. The results from this thesis shows an LCOE of 42.7 USD/MWh, 44.8 USD/MWh, and 39.9 USD/MWh at the solar-based, wind-based and hybrid scenario, respectively. When compared to global averages in 2020, the results from this thesis are below the 57 USD/MWh global average for solar PV and are just slightly above the 39 USD/MWh global average for onshore wind, with offshore wind coming in at a considerably higher average of 84 USD/MWh IRENA (2021b). Thus indicating highly market

competitive cost of electricity from the solar-based scenario in Tan-Tan, and relatively average values in Utsira and Patagonia. One would initially assume, both Utsira and Patagonia to display below-average costs, rather than average costs because of their abundant weather resources. However, parameters chosen for this thesis' particular calculations such as CAPEX and OPEX values, discount rates, plant lifetimes etc. could all impact the cost of electricity, and cause discrepancies towards real-life scenarios.

The differences in LCOE from renewables in this study, compared to the LCOE for industrial use (not households) in Europe in the first quarter of 2022, is noteworthy. The recorded LCOE in Europe was around 200 USD/MWh, which is over four times the cost of the renewable-generated LCOE in our different scenarios Eurostat (2022). As of 2021, the European electricity mix was 40% fossil based, 25% nuclear and 35% renewable Eurostat (2023). This indicates that generating electricity solely from renewable sources, as demonstrated in the scenarios considered in this thesis, can potentially offer significant economic value compared to the fossil-fuel based European grid in terms of LCOE.

When it comes to the hydrogen production cost, the solar-based scenario resulted in an LCOH of 3.14 USD/kgH_2, the wind-based scenario at 2.80 USD/kgH_2 and the hybrid scenario at 2.51 USD/kgH_2. These cost are dominated by the cost of renewable energy generation, i.e., LCOE, as well as capital cost of the electrolyzers. According to International Energy Agency (2021), the average cost of producing hydrogen from renewables today (2021) is around 3.5-7.5 USD/kgH_2, with the prices expected to drop to to around 1.5-3.5 USD/kgH_2 in 2030 and 1-2.5 USD/kgH_2 in 2050. In contrast, hydrogen from natural gas is today around 1.5 USD/kgH_2 and natural gas with CCS (blue hydrogen) at around 2 USD/kgH_2 IEA (2022). From this, it is evident that the hydrogen production in favorable renewable locations (ref Tan-Tan, Utsira, and Patagonia) is able to achieve hydrogen prices similar to that of the 2030 estimated prices. Thus indicating that the LCOH obtained from our studies are to be considered good as of 2023 standards.

Lastly, the attention is turned to the levelized cost of ammonia (LCOA) which is greatly influenced by both the LCOE and the LCOH. As we've discussed, a decrease in the LCOE leads to a decrease in the LCOH, which subsequently leads to a decrease in the LCOA. In our study, the LCOA for the solar-based scenario was calculated to be 595 USD/tNH_3, the wind-based scenario at 599 USD/tNH_3 and the hybrid scenario at 501 USD/tNH_3. This is in range with other similar green ammonia projects, where the results typically show an LCOA in the range of 447 - 750 USD/tNH_3, as shown in Appendix A. It is also beneficial to provide some context by comparing the LCOA with the prices of conventional fossil fuel-based ammonia. Historically, these prices have ranged from 200-600 USD/tNH_3 Cesaro et al. (2021); Fasihi et al. (2021). However, in the face of recent disruptions such as the Covid-19 pandemic and the Russian-Ukrainian war, these prices have surged significantly, and reached 1200 USD/tNH_3 in 2021 U.S. Energy Information Administration (2022), before dropping to 600 USD/tNH_3 again the first quarter of 2023 Kim Chipman and Elizabeth Elkin (2023).

The primary reason for this surge is the increase in prices of natural gas and coal, which have a direct correlation with the price of traditional ammonia production, as it provides feedstock to the hydrogen production - essential to production of ammonia. However, the production of green ammonia, only relies on renewable energy sources, and is not affected

in the same manner. This major difference in price range underscores the instability of fossil fuel-based ammonia prices, which are subject to fluctuation due to external factors. On the contrary, green ammonia demonstrates potential for economic stability and competitiveness.

Our study's calculated LCOA values, especially for the hybrid scenario, demonstrate the economic viability and competitiveness of green ammonia production in the regions under consideration, as they align with recent prices for conventional ammonia. Additionally, the simulation emphasizes how reductions in LCOE and LCOH contribute significantly to achieving competitive LCOA values, which will be important if the LCOA is to be decreased even further.

6.3 Use of resources

The sustainable and efficient use of resources is an important part in the development and implementation of any industrial process. For the production of green ammonia, it's important to also evaluate the impact of the process on resources such as land, water, and materials. These factors are important to consider as they can influence the environmental footprint, as well as the scalability of green ammonia production.

Land use

The land use, or land footprint of the green ammonia plant is critical when dealing with large scale industrial installations. A 1500 tpd green ammonia plant needs extreme land availability if implementation is to be considered feasible. The renewables are especially resource-demanding in terms of land use, with wind turbines typically requiring around 150 km^2/GW, while the solar PV usually requires around 20 km^2/GW NREL (2016); Obane et al. (2020). The direct land use of wind turbines are only a fraction of the given number, however, in order to mitigate wake effects (turbulence, or reduced wind speed downstream), the wind turbines must be spaced a part from one another. As a result, the wind turbines requires more dedicated land area than the solar PV. Another interesting fact regarding the solar PV is that the modules in theory could be placed anywhere, on top of buildings, hovering over agricultural lands or parking lots, floating on water etc. These synergies could potentially aid in the large scale implementation of solar PV.

The land use of the electrolyzers and battery storage systems on the other hand, are not as widespread. Both come in modular installations and has the possibility of being installed in multi-floor configurations within industrial buildings, exemplified by YARA's 24 MW modular PEM installation within an old factory building on-site YARA (2022). Table 6.1 shows the land use of the various components in each scenario investigated in this thesis.

Table 6.1: Calculated land footprint for each scenario.

Description	**Solar-based scenario**	**Wind-based scenario**	**Hybrid-based scenario**
Solar PV (km^2)	65	-	7.8
Wind Turbines (km^2)	-	221	170
Electrolyzers (km^2)	0.0389	0.0227	0.0205
Batteries (km^2)	0.0159	0.0045	0.0045
Total (km^2)	65.1	221.1	177.9

In the solar-based scenario, the primary land use is for solar PV installations, requiring approximately 65 km^2 of land area, or about the same size as Manhattan. Conversely, in the wind-based scenario, wind turbines dominate the land use with about 221 km^2, around the size of the island Malta. The hybrid-based scenario uses both solar PV and wind turbines, leading to a total land use of approximately 177.9 km^2. The electrolyzers and battery banks require significantly less land area, and the areas calculated and presented in the table is a worst-case scenario where the installations are on a single plan, and not multi-floor. In this thesis, the electrolyzer installation in the wind-based scenario would take up around half a football field. However, installed on several floors the ground space would be halved, or even three times less depending on the number of floors. The same idea is valid for the battery storage system.

It is safe to say that GW scale renewable installations requires enormous land areas. This is why location is key. Fortunately, the off-grid ammonia plants considered in this thesis can be placed anywhere as long as the weather resources (wind speed and solar irradiation) is abundant. That allows us them to be situated at suitable locations where there is enough available land-area.

Water use

Water security should not be compromised and, therefore, desalinated sea water should be used for gigawatt-scale ammonia plants in most locations. The annual water consumption for production of hydrogen through electrolysis is 970 million liters. Put in perspective, the annual water consumption of a Norwegian citizen is estimated to be 51,000 liter per year, or 140 l/day Norsk Vann (2021). This means that the annual water consumed by the ammonia plant equals the annual water consumed by 19,000 Norwegian citizens, or enough to fill 388 Olympic swimming pools. This amount of fresh water consumption may cause problems, especially in areas were availability is already scarce, such as Tan-Tan, Morocco (solar-based scenario). However desalination of seawater is a cheap and good alternative to the scarce freshwater. This is also a possibility in the aforementioned location, which is situated near the ocean. High quality and pure water can be obtained from desalination at an estimated cost less than 1% of the electrolyzer costs Babarit et al. (2018), meaning that providing water for the large scale green ammonia plant is feasible at appropriate

locations, either with good freshwater resources, or close to seawater where desalination can be implemented.

Material use

The materials used in the green ammonia process, particularly in the electrolyzers, are an important consideration, especially in terms of potential shortages and the impact on large-scale deployment. Proton Exchange Membrane (PEM) electrolysis relies on precious metals such as platinum and iridium, as they are required for stable and efficient operation in the acidic membrane environment. The earth's crust shortage of iridium (only 8.17 tonnes produced annually) is particularly important to consider, given the current dependence on iridium as an electrocatalyst for PEM electrolyzers, where 1 GW of PEM electrolyzer typically requires around 0.75 tonnes of iridium Erik Eikeng (2022); IRENA and AEA (2022).

From the results of the optimization in our study, the installed capacity of the electrolyzers was found to be 1.44 GW, 0.84 GW, and 0.76 GW for the solar, wind, and hybrid scenarios respectively (Table 5.1). With these installed capacities, the iridium requirements would be approximately 1.08, 0.63, and 0.57 tonnes respectively, based on the current design of PEM electrolyzers, which is up to 1/8th of the global annual suppl iridium supply. As a result, material shortage is a real concern in the deployment of GW scale electrolyzers. This could potentially be a bottleneck for large scale implementation of green ammonia plants. Thus, a reduction in iridium amount in the electrolyzer is crucial. The best alternative as of today - ruthenium, is also a critical raw material, but without the reserve limitations that iridium suffers from. Nevertheless, further research on alternative materials must be conducted if PEM electrolyzers is to be part of future large scale implementation Erik Eikeng (2022).

On the other hand, alkaline electrolysis, which relies on more abundant materials like nickel, and solid oxide electrolysis, which uses yttrium, do not currently face the same material shortage issues. Thus, the choice of electrolysis technology as well as water source can greatly impact the sustainability and scalability of renewable ammonia production IRENA and AEA (2022).

6.4 Environmental impact

There is a substantial potential for reduction of CO_2 emissions in a green ammonia plant compared to a conventional fossil-fuel based ammonia plant. As presented in section 2.3, conventional natural gas-based (gray) ammonia production emits about 1.8 tonnes of CO_2 per tonne of ammonia. By contrast, green ammonia production can lower these emissions to below 0.1 tonne CO_2 per tonne of ammonia.

The green ammonia plant discussed in this thesis, has a production of 1500 tonnes ammonia per day, or 540,000 tonnes per year. A conventional ammonia plant of this size would emit 972,000 tonnes CO_2 per year. By contrast, the green ammonia plant would only emit around 54,000 tonnes CO_2 per year. By replacing the conventional plant with a green plant, one could potentially reduce emissions by 918,000 tonnes annually (95% reduction), equivalent to removing around 200,000 cars off the road (an average car emits

around 4.6 tonnes of CO_2 per year US EPA (2016))

In addition to the environmental benefit, the reduced emission may also provide economical benefits in terms of reduction in carbon taxes. In the EU, carbon taxes are applied with current levels around 75 USD/tNH_3, but outside of EU they are typically much lower, anywhere from 1 to 60 USD/tNH_3, and fluctuating IRENA and AEA (2022). With the potential reduction in emissions mentioned above, this could save a green ammonia plant over 68 MUSD in carbon taxes annually, compared to a conventional ammonia plant. Should the taxes increase even further, it could facilitate the establishment of green ammonia as not just an environmentally friendly alternative, but also as a more economically competitive choice compared to conventional ammonia.

6.5 The future of green ammonia

The present and future of green ammonia are dependant on several key factors. As of now, its economic competitiveness with conventional fossil-fuel based ammonia is hindered by high cost of production. This is primarily due to production of hydrogen caused by expensive electrolyzers as well as high power demands during electrolysis. If the green ammonia production is to become competitive, these cost must be lowered.

In recent years, progress has been made on these fronts. The global installed electrolyzer capacity was 0.3 GW in 2020, reached 2 GW by 2022, and will reach around 6 GW this year (2023) IEA (2023). For reference, the installed electrolyzer capacity in the solar-based scenario investigated in this thesis was 1.44 GW, almost equalling the total installed global capacity in 2022. The electrolyzer manufacturing is also expanding, and has doubled from last year (2022) to nearly 8GW per year (2023) International Renewable Energy Agency (2022-09). By this increasing rate, and by realisation of projects that have already been announced, the total installed electrolyzer capacity can reach 240GW by 2030. This will trigger economies of scale, and the electrolyzer manufacturing will see a decrease of cost, thus decreasing the cost of installing electrolyzers.

Decreasing the cost of energy is also a key part. CAPEX of the renewables constitutes nearly half the total CAPEX for the green ammonia plants. By reducing these costs, the overall cost and LCOA would be lowered as well. Fortunately, renewable energy sources are becoming more affordable. For instance, the cost of solar PV has seen a remarkable drop over the past decade, making it an increasingly viable power source for green ammonia plants. The trend of declining renewable energy costs is expected to continue, further enhancing the feasibility of green ammonia production.

Carbon taxing, as mentioned before, can also help increase green ammonia competitiveness by attributing a cost to CO_2 emissions. This economic incentive drives industries towards cleaner alternatives, and will be important if the conventional ammonia plants is to be replaced by green plants. Additionally, flexibility in the Haber-Bosch (H-B) process can also enhance the economic viability of renewable-based ammonia plants. By being able to adapt to variable energy inputs, flexible H-B units reduce the need for large, expensive energy storage solutions like batteries and hydrogen tanks. This can lead to significant cost savings, making green ammonia plants more competitive.

7 Conclusions

The purpose of this thesis has been to construct and utilize a computational framework for optimal design of a green ammonia plant. This versatile tool can be applied to any location in the world, and generate an optimal green ammonia plant solution on demand. The computations are based of off-grid wind and/or solar energy in combination with battery energy storage systems, as well as hydrogen buffer tanks. The inclusion of energy and hydrogen storage is done in order to cope with the intermittent renewable energy supply, and to provide reliable production of green ammonia. The framework further facilitates the determination of the optimal sizing of all system components, ensuring a reliable supply of ammonia at the most cost-effective point of operation.

The applicability of the framework was tested for production of 1500 tonnes of ammonia per day at three different locations/scenarios; a solar-based scenario in Tan-Tan, Morocco, a wind-based scenario in Utsira, Norway, and a hybrid scenario in Patagonia, Argentina. These diverse locations demonstrated the framework's adaptability to various renewable energy profiles and its ability to generate optimal green ammonia production strategies for any location. Additionally, it provided valuable insight into the techno-economical feasibility of large scale green ammonia implementation.

From the results of the framework, in addition to a literature review, and an in-depth background theory search, the techno-economical feasibility of the green ammonia plant has been evaluated. From an economical point of view, the levelized cost of ammonia (LCOA) is the defining cost parameter of the green ammonia plant. The LCOA obtained from the study was valued at 595 USD/tNH_3 for the solar-based scenario, 599 USD/tNH_3 for the wind based scenario, and 501 USD/tNH_3 for the hybrid scenario. The results are in line with similar research done in the field, but are still higher than the historical price point of conventional fossil-fuel based ammonia, priced around 200-600 USD/tNH_3.

Furthermore, the economical analysis provided valuable information regarding the required capital investment (CAPEX), and the annual operational costs (OPEX) for each scenario. The solar-based scenario requires a CAPEX of 3,044 MUSD and an OPEX of 67.7 MUSD, and the wind-based scenario a CAPEX of 3,198 MUSD and an OPEX of 57.2 MUSD. The hybrid scenario, on the other hand, resulted in a CAPEX of 2,626 MUSD and an OPEX of 51.8 MUSD. These cost evaluations may provide meaningful information for decision-makers and stakeholders in the green ammonia industry.

In conclusion, the computational framework developed in this thesis demonstrates the feasibility of designing optimal green ammonia plants powered by renewable energy sources. Its application to different geographic locations and at different scenarios underscores the frameworks versatility. Additionally, the economic analyses performed contribute to useful insights. While the costs associated with production of green ammonia are still higher than conventional methods, the benefits of a carbon-neutral process make green ammonia an increasingly attractive option for the future. Both the solar-based and wind-based scenarios show competitiveness, but the hybrid scenario, utilizing the synergies between solar and wind energy, sails ahead as a more stable and efficient solution, by reducing the reliance on battery storage and hydrogen storage, and providing a more continous flow of energy into the system.

8 Further work

Based on the findings of this thesis, as well as what has been discussed and concluded, some potential further work will be suggested here.

Integrate the flexible ammonia synthesis unit

The framework created in this thesis is based on a non-flexible ammonia synthesis unit (Haber-Bosch + ASU) which is operated either continuously at full rate, or is shut down. This is the conventional way, but recent research suggests that flexible units are possible. By modifying the strategy for controlling power and hydrogen flows presented in the methodology, a flexible ammonia synthesis unit could be implemented in the framework.

Include ramp-up and ramp-down times

Another aspect that should be addressed further is the inclusion of ramp-up and ramp-down times. When simulating operation of the green ammonia plant, both the electrolyzers and the ammonia synthesis unit should have ramp-up and ramp-down included. In the current framework, however, this is neglected, and both components are assumed to have instantaneous ramping times. This will necessarily overestimate the actual production and efficiency of the system, and needs to be included for a more realistic simulation.

Consider stack replacement costs

As mentioned in the discussion part of the thesis, the framework does not include replacement of electrolyzer stacks. The lifetime of the electrolyzers are typically much shorter than the plant lifetime, and must be replaced at some point during the lifetime of the plant. Including this, would mean additional costs, which would impact the assessment of the optimal plant configuration. Further work should consider the inclusion of these replacement costs to increase the accuracy of the model.

Perform sensitivity analysis

Additionally, a sensitivity analysis would provide valuable insights into how the green ammonia plant is affected by adjusting various input variables. It would be interesting to run the optimization model for various input parameters, such as different CAPEX values for all system components or various levels of flexibility for the electrolyzers and ammonia synthesis unit. Additionally, it would be beneficial to see how various amount of system shutdown (TAD), or the reliability level, would impact cost as well as point of optimal plant sizing. By allowing for more or less days of shut down would mean more or less need for energy and hydrogen storage. Running these simulations would provide useful data.

Improve computational efficiency

The current framework utilizes an iterative optimization approach, which, while straightforward and easy to implement, can be time-consuming for large-scale simulations. Exploring alternative optimization algorithms, such as linear programming, non-linear heuristic optimization methods, or parallel computing could potentially reduce the computational time and decrease the run-time of the optimization framework.

9 References

Z. Abdin and W. Mérida. Hybrid energy systems for off-grid power supply and hydrogen production based on renewable energy: A techno-economic analysis. *Energy Conversion and Management*, 196:1068–1079, September 2019. ISSN 0196-8904. doi: 10.1016/j.enconman.2019.06.068. URL https://www.sciencedirect.com/science/article/pii/S0196890419307381.

Sina Akhavan Shams and Rouhollah Ahmadi. Dynamic optimization of solar-wind hybrid system connected to electrical battery or hydrogen as an energy storage system. *International Journal of Energy Research*, 45(7):10630–10654, 2021. ISSN 1099-114X. doi: 10.1002/er.6549. URL https://onlinelibrary.wiley.com/doi/abs/10.1002/er.6549. _eprint: https://onlinelibrary.wiley.com/doi/pdf/10.1002/er.6549.

Abdulrahman S. Al-Buraiki and Abdullah Al-Sharafi. Hydrogen production via using excess electric energy of an off-grid hybrid solar/wind system based on a novel performance indicator. *Energy Conversion and Management*, 254:115270, February 2022. ISSN 0196-8904. doi: 10.1016/j.enconman.2022.115270. URL https://www.sciencedirect.com/science/article/pii/S0196890422000668.

Abdullah Al-Sharafi, Ahmet Z. Sahin, Tahir Ayar, and Bekir S. Yilbas. Techno-economic analysis and optimization of solar and wind energy systems for power generation and hydrogen production in Saudi Arabia. *Renewable and Sustainable Energy Reviews*, 69:33–49, March 2017. ISSN 1364-0321. doi: 10.1016/j.rser.2016.11.157. URL https://www.sciencedirect.com/science/article/pii/S136403211630908X.

Aida Alami. How Morocco went big on solar energy, November 2021. URL https://www.bbc.com/future/article/20211115-how-morocco-led-the-world-on-clean-solar-energy.

Souad Anouar. Morocco Has Invested $5.2 Billion in Solar Energy Projects, August 2022. URL https://www.moroccoworldnews.com/2022/08/350593/morocco-has-invested-5-2-billion-in-solar-energy-projects.

Julien Armijo and Cédric Philibert. Flexible production of green hydrogen and ammonia from variable solar and wind energy: Case study of Chile and Argentina. *International Journal of Hydrogen Energy*, 45(3):1541–1558, January 2020. ISSN 0360-3199. doi: 10.1016/j.ijhydene.2019.11.028. URL https://www.sciencedirect.com/science/article/pii/S0360319919342089.

Carlos Arnaiz del Pozo and Schalk Cloete. Techno-economic assessment of blue and green ammonia as energy carriers in a low-carbon future. *Energy Conversion and Management*, 255:115312, March 2022. ISSN 0196-8904. doi: 10.1016/j.enconman.2022.115312. URL https://www.sciencedirect.com/science/article/pii/S019689042200108X.

A. Babarit, J. C. Gilloteaux, G. Clodic, M. Duchet, A. Simoneau, and M. F. Platzer. Techno-economic feasibility of fleets of far offshore hydrogen-producing wind energy converters. *International Journal of Hydrogen Energy*, 43(15):7266–7289, 2018. doi: 10.1016/j.ijhydene.2018.02.144.

Bastien Bonnet-Cantalloube, Marie Espitalier-Noël, Priscilla Ferrari de Carvalho, Joana Fonseca, and Grzegorz Pawelec. Clean Ammonia in the future energy system. March 2023. URL https://hydrogeneurope.eu/wp-content/uploads/2023/03/2023.03_H2Europe_Clean_Ammonia_Report_DIGITAL_FINAL.pdf.

René Bañares, Dericks Gerard, Fiaschetti Maurizio, and Grünewald Philipp. Analysis of Islanded Ammonia-based Energy Storage Systems. *University of Oxford*, page 158, September 2015. URL https://eng.ox.ac.uk/media/11082/ammonia-based_ess.pdf.

Dmitri Bessarabov, Haijiang Wang, Hui Li, and Nana Zhao. *PEM Electrolysis for Hydrogen Production: Principles and Applications*. CRC Press, 2016. ISBN 978-1-4822-5232-3. Google-Books-ID: BNuYCgAAQBAJ.

Michael Birnbaum. Europe needs energy. Moroccan solar may be a clean solution. *Washington Post*, April 2023. ISSN 0190-8286. URL https://www.washingtonpost.com/climate-solutions/2023/04/13/morocco-europe-solar-desert/.

Loz Blain. World's new largest wind turbine sweeps 10 football fields per spin, January 2023. URL https://newatlas.com/energy/h260-18mw-biggest-wind-turbine/. Section: Energy.

Bob Dylan. The Times They Are A-Changin', 1963. URL http://www.bobdylan.com/songs/times-they-are-changin/.

Jörn Brauns and Thomas Turek. Alkaline water electrolysis powered by renewable energy: A review. 8(2):248, 2020. ISSN 2227-9717. doi: 10.3390/pr8020248. URL https://www.mdpi.com/2227-9717/8/2/248. Number: 2 Publisher: Multidisciplinary Digital Publishing Institute.

Silje Nornes Bryntesen, Anders Hammer Strømman, Ignat Tolstorebrov, Paul Robert Shearing, Jacob Joseph Lamb, and Odne Stokke Burheim. Opportunities for the state-of-the-art production of LIB Electrodes – A review. *1406-?*, 2021. ISSN 1996-1073. doi: 10.3390/en14051406. URL https://ntnuopen.ntnu.no/ntnu-xmlui/handle/11250/2732096. Accepted: 2021-03-08T09:59:06Z Publisher: MDPI.

Abba Lawan Bukar and Chee Wei Tan. A review on stand-alone photovoltaic-wind energy system with fuel cell: System optimization and energy management strategy. *Journal of Cleaner Production*, 221:73–88, June 2019. ISSN 0959-6526. doi: 10.1016/j.jclepro.2019.02.228. URL https://www.sciencedirect.com/science/article/pii/S095965261930633X.

Odne Stokke Burheim. Chapter 8 - hydrogen for energy storage. In Odne Stokke Burheim, editor, *Engineering Energy Storage*, pages 147–192. Academic Press, 2017. ISBN 978-0-12-814100-7. doi: https://doi.org/10.1016/B978-0-12-814100-7.00008-0. URL https://www.sciencedirect.com/science/article/pii/B9780128141007000080.

Tony Burton, Nick Jenkins, and David Sharpe. *Wind Energy Handbook*. John Wiley & Sons, Ltd, 2011. ISBN 9781119992714. doi: https://doi.org/10.1002/9781119992714.ch1. URL https://onlinelibrary.wiley.com/doi/abs/10.1002/9781119992714.ch1.

Marcelo Carmo, David L. Fritz, Jürgen Mergel, and Detlef Stolten. A comprehensive review on PEM water electrolysis. 38(12):4901–4934, 2013. ISSN 0360-3199. doi: https://doi.org/10.1016/j.ijhydene.2013.01.151. URL https://www.sciencedirect.com/science/article/pii/S0360319913002607.

W. F Castle. Air separation and liquefaction: recent developments and prospects for the beginning of the new millennium. *International Journal of Refrigeration*, 25(1): 158–172, January 2002. ISSN 0140-7007. doi: 10.1016/S0140-7007(01)00003-2. URL https://www.sciencedirect.com/science/article/pii/S0140700701000032.

Zac Cesaro, Matthew Ives, Richard Nayak-Luke, Mike Mason, and René Bañares-Alcántara. Ammonia to power: Forecasting the levelized cost of electricity from green ammonia in large-scale power plants. *Applied Energy*, 282:116009, January 2021. ISSN 0306-2619. doi: 10.1016/j.apenergy.2020.116009. URL https://www.sciencedirect.com/science/article/pii/S0306261920314549.

Marian Chatenet, Bruno G. Pollet, Dario R. Dekel, Fabio Dionigi, Jonathan Deseure, Pierre Millet, Richard D. Braatz, Martin Z. Bazant, Michael Eikerling, Iain Staffell, Paul Balcombe, Yang Shao-Horn, and Helmut Schäfer. Water electrolysis: from textbook knowledge to the latest scientific strategies and industrial developments. 51(11): 4583–4762, 2022. doi: 10.1039/D0CS01079K. URL http://dx.doi.org/10.1039/D0CS01079K. Publisher: The Royal Society of Chemistry.

Sudipta Chatterjee, Rajesh Kumar Parsapur, and Kuo-Wei Huang. Limitations of Ammonia as a Hydrogen Energy Carrier for the Transportation Sector. *ACS Energy Letters*, 6(12):4390–4394, December 2021. doi: 10.1021/acsenergylett.1c02189. URL https://doi.org/10.1021/acsenergylett.1c02189. Publisher: American Chemical Society.

Mao Cheng, Piyush Verma, Zhiwei Yang, and Richard L. Axelbaum. Flexible cryogenic air separation unit—An application for low-carbon fossil-fuel plants. *Separation and Purification Technology*, 302:122086, December 2022. ISSN 1383-5866. doi: 10.1016/j.seppur.2022.122086. URL https://www.sciencedirect.com/science/article/pii/S1383586622016410.

Jun Chi and Hongmei Yu. Water electrolysis based on renewable energy for hydrogen production. 39(3):390–394, 2018. ISSN 1872-2067. doi: https://doi.org/10.1016/S1872-2067(17)62949-8. URL https://www.sciencedirect.com/science/article/pii/S1872206717629498.

Dan Chiras. *Wind Power Basics: A Green Energy Guide*. New Society Publishers, 2010. ISBN 9780865716179.

Barun K. Das, Majed A. Alotaibi, Pronob Das, M. S. Islam, Sajal K. Das, and Md Alamgir Hossain. Feasibility and techno-economic analysis of stand-alone and grid-connected PV/Wind/Diesel/Batt hybrid energy system: A case study. *Energy Strategy Reviews*, 37:100673, September 2021. ISSN 2211-467X. doi: 10.1016/j.esr.2021.100673. URL https://www.sciencedirect.com/science/article/pii/S2211467X21000596.

S. Diaf, D. Diaf, M. Belhamel, M. Haddadi, and A. Louche. A methodology for optimal sizing of autonomous hybrid PV/wind system. *Energy Policy*, 35(11):5708–5718, November 2007. ISSN 0301-4215. doi: 10.1016/j.enpol.2007.06.020. URL https://www.sciencedirect.com/science/article/pii/S0301421507002893.

S. Diaf, M. Belhamel, M. Haddadi, and A. Louche. Technical and economic assessment of hybrid photovoltaic/wind system with battery storage in Corsica island. *Energy Policy*, 36(2):743–754, February 2008a. ISSN 0301-4215. doi: 10.1016/j.enpol.2007.10.028. URL https://www.sciencedirect.com/science/article/pii/S0301421507004788.

S. Diaf, G. Notton, M. Belhamel, M. Haddadi, and A. Louche. Design and techno-economical optimization for hybrid PV/wind system under various meteorological conditions. *Applied Energy*, 85(10):968–987, October 2008b. ISSN 0306-2619. doi: 10.1016/j.apenergy.2008.02.012. URL https://www.sciencedirect.com/science/article/pii/S0306261908000470.

Chuancheng Duan, Robert Kee, Huayang Zhu, Neal Sullivan, Liangzhu Zhu, Liuzhen Bian, Dylan Jennings, and Ryan O'Hayre. Highly efficient reversible protonic ceramic electrochemical cells for power generation and fuel production. 4(3):230–240, 2019. ISSN 2058-7546. doi: 10.1038/s41560-019-0333-2. URL https://www.nature.com/articles/s41560-019-0333-2. Number: 3 Publisher: Nature Publishing Group.

Chuancheng Duan, Jake Huang, Neal Sullivan, and Ryan O'hayre. Proton-conducting oxides for energy conversion and storage. *Applied Physics Reviews*, 7:11314, 03 2020. doi: 10.1063/1.5135319.

Sune Dalgaard Ebbesen, Søren Højgaard Jensen, Anne Hauch, and Mogens Bjerg Mogensen. High temperature electrolysis in alkaline cells, solid proton conducting cells, and solid oxide cells. 114(21):10697–10734, 2014. ISSN 0009-2665. doi: 10.1021/cr5000865. URL https://doi.org/10.1021/cr5000865. Publisher: American Chemical Society.

Jonas Egerer, Veronika Grimm, Kiana Niazmand, and Philipp Runge. The economics of global green ammonia trade – "Shipping Australian wind and sunshine to Germany". *Applied Energy*, 334:120662, March 2023. ISSN 0306-2619. doi: 10.1016/j.apenergy.2023.120662. URL https://www.sciencedirect.com/science/article/pii/S0306261923000260.

Erik Eikeng and Oscar Rogneby. A feasibility study of large scale wind powered hydrogen production. B.S. thesis, NTNU, 2021. URL https://hdl.handle.net/11250/2779955.

Elisabeth Kriegsmann. Patagonia: Argentina's Wind Energy Powerhouse and Green Hydrogen Catalysator, August 2021. URL https://ptx-hub.org/patagonia-argentinas-wind-energy-powerhouse-and-green-hydrogen\-catalysator/.

Energidepartementet. Regjeringen går videre i sin satsing på havvind, December 2022. URL https://www.regjeringen.no/no/aktuelt/regjeringen-gar-videre-i-sin-satsing-pa-havvind/id2949762/. Publisher: regjeringen.no.

Energidepartementet. Utsira Nord, May 2023. URL https://www.regjeringen.no/no/tema/energi/landingssider/havvind/utsira-nord/id2967232/. Publisher: regjeringen.no.

Eric R. Morgan. *Techno-Economic Feasibility Study of Ammonia Plants Powered by Offshore Wind*. Dissertation, University of Massachusetts Amherst, February 2013. URL https://scholarworks.umass.edu/cgi/viewcontent.cgi?article=1704&context=open_access_dissertations.

Erico Spinadel. Argentina - Wind Sector Overview, 2021. URL https://library.wwindea.org/listing/argentina/.

Erik Eikeng. Critical and Strategical Raw Materials for Electrolyzers. Specialization Project, Norwegian University of Science and Technology, Trondheim, December 2022.

Eurostat. Electricity price statistics, 2022. URL https://ec.europa.eu/eurostat/statistics-explained/index.php?title=Electricity_price_statistics.

Eurostat. Electricity production, consumption and market overview, 2023. URL https://ec.europa.eu/eurostat/statistics-explained/index.php?title=Electricity_production,_consumption_and_market_overview.

Mahdi Fasihi, Robert Weiss, Jouni Savolainen, and Christian Breyer. Global potential of green ammonia based on hybrid PV-wind power plants. *Applied Energy*, 294:116170, July 2021. ISSN 0306-2619. doi: 10.1016/j.apenergy.2020.116170. URL https://www.sciencedirect.com/science/article/pii/S0306261920315750.

Felipe Ignacio Gallardo, Andrea Monforti Ferrario, Mario Lamagna, Enrico Bocci, Davide Astiaso Garcia, and Tomas E. Baeza-Jeria. A Techno-Economic Analysis of solar hydrogen production by electrolysis in the north of Chile and the case of exportation from Atacama Desert to Japan. *International Journal of Hydrogen Energy*, 46(26): 13709–13728, April 2021. ISSN 0360-3199. doi: 10.1016/j.ijhydene.2020.07.050. URL https://www.sciencedirect.com/science/article/pii/S0360319920325842.

Frank Gambou, Damien Guilbert, Michel Zasadzinski, and Hugues Rafaralahy. A comprehensive survey of alkaline electrolyzer modeling: Electrical domain and specific electrolyte conductivity. *Energies*, 15(9), 2022. ISSN 1996-1073. doi: 10.3390/en15093452. URL https://www.mdpi.com/1996-1073/15/9/3452.

Germán Bersalli and Natalia Realpe Carrillo. An opportunity to transform the Argentinean energy system | Research Institute for Sustainability, August 2021. URL https://www.rifs-potsdam.de/en/blog/2021/08/opportunity-transform-argentinean-energy-system.

Manish Goswami and V K Goyal. Causes of Downtime in Ammonia-Urea Plants. 2012. URL https://www.faidelhi.org/Maintenance%20Practices%20and%20Case%20Studies/Downtime%20in%20ammonia-IJF%20aug%20%2012.pdf.

S. A. Grigoriev, V. N. Fateev, D. G. Bessarabov, and P. Millet. Current status, research trends, and challenges in water electrolysis science and technology. 45(49):26036–26058, 2020. ISSN 0360-3199. doi: https://doi.org/10.1016/j.ijhydene.2020.03.109. URL https://www.sciencedirect.com/science/article/pii/S0360319920310715.

Yujing Guo, Gendi Li, Junbo Zhou, and Yong Liu. Comparison between hydrogen production by alkaline water electrolysis and hydrogen production by PEM electrolysis. *IOP Conference Series: Earth and Environmental Science*, 371(4):042022, 2019. doi: 10.1088/1755-1315/371/4/042022. URL https://doi.org/10.1088/1755-1315/371/4/042022.

Haldor Topsøe and Alfa Laval. Ammonfuel An industrial view of ammonia as a marine fuel. *Siemens Gamesa Renewable Energy'*, page 59, August 2020. URL https://www.topsoe.com/hubfs/DOWNLOADS/DOWNLOADS%20-%20White%20papers/Ammonfuel%20Report%20Version%2009.9%20August%203_update.pdf.

Steven Hegedus and Antonio Luque. *Handbook of Photovoltaic Science and Engineering, Second Edition*. 03 2011. ISBN 9780470974704. doi: 10.1002/9780470974704.ch1.

Dirk Henkensmeier, Malikah Najibah, Corinna Harms, Jan Žitka, Jaromír Hnát, and Karel Bouzek. Overview: State-of-the art commercial membranes for anion exchange membrane water electrolysis. 18(2), 2020. ISSN 2381-6872. doi: 10.1115/1.4047963. URL https://doi.org/10.1115/1.4047963.

HUASUN. Himalaya G12 Series 615-635W. *Huasun Energy*, 2022. URL https://www.pvselected.com/wp-content/uploads/download/solarpanel/huasun/G12-120.pdf.

IEA. Global average levelised cost of hydrogen production by energy source and technology, 2019 and 2050 – Charts – Data & Statistics, October 2022. URL https://www.iea.org/data-and-statistics/charts/global-average-levelised-cost-of-hydrogen-production-by-energy\protect\discretionary{\char\hyphenchar\font}{}{}source-and-technology-2019-and-2050.

IEA. Electrolysers – Analysis, 2023. URL https://www.iea.org/reports/electrolysers.

Jussi Ikäheimo, Juha Kiviluoma, Robert Weiss, and Hannele Holttinen. Power-to-ammonia in future North European 100 % renewable power and heat system. *International Journal of Hydrogen Energy*, 43(36):17295–17308, September 2018. ISSN 0360-3199. doi: 10.1016/j.ijhydene.2018.06.121. URL https://www.sciencedirect.com/science/article/pii/S0360319918319931.

International Energy Agency. *Ammonia Technology Roadmap: Towards more sustainable nitrogen fertiliser production*. OECD, October 2021. ISBN 978-92-64-96568-3. doi: 10.1787/f6daa4a0-en. URL https://www.oecd-ilibrary.org/energy/ammonia-technology-roadmap_f6daa4a0-en.

IEA International Energy Agency. Net zero by 2050 a roadmap for the global energy sector. 2021. URL https://www.iea.org/reports/net-zero-by-2050.

International Renewable Energy Agency. Electrolysers – analysis, 2022-09. URL https://www.iea.org/reports/electrolysers.

International Renewable Energy Agency, IRENA. World energy transitions outlook: 1.5°c pathway 2021 edition, 2021. URL https://irena.org/publications/2021/March/World-Energy-Transitions-Outlook.

IRENA. Renewable power generation costs in 2021. 2021a. URL https://www.irena.org/-/media/Files/IRENA/Agency/Publication/2022/Jul/IRENA_Power_Generation_Costs_2021.pdf?rev=34c22a4b244d434da0accde7de7c73d8.

IRENA. Renewable Power Generation Costs, 2021b. URL https://www.irena.org/Data/View-data-by-topic/Costs/Global-Trends.

IRENA. Record Growth in Renewables Achieved Despite Energy Crisis, March 2023a. URL https://www.irena.org/News/pressreleases/2023/Mar/Record-9-point-6-Percentage-Growth-in-Renewables-.

IRENA. Renewable capacity statistics 2023, March 2023b. URL https://www.irena.org/Publications/2023/Mar/Renewable-capacity-statistics-2023.

IRENA and AEA. Innovation Outlook: Renewable Ammonia. *International Renewable Energy Agency*, 2022. URL https://www.irena.org/-/media/Files/IRENA/Agency/Publication/2022/May/IRENA_Innovation_Outlook_Ammonia_2022.pdf.

IRENA and AfDB. Renewable Energy Market Analysis: Africa and its Regions. , *International Renewable Energy Agency*, 2022. URL https://www.irena.org/-/media/Files/IRENA/Agency/Publication/2022/Jan/IRENA_Market_Africa_2022.pdf?rev=bb73e285a0974bc996a1f942635ca556.

Nikolas Ironside. Electrolysis: The backbone of the green transition. 2022. URL https://www.cowi.com/insights/electrolysis-the-backbone-of-the-green-transition.

Svetlana Ivanova and Robert Lewis. Producing Nitrogen via Pressure Swing Adsorption. *Chemical Engineering Progress*, 108(6):38–42, June 2012. ISSN 03607275. URL https://www.proquest.com/docview/1022298802/abstract/170DEF6E2E71422EPQ/1. Num Pages: 5 Place: New York, United States Publisher: American Institute of Chemical Engineers Section: Reactions and Separations.

Milind Jain, Rithu Muthalathu, and Xiao-Yu Wu. Electrified ammonia production as a commodity and energy storage medium to connect the food, energy, and trade sectors. *iScience*, 25(8):104724, August 2022. ISSN 2589-0042. doi: 10.1016/j.isci.2022.104724. URL https://www.sciencedirect.com/science/article/pii/S2589004222009968.

Pramod Jain. *Wind Energy Engineering*. McGraw-Hill Professional, 1 edition, 2010. ISBN 0071714774.

J.F Manwell, J.G McGowan, and A.L Rogers. *Wind Energy Eplained - Theory, design and application*, volume Second edition. Wiley, 2009.

A. Kaabeche, M. Belhamel, and R. Ibtiouen. Sizing optimization of grid-independent hybrid photovoltaic/wind power generation system. *Energy*, 36(2):1214–1222, February 2011. ISSN 0360-5442. doi: 10.1016/j.energy.2010.11.024. URL https://www.sciencedirect.com/science/article/pii/S0360544210006699.

Kim Chipman and Elizabeth Elkin. Farmers Catch a Break as Fertilizer Costs Fall to Pre-War Levels. *Bloomberg.com*, February 2023. URL https://www.bloomberg.com/news/articles/2023-02-24/farmers-catch-a-break-as-fertilizer-costs-fall-to-pre-war-levels.

Kiane de Kleijne, Heleen de Coninck, Rosalie van Zelm, Mark A. J. Huijbregts, and Steef V. Hanssen. The many greenhouse gas footprints of green hydrogen. *Sustainable Energy & Fuels*, 6(19):4383–4387, 2022. doi: 10.1039/D2SE00444E. URL https://pubs.rsc.org/en/content/articlelanding/2022/se/d2se00444e. Publisher: Royal Society of Chemistry.

Hossein Kord and Ahmad Rouhani. An Integrated Hybrid Power Supply for Off-Grid Applications Fed by Wind/Photovoltaic/Fuel Cell Energy Systems. *International power system conference 2009*, 2009.

S. Shiva Kumar and V. Himabindu. Hydrogen production by PEM water electrolysis – a review. 2(3):442–454, 2019. ISSN 2589-2991. doi: https://doi.org/10.1016/j.mset.2019.03.002. URL https://www.sciencedirect.com/science/article/pii/S2589299119300035.

Long Q. Le, Carolina Herradon Hernandez, Marcos Hernandez Rodriguez, Liangzhu Zhu, Chuancheng Duan, Hanping Ding, Ryan P. O'Hayre, and Neal P. Sullivan. Proton-conducting ceramic fuel cells: Scale up and stack integration. 482:228868, 2021. ISSN 0378-7753. doi: 10.1016/j.jpowsour.2020.228868. URL https://www.sciencedirect.com/science/article/pii/S0378775320311721.

Long Q. Le, Charlie Meisel, Carolina H. Hernandez, Jake Huang, Youdong Kim, Ryan O'Hayre, and Neal P. Sullivan. Performance degradation in proton-conducting ceramic fuel cell and electrolyzer stacks. 537:231356, 2022. ISSN 0378-7753. doi: 10.1016/j.jpowsour.2022.231356. URL https://www.sciencedirect.com/science/article/pii/S0378775322003688.

Markus Lehner, Robert Tichler, Horst Steinmüller, and Markus Koppe. Water electrolysis. In *Power-to-Gas: Technology and Business Models*, pages 19–39. Springer International Publishing, 2014. ISBN 978-3-319-03995-4. doi: 10.1007/978-3-319-03995-4_3. URL https://doi.org/10.1007/978-3-319-03995-4_3.

R. L. LeRoy. Industrial water electrolysis: Present and future. 8(6):401–417, 1983. ISSN 0360-3199. doi: https://doi.org/10.1016/0360-3199(83)90162-3. URL https://www.sciencedirect.com/science/article/pii/0360319983901623.

Charles Lhuillier, Pierre Brequigny, Francesco Contino, and Christine Rousselle. Combustion Characteristics of Ammonia in a Modern Spark-Ignition Engine. October 2019. doi: 10.4271/2019-24-0237. URL https://www.sae.org/content/2019-24-0237/.

Douglas R. MacFarlane, Pavel V. Cherepanov, Jaecheol Choi, Bryan H. R. Suryanto, Rebecca Y. Hodgetts, Jacinta M. Bakker, Federico M. Ferrero Vallana, and Alexandr N. Simonov. A Roadmap to the Ammonia Economy. *Joule*, 4(6):1186–1205, June 2020. ISSN 2542-4351. doi: 10.1016/j.joule.2020.04.004. URL https://www.sciencedirect.com/science/article/pii/S2542435120301732.

Akbar Maleki and Alireza Askarzadeh. Artificial bee swarm optimization for optimum sizing of a stand-alone PV/WT/FC hybrid system considering LPSP concept. *Solar Energy*, 107:227–235, September 2014. ISSN 0038-092X. doi: 10.1016/j.solener.2014.05.016. URL https://www.sciencedirect.com/science/article/pii/S0038092X1400245X.

Akbar Maleki and Fathollah Pourfayaz. Optimal sizing of autonomous hybrid photovoltaic/wind/battery power system with LPSP technology by using evolutionary algorithms. *Solar Energy*, 115:471–483, May 2015. ISSN 0038-092X. doi: 10.1016/j.solener.2015.03.004. URL https://www.sciencedirect.com/science/article/pii/S0038092X1500119X.

Augustin Mcevoy, T. Markvart, and Luis Castañer. *Practical Handbook of Photovoltaics*. 01 2012. doi: 10.1016/C2011-0-05723-X.

Esmail M. A. Mokheimer, Abdullah Al-Sharafi, Mohamed A. Habib, and Iyad Alzaharnah. A New Study for Hybrid PV/Wind off-Grid Power Generation Systems with the Comparison of Results from Homer. *International Journal of Green Energy*, 12(5):526–542, May 2015. ISSN 1543-5075. doi: 10.1080/15435075.2013.833929. URL https://doi.org/10.1080/15435075.2013.833929. Publisher: Taylor & Francis _eprint: https://doi.org/10.1080/15435075.2013.833929.

Eric Morgan, James Manwell, and Jon McGowan. Wind-powered ammonia fuel production for remote islands: A case study. *Renewable Energy*, 72:51–61, December 2014. ISSN 0960-1481. doi: 10.1016/j.renene.2014.06.034. URL https://www.sciencedirect.com/science/article/pii/S0960148114003747.

Eric R. Morgan, James F. Manwell, and Jon G. McGowan. Sustainable Ammonia Production from U.S. Offshore Wind Farms: A Techno-Economic Review. *ACS Sustainable Chemistry & Engineering*, 5(11):9554–9567, November 2017. doi: 10.1021/acssuschemeng.7b02070. URL https://doi.org/10.1021/acssuschemeng.7b02070. Publisher: American Chemical Society.

Richard Müller, Uwe Pfeifroth, Christine Träger-Chatterjee, Roswitha Cremer, Jörg Trentmann, and Rainer Hollmann. Surface Solar Radiation Data Set - Heliosat (SARAH) - Edition 1, February 2015. URL http://wui.cmsaf.eu/safira/action/viewDoiDetails?acronym=SARAH_V001. Artwork Size: 3.6 TiB Pages: 3.6 TiB.

Youssef Naimi and Amal Antar. Hydrogen generation by water electrolysis. In Murat Eyvaz, editor, *Advances In Hydrogen Generation Technologies*, chapter 1. IntechOpen, Rijeka, 2018. doi: 10.5772/intechopen.76814. URL https://doi.org/10.5772/intechopen.76814.

NASA earth observatory. Climate and Earth's Energy Budget, January 2009. URL https://earthobservatory.nasa.gov/features/EnergyBalance/page2.php. Publisher: NASA Earth Observatory.

United Nations. COP26: Together for our planet, 2021. URL https://www.un.org/en/climatechange/cop26. Publisher: United Nations.

Richard Nayak-Luke, René Bañares-Alcántara, and Ian Wilkinson. "Green" Ammonia: Impact of Renewable Energy Intermittency on Plant Sizing and Levelized Cost of Ammonia. *Industrial & Engineering Chemistry Research*, 57(43):14607–14616, October 2018. ISSN 0888-5885. doi: 10.1021/acs.iecr.8b02447. URL https://doi.org/10.1021/acs.iecr.8b02447. Publisher: American Chemical Society.

Nel Hydrogen Electrolysers. The World's Most Efficient and Reliable Electrolysers. *Nel hydrogen*, 2021. URL https://nelhydrogen.com/wp-content/uploads/2020/03/Electrolysers-Brochure-Rev-D.pdf.

Nhut Tien Nguyen, Ryuji Matsuhashi, and Tran Thi Bich Chau Vo. A design on sustainable hybrid energy systems by multi-objective optimization for aquaculture industry. *Renewable Energy*, 163:1878–1894, January 2021. ISSN 0960-1481. doi: 10.1016/j.renene.2020.10.024. URL https://www.sciencedirect.com/science/article/pii/S0960148120315901.

Norsk Vann. Vannforsyning og drikkevann, August 2021. URL https://norskvann.no/vannforsyning-og-drikkevann/.

Shahmir Ali Nosherwani and Rui Costa Neto. Techno-economic assessment of commercial ammonia synthesis methods in coastal areas of Germany. *Journal of Energy Storage*, 34:102201, February 2021. ISSN 2352-152X. doi: 10.1016/j.est.2020.102201. URL https://www.sciencedirect.com/science/article/pii/S2352152X20320247.

NREL. Land Use by System Technology, 2016. URL https://www.nrel.gov/analysis/tech-size.html.

NVE. Data for utbygde vindkraftverk i Norge, April 2023. URL https://www.nve.no/energi/energisystem/vindkraft/data-for-utbygde-vindkraftverk-i-norge/.

Hideaki Obane, Yu Nagai, and Kenji Asano. Assessing land use and potential conflict in solar and onshore wind energy in Japan. *Renewable Energy*, 160:842–851, November 2020. ISSN 0960-1481. doi: 10.1016/j.renene.2020.06.018. URL https://www.sciencedirect.com/science/article/pii/S0960148120309125.

Ola Osman, Sgouris Sgouridis, and Andrei Sleptchenko. Scaling the production of renewable ammonia: A techno-economic optimization applied in regions with high insolation. *Journal of Cleaner Production*, 271:121627, June 2020. doi: 10.1016/j.jclepro.2020.121627. URL https://www.sciencedirect.com/science/article/pii/S0959652620316747.

Stefan Pfenninger and Iain Staffell. Renewables ninja. Available at: https://www.renewables.ninja/, 2022. URL https://www.renewables.ninja/.

PVGIS. PVGIS data sources & calculation methods, 2021. URL https://joint-research-centre.ec.europa.eu/pvgis-online-tool/getting-started-pvgis/pvgis-data-sources-calculation-methods_en.

Mamoon Rashid, Mohammed Al Mesfer, Hamid Naseem, and Mohd Danish. Hydrogen production by water electrolysis: A review of alkaline water electrolysis, pem water electrolysis and high temperature water electrolysis. *International Journal of Engineering and Advanced Technology*, ISSN:2249–8958, 02 2015. URL https://www.researchgate.net/publication/273125977_Hydrogen_Production_by_Water_Electrolysis_A_Review_of_Alkaline_Water_Electrolysis_PEM_Water_Electrolysis_and_High_Temperature_Water_Electrolysis.

Reiner Korthauer. *Lithium-Ion Batteries: Basics and Applications*. Springer-Verlag Berlin and Heidelberg GmbH & Co. K, 2018. URL https://www.bokkilden.no/energi-kraftproduksjon-distribusjon-og-lagring/lithium-ion-batteries-basics-and-applications-reiner-korthauer/produkt.do?produktId=14470530.

Michele M. Rienecker, Max J. Suarez, Ronald Gelaro, Ricardo Todling, Julio Bacmeister, Emily Liu, Michael G. Bosilovich, Siegfried D. Schubert, Lawrence Takacs, Gi-Kong Kim, Stephen Bloom, Junye Chen, Douglas Collins, Austin Conaty, Arlindo Da Silva, Wei Gu, Joanna Joiner, Randal D. Koster, Robert Lucchesi, Andrea Molod, Tommy Owens, Steven Pawson, Philip Pegion, Christopher R. Redder, Rolf Reichle, Franklin R. Robertson, Albert G. Ruddick, Meta Sienkiewicz, and Jack Woollen. MERRA: NASA's Modern-Era Retrospective Analysis for Research and Applications. *Journal of Climate*, 24(14):3624–3648, July 2011. ISSN 0894-8755, 1520-0442. doi: 10.1175/JCLI-D-11-00015.1. URL http://journals.ametsoc.org/doi/10.1175/JCLI-D-11-00015.1.

Kevin H. R. Rouwenhorst, Aloijsius G. J. Van der Ham, Guido Mul, and Sascha R. A. Kersten. Islanded ammonia power systems: Technology review & conceptual process design. *Renewable and Sustainable Energy Reviews*, 114:109339, October 2019. ISSN 1364-0321. doi: 10.1016/j.rser.2019.109339. URL https://www.sciencedirect.com/science/article/pii/S1364032119305477.

Kevin Hendrik Reindert Rouwenhorst. *Power-to-ammonia-to-power (P2A2P) for local electricity storage in 2025: Current developments, process proposal & future research required*. PhD thesis, August 2018.

Nicholas Salmon and René Bañares-Alcántara. A global, spatially granular techno-economic analysis of offshore green ammonia production. *Journal of Cleaner Production*, 367:133045, September 2022. ISSN 0959-6526. doi: 10.1016/j.jclepro.2022.133045. URL https://www.sciencedirect.com/science/article/pii/S0959652622026361.

M. M. Samy, S. Barakat, and H. S. Ramadan. Techno-economic analysis for rustic electrification in Egypt using multi-source renewable energy based on PV/ wind/ FC. *International Journal of Hydrogen Energy*, 45(20):11471–11483, April 2020. ISSN 0360-3199. doi: 10.1016/j.ijhydene.2019.04.038. URL https://www.sciencedirect.com/science/article/pii/S0360319919314296.

O. Schmidt, A. Gambhir, I. Staffell, A. Hawkes, J. Nelson, and S. Few. Future cost and performance of water electrolysis: An expert elicitation study. *International Journal of Hydrogen Energy*, 42(52):30470–30492, 2017. ISSN 0360-3199. doi: https://doi.org/10.1016/j.ijhydene.2017.10.045.

Xiaofei Shi, Yu Qian, and Siyu Yang. Fluctuation Analysis of a Complementary Wind–Solar Energy System and Integration for Large Scale Hydrogen Production. *ACS Sustainable Chemistry & Engineering*, 8(18):7097–7110, May 2020. doi: 10.1021/acssuschemeng.0c01054. URL https://doi.org/10.1021/acssuschemeng.0c01054. Publisher: American Chemical Society.

Yixiang Shi, Ningsheng Cai, Tianyu Cao, and Jiujun Zhang. *High-Temperature Electrochemical Energy Conversion and Storage: Fundamentals and Applications*. CRC Press, 2017. doi: 10.1201/b22506.

J. Sigurvinsson, C. Mansilla, P. Lovera, and F. Werkoff. Can high temperature steam electrolysis function with geothermal heat? 32(9):1174–1182, 2007. ISSN 0360-3199. doi: https://doi.org/10.1016/j.ijhydene.2006.11.026. URL https://www.sciencedirect.com/science/article/pii/S0360319906005829.

E. Skoplaki and J. A. Palyvos. On the temperature dependence of photovoltaic module electrical performance: A review of efficiency/power correlations. *Solar Energy*, 83 (5):614–624, May 2009. ISSN 0038-092X. doi: 10.1016/j.solener.2008.10.008. URL https://www.sciencedirect.com/science/article/pii/S0038092X08002788.

Mariem Smaoui, Achraf Abdelkafi, and Lotfi Krichen. Optimal sizing of stand-alone photovoltaic/wind/hydrogen hybrid system supplying a desalination unit. *Solar Energy*, 120:263–276, October 2015. ISSN 0038-092X. doi: 10.1016/j.solener.2015.07.032. URL https://www.sciencedirect.com/science/article/pii/S0038092X1500403X.

Luca Spelorzi. *Technical-economic feasibility analysis of green hydrogen production in Patagonia through wind energy, and transport to Italy for the decarbonisation of steel industry*. laurea, Politecnico di Torino, October 2022. URL https://webthesis.biblio.polito.it/24216/.

E. Taibi, H. Blanco, R. Miranda, M. Carmo, D. Gielen, and R. Roesch. Green hydrogen cost reduction: Scaling up electrolysers to meet the 1.5C climate goal. *IRENA*, 2020. URL https://www.irena.org/publications/2020/Dec/Green-hydrogen-cost-reduction.

H. Tebibel. Battery energy storage system for enhancing the electrolyzer capacity factor in small-scale WindtH2 system with a smoothing control strategy: Constrained multi-objective Pareto optimization and case study in Algeria. *Journal of Energy Storage*, 52: 105017, August 2022. ISSN 2352-152X. doi: 10.1016/j.est.2022.105017. URL https://www.sciencedirect.com/science/article/pii/S2352152X22010209.

Hammou Tebibel. Methodology for multi-objective optimization of wind turbine/battery/electrolyzer system for decentralized clean hydrogen production using an adapted power management strategy for low wind speed conditions. *Energy Conversion and Management*, 238:114125, June 2021. ISSN 0196-8904. doi: 10.1016/j.enconman.2021.114125. URL https://www.sciencedirect.com/science/article/pii/S0196890421003010.

The royal society. The role of hydrogen and ammonia in meeting the net zero challenge. *CLIMATE CHANGE : SCIENCE AND SOLUTIONS*, 2021.

The royal society of chemistry. Periodic Table – Royal Society of Chemistry, 2023. URL https://www.rsc.org/periodic-table/.

TRACTEBEL ENGIE and HINICIO. Study on early business cases for H2 in energy storage and more broadly power to H2 applications. *Fuel Cells and Hydrogen Joint Undertaking (FCHJU)*, 2017.

Alfredo Ursua, Luis M. Gandía, and Pablo Sanchis. Hydrogen production from water electrolysis: Current status and future trends. *Proceedings of the IEEE*, 100:410–426, 02 2012. doi: 10.1109/JPROC.2011.2156750.

U.S. Department of Energy. Potential Roles of Ammonia in a Hydrogen Economy. *U.S. Department of Energy*, 2006. URL https://www.energy.gov/eere/fuelcells/articles/potential-roles-ammonia-hydrogen-economy.

U.S. Energy Information Administration. U.S. ammonia prices rise in response to higher international natural gas prices, May 2022. URL https://www.eia.gov/todayinenergy/detail.php?id=52358.

OAR US EPA. Tailpipe Greenhouse Gas Emissions from a Typical Passenger Vehicle, January 2016. URL https://www.epa.gov/greenvehicles/tailpipe-greenhouse-gas-emissions-typical-passenger-vehicle.

Kevin Verleysen, Alessandro Parente, and Francesco Contino. How does a resilient, flexible ammonia process look? Robust design optimization of a Haber-Bosch process with optimal dynamic control powered by wind. *Proceedings of the Combustion Institute*, July 2022. ISSN 1540-7489. doi: 10.1016/j.proci.2022.06.027. URL https://www.sciencedirect.com/science/article/pii/S1540748922000347.

Vestas. EnVentus, 2023. URL https://nozebra.ipapercms.dk/Vestas/Communication/Productbrochure/enventus/enventus-platform-brochure/?page=12.

Immanuel Vincent and Dmitri Bessarabov. Low cost hydrogen production by anion exchange membrane electrolysis: A review. 81:1690–1704, 2018. ISSN 1364-0321. doi: 10.1016/j.rser.2017.05.258. URL https://www.sciencedirect.com/science/article/pii/S1364032117309127.

Changlong Wang, Stuart D. C. Walsh, Thomas Longden, Graham Palmer, Israel Lutalo, and Roger Dargaville. Optimising renewable generation configurations of off-grid green ammonia production systems considering Haber-Bosch flexibility. *Energy Conversion and Management*, 280:116790, March 2023. ISSN 0196-8904. doi: 10.1016/j.enconman.2023.116790. URL https://www.sciencedirect.com/science/article/pii/S019689042300136X.

Shan Wang, Aolin Lu, and Chuan-Jian Zhong. Hydrogen production from water electrolysis: role of catalysts. 8(1):4, 2021. ISSN 2196-5404. doi: 10.1186/s40580-021-00254-x. URL https://doi.org/10.1186/s40580-021-00254-x.

Philip R. Wolfe. *The Solar Generation: Childhood and Adolescence of Terrestrial Photovoltaics*. John Wiley & Sons, May 2018. ISBN 978-1-119-42558-8. Google-Books-ID: WbpaDwAAQBAJ.

Feixiang Wu, Joachim Maier, and Yan Yu. Guidelines and trends for next-generation rechargeable lithium and lithium-ion batteries. *Chemical Society Reviews*, 49(5):1569–1614, 2020. doi: 10.1039/C7CS00863E. URL https://pubs.rsc.org/en/content/articlelanding/2020/cs/c7cs00863e. Publisher: Royal Society of Chemistry.

Zhimin Yang, Yi Chai, Hongpeng Yin, and Songbing Tao. LPV Model Based Sensor Fault Diagnosis and Isolation for Permanent Magnet Synchronous Generator in Wind Energy Conversion Systems. *Applied Sciences*, 8(10):1816, October 2018. ISSN 2076-3417. doi: 10.3390/app8101816. URL https://www.mdpi.com/2076-3417/8/10/1816. Number: 10 Publisher: Multidisciplinary Digital Publishing Institute.

YARA. Åpner for historisk satsing på grønt hydrogen og grønn ammoniakk i Norge | Yara International, February 2021. URL https://www.yara.com/corporate-releases/apner-for-historisk-satsing-pa-gront-hydrogen-og-gronn-ammoniakk-i-norge/.

YARA. Yara and Linde Engineering agree to build a 24 MW green hydrogen demonstration plant in Norway. Both companies aim to achieve a significant carbon dioxide reduction in the production of fertilizers in Norway | Yara International, January 2022. Available online: https://www.yara.com/corporate-releases/yara-and-linde-engineering-agree\-to-build-a-24-mw-green-hydrogen-demonstration-plant-in-norway.-both-companies\-aim-to-achieve-a-significant-\carbon-dioxide-reduction-in-the-production-of-fertilizers-in-norway/.

A Appendix

Presentation of the various LCOA calculations obtained from literature study.

Table A.1: Comparison of LCOA across different scenarios and studies

Scenario/Study	**LCOA (USD/tNH_3)**
Hybrid scenario from this thesis	501
Solar-based scenario from this thesis	595
Wind-based scenario from this thesis	599
Morgan's wind-based scenario[3]	447-942
Wang's hybrid scenario[5]	530
Egerer's hybrid scenario[9]	590
Arnaiz del Pozo's hybrid scenarios[8]	569-772
Cesaro's Solar-based scenario[1]	634
Armijo's hybrid scenarios[2]	487-710
Wang's solar-based scenario[5]	670
Osman's solar-based scenario[6]	718
Nayak-Luke's hybrid scenario[7]	720
Wang's wind-based scenario[5]	750

[1](Cesaro et al., 2021), [2](Armijo and Philibert, 2020), [3](Morgan et al., 2014), [4](Bañares et al., 2015), [5](Wang et al., 2023), [6](Osman et al., 2020), [7](Nayak-Luke et al., 2018), [8](Arnaiz del Pozo and Cloete, 2022), [9](Egerer et al., 2023),

B Appendix

Illustration of the hours during one year of production where the system is shut down for all the scenario evaluated in the thesis.

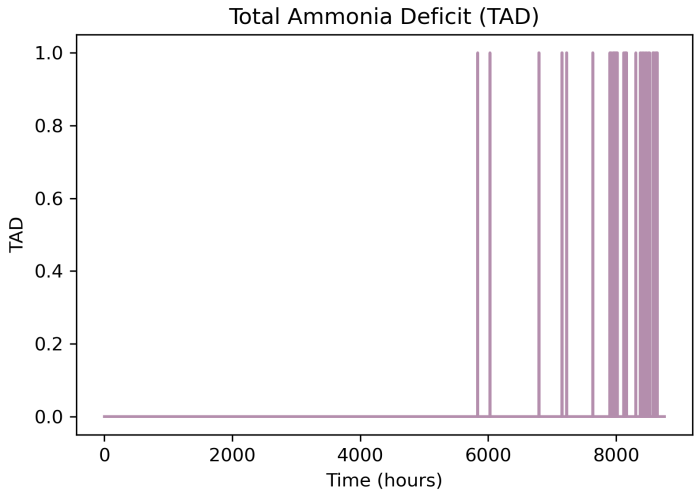

Figure B.1: Hourly total ammonia deficit of the Solar-based scenario

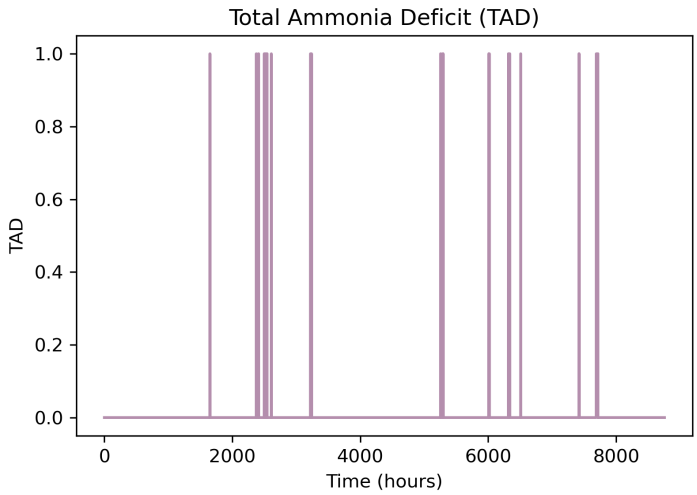

Figure B.2: Hourly total ammonia deficit of the Wind-based scenario

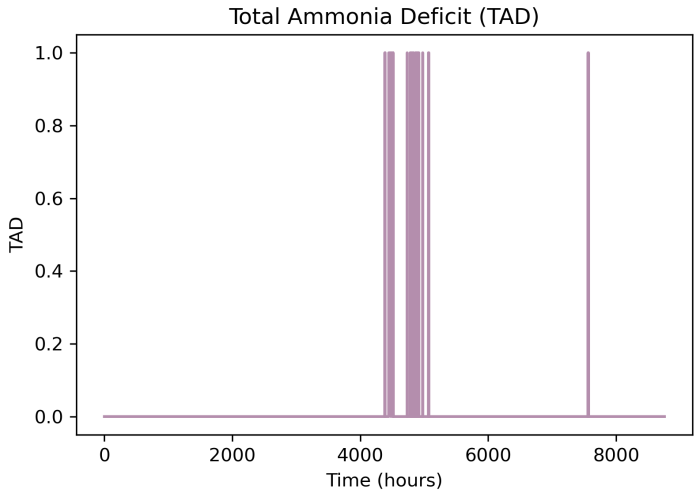

Figure B.3: Hourly total ammonia deficit of the hybrid scenario

C Appendix

Illustration of the energy requirement breakdown for the power demanding components in the green ammonia plant.

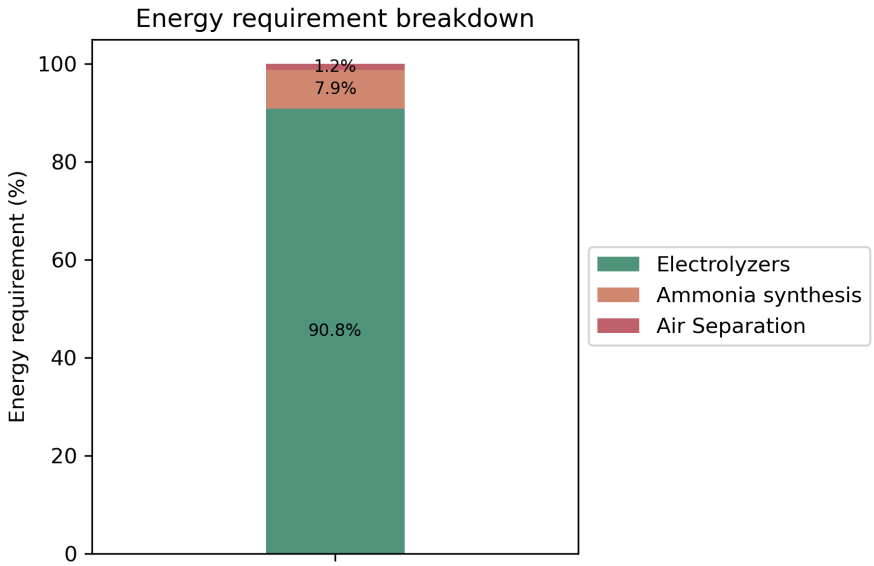

Figure C.1: Energy requirement breakdown for the green ammonia plant

D Appendix

The python script used to calculate hourly energy production from a 1 kW wind turbine and a 1 kW solar PV. This is for scaling up during the optimization algorithm.

```
""" Calculate energy production from solar PV and wind turbine """

import pandas as pd

# Read the irradiation and wind speed CSV files into a Pandas DataFrame
solar_df = pd.read_csv('G:/My Drive/Masters Project/Excel
↪  files/TEST_PV.csv', skiprows=10)
wind_df = pd.read_csv('G:/My Drive/Masters Project/Excel
↪  files/TEST_WT.csv', skiprows=2)

# Extract the solar irradtion data in column F (6th column, hence 5)
# from row 12 to row 8771. Also add all values to a list
solar_irradiation = solar_df.iloc[0:8760, 5].tolist()

# Extract the ambiant air temperature data in column H (8th column, hence
↪  7) from row 12 to row 8771. Also add all values to a list
ambient_temperature = solar_df.iloc[0:8760, 7].tolist()

# Extract the wind data in column F (6th column, hence 5) from row 4 to
↪  row 8767
wind_speed = wind_df.iloc[0:8765, 5].tolist()

# Define parameters for the PV system
Df = 0.9 # derating factor (decimal point)
G_ref = 1000 # reference irradiation (W)
NOCT = 44 # nominal cell operating temperatured (degC)
Kt = -3.7E-3 # 1/degC
P_rated = 1000 # rated installed capacity of PV module (W)
T_ref = 25 # reference cell temperature (degC)
eta = 0.24 # solar PV efficiency (decimal point)

# Define a function to calculate the PV output in kW for each timestep
def calculate_pv_output(solar_irradiation, ambient_temperature):
    P_pv = P_rated * Df * (solar_irradiation / G_ref) * (1 + Kt *
    ↪  ((ambient_temperature - T_ref) / 5) * ((NOCT - 20) / 80))
    return P_pv

# Calculate the PV output for each timestep using empty lists
pv_output = []
for i in range(len(solar_irradiation)):
```

```
    pv_output.append(calculate_pv_output(solar_irradiation[i],
    ↪  ambient_temperature[i]))

# Define parameters for the Wind Turbine system
P_rated = 1000 # rated installed capacity of wind turbine (W)
v_ci = 3 # cut in wind speed (m/s)
v_co = 25 # cut out wind speed (m/s
v_r = 12 # rated wind speed (m/s)

# Define a function to calculate the wind turbine output in kW for each
↪  timestep
def calculate_wt_output(wind_speed):
    if wind_speed <= v_ci or wind_speed >= v_co:
        P_wt = 0
    elif v_ci < wind_speed < v_r:
        P_wt = P_rated * ((wind_speed**3 - v_ci**3)/(v_r**3 - v_ci**3))
    elif v_r <= wind_speed < v_co:
        P_wt = P_rated
    else:
        P_wt = 0
    return P_wt

# Calculate the PV output for each timestep using empty lists
wt_output = []
for i in range(len(wind_speed)):
    wt_output.append(calculate_wt_output(wind_speed[i]))


""" End of wind and solar pv production calculation """
```

E Appendix

The script representing the optimization framework, or the iterative optimization code used for calculations performed in this thesis. This script mimics the system behaviour of a green ammonia plant.

```
""" Read input data from wind and solar pv production"""


# Read the pv and wind data CSV files into a Pandas DataFrame
solar_df = pd.read_csv("C:/Users/Bruker/Downloads/ninja_pv_patagonia.csv",
↪  skiprows=3)
wind_df =
↪  pd.read_csv("C:/Users/Bruker/Downloads/ninja_wind_patagonia.csv",
↪  skiprows=3)

# Extract and list the hourly solar power from 1kWp data over 1 year
solar_power_1kwp = solar_df["electricity"].iloc[0:8760].values.tolist()

# Extract and list the hourly wind power from 1kWp data over 1 year
wind_power_1kwp = wind_df["electricity"].iloc[0:8765].values.tolist()

# Define simulation time step  and period in hours
dt = 1 # timestep (h)
t_sim = 8760 # period (h)

# Introduce TAD threshold to limit number of iterations
TAD_threshold = (24*5)
TAD_threshold_days = TAD_threshold/24

""" Define parameters and initial conditions """

# Define energy consumption parameters
e_elz_h2 = 49 # energy demand by electrolyzers (kWh/kgH2)
e_elz_nh3 = 8.71 # energy demand by electrolyzers (kWh/kgNH3)
e_hb = 0.6 # energy demand for haber bosch unit for NH3 prod (kWh/kgNH3)
e_psa = 0.119 # energy demand for air separation unit for N2 prod
↪  (kWh/kgNH2)
e_syngas_compression = 0.16 # energy demand for pre-compression of syngas
↪  (kWh/kgNH3)
e_as = e_hb + e_psa + e_syngas_compression # energy demand for continuous
↪  ammonia synthesis (kWh/kgNH3)
h2O_demand = 10 # l H2O/kgH2


# Define initial conditions
```

```
tonnes_nh3_prod_day = 1500
tonnes_nh3_prod_year = tonnes_nh3_prod_day * (365-TAD_threshold_days) #
↪  yearly ammonia production (tonnesNH3/y)
tonnes_nh3_prod_year_real = tonnes_nh3_prod_day * (335)
kg_nh3_prod_year = tonnes_nh3_prod_year * 1000 # yearly ammonia production
↪  (kgNH3/y)
kg_nh3_prod_hour = kg_nh3_prod_year * (1/8760) # hourly ammonia production
↪  (kgNH3/h)
m_h2_asu_year = kg_nh3_prod_year * 0.1777 # yearly h2 demand for asu
↪  (kgH2/y)
m_h2_asu_hour = kg_nh3_prod_hour * 0.1777 # hourly h2 demand for asu
↪  (kgH2/h)
m_n2_asu_year = kg_nh3_prod_year * 0.8223 # yearly n2 demand for asu
↪  (kgH2/y)
m_n2_asu_hour = kg_nh3_prod_hour * 0.8223 # hourly n2 demand for asu
↪  (kgH2/h)
p_hb_installed = kg_nh3_prod_hour * e_hb # installed haber-bosch cap (kW)
p_psa_installed =  m_n2_asu_hour * e_psa # installed PSA cap (kW)
p_syngas_compression = kg_nh3_prod_hour * e_syngas_compression # installed
↪  cap of syngas compressor (kW)
p_asu_installed = p_hb_installed + p_psa_installed + p_syngas_compression
↪  # installed ammonia synthesis unit cap (kW)
p_elz_installed = m_h2_asu_hour * e_elz_h2 # theoretically minimum
↪  required installed electrolyzer capacity kW
p_total = p_elz_installed + p_asu_installed # kW (used for finding
↪  ranges)

""" Adjust system component installed cap ranges based on annual NH3
↪  demand """

# Calculate dynamic step sizes based on demand
wt_step = max(p_total * 0.05, 0.05)
pv_step = max(p_total * 0.05, 0.05)
elz_step = max(p_elz_installed * 0.03, 0.5)
bat_step = max(p_asu_installed * 6, 0.5)
h2tank_step = max(m_h2_asu_hour * 12, 0.1)

# Adjust the ranges based on demand and dynamic step sizes
wt_min, wt_max = (p_total * 1.5), (p_total * 3)
pv_min, pv_max = (p_total * 0.1), (p_total * 0.6)
elz_min, elz_max = (p_elz_installed * 1), (p_elz_installed * 1.3)
bat_min, bat_max = (p_asu_installed), (p_asu_installed * (24))
h2tank_min, h2tank_max = (m_h2_asu_hour * (24*2)), (m_h2_asu_hour *
↪  (24*6))
wt_range = np.arange(wt_min, wt_max + wt_step, wt_step)
pv_range = np.arange(pv_min, pv_max + pv_step, pv_step)
```

```
elz_range = np.arange(elz_min, elz_max + elz_step, elz_step)
bat_range = np.arange(bat_min, bat_max + bat_step, bat_step)
h2tank_range = np.arange(h2tank_min, h2tank_max + h2tank_step,
↪  h2tank_step)

# Calculate dynamic step sizes based on demand
wt_step = max(p_total * 0.025, 0.05)
pv_step = max(p_total * 0.025, 0.05)
elz_step = max(p_elz_installed * 0.03, 0.5)
bat_step = max(p_asu_installed * 6, 0.5)
h2tank_step = max(m_h2_asu_hour * 12, 0.1)

# Adjust the ranges based on demand and dynamic step sizes
wt_min, wt_max = (p_total * 1.92), (p_total * 1.99)
pv_min, pv_max = (p_total * 0.64), (p_total * 0.78)
elz_min, elz_max = (p_elz_installed * 1.35), (p_elz_installed * 1.45)
bat_min, bat_max = (p_asu_installed), (p_asu_installed * (24))
h2tank_min, h2tank_max = (m_h2_asu_hour * (24)), (m_h2_asu_hour * (24*6))
wt_range = np.arange(wt_min, wt_max + wt_step, wt_step)
pv_range = np.arange(pv_min, pv_max + pv_step, pv_step)
elz_range = np.arange(elz_min, elz_max + elz_step, elz_step)
bat_range = np.arange(bat_min, bat_max + bat_step, bat_step)
h2tank_range = np.arange(h2tank_min, h2tank_max + h2tank_step,
↪  h2tank_step)


""" Define empty arrays and lists for storing simulation data """


# Define arrays to store system operation results found from iterations
p_wt = np.zeros(t_sim) # power produced by wt
p_pv = np.zeros(t_sim) # power produced by pv
p_re = np.zeros(t_sim) # total power produced (by wt and pv combined)
p_tot = np.zeros(t_sim) # total power available after asu has recievied
↪  input
c_h2tank = np.zeros(t_sim) # state of charge of h2 tank (kgH2)
c_bat = np.zeros(t_sim) # state of charge of batteries (kWh)
p_elz = np.zeros(t_sim) # power consumed by electrolyzers (kW)
p_bat_in = np.zeros(t_sim) # power charged from batteries (kW)
p_bat_out = np.zeros(t_sim) # power discharged by batteries (kW)
p_asu = np.zeros(t_sim) # power consusmed by ammonia synthesis unit (kW)
m_h2_elz = np.zeros(t_sim) # hydrogen produced by electrolyzers (kgH2/h)
m_h2_asu = np.zeros(t_sim) # hydrogen consumed by ammonia synthesis unit
↪  (kgH2/h)
m_h2tank_in = np.zeros(t_sim) # hydrogen charged into h2 tanks (kgH2/h)
```

```
m_h2tank_out = np.zeros(t_sim) # hydrogen discharged from h2 tanks
↪  (kgH2/h)
energy_curt = np.zeros(t_sim) # energy curtailed. i.e., excess prodcution

# Create empty list for storing simulation results
simulation_results = []


""" Define functions to calculate CAPEX, OPEX and LCOA """


# Calculate CAPEX of system comp and give output as capex array
def calculate_capex(wt, pv, elz, bat, h2tank, p_hb_installed,
↪  p_syngas_compression, p_psa_installed):
    """ calculates the capex for each system component based on the
        system components installed capacity """

    capex_wt = 1150 * wt # USD
    capex_pv = 475 * pv # USD
    capex_bat = 250 * bat # USD
    capex_elz = 610 * elz # USD
    capex_h2tank = 400 * h2tank # USD
    capex_asu = 2837 * (p_hb_installed + p_syngas_compression) # USD
    capex_psa = 3490 * (p_psa_installed) # USD

    capex = np.array([capex_wt, capex_pv, capex_bat, capex_elz,
    ↪  capex_h2tank, capex_asu, capex_psa])
    return capex

def calculate_opex(capex):
    """ calculates the opex for each system component based on the
        capex array for each component """

    opex_wt = 0.02 * capex[0] # 2% of CAPEX
    opex_pv = 0.02 * capex[1] # 2% of CAPEX
    opex_bat = 0.01 * capex[2] # 1% of CAPEX
    opex_elz = 0.03 * capex[3] # 3% of CAPEX
    opex_h2tank = 0 * capex[4] # 0% of CAPEX
    opex_asu = 0.05 * capex[5] # 5% of CAPEX
    opex_psa = 0.02 * capex[6] # 2% of CAPEX

    opex = np.array([opex_wt, opex_pv, opex_bat, opex_elz, opex_h2tank,
    ↪  opex_asu, opex_psa])
    return opex

def calculate_lcoa(capex, opex, annual_ammonia_prod):
```

```
    """ calculates LCOA for a system given capex and opex arrays for each
        system component and annual ammonia prod"""
    plant_lifetime = 30  # years
    discount_rate = 0.075  # 10% per year

    # Calculate the annualized capital cost (ann_capex) for each
    ↪ component
    ann_capex = (capex * (discount_rate * (1 +
    ↪ discount_rate)**plant_lifetime)) / ((1 +
    ↪ discount_rate)**plant_lifetime -1)

    # Calculate the total annual cost (TAC) for each component
    tac = ann_capex + opex

    # Calculate the Levelized Cost of Ammonia (LCOA)
    lcoa = np.sum(tac) / annual_ammonia_prod  # USD/tonneNH3
    return lcoa


""" Define function to calculate elz constraints """


# Define a function to calculate the electrolyzer operational constraints
↪ based on the given capacity
def calculate_elz_constraints(elz):
    p_elz_max = elz * 1.15
    p_elz_min = elz * 0.15
    return p_elz_max, p_elz_min


""" Create variable to store configurations and lcoa """


# Create a variable to store the system configuration with the lowest
↪ LCOA
min_lcoa = float('inf')
best_config = None
best_results = None
best_hourly_results = None


""" Start the system simulations """


# Start the nested loop, iterative procedure to find the solutions and
↪ results
```

```
for wt in wt_range:  # wt is the installed wt capacity for this sys config
↪  (kW)
    for pv in pv_range:  # pv is the installed pv capacity (kW)
        for elz in elz_range:  # elz is the installed electrolyzer
        ↪  capacity (kW)
            # Calculate electrolyzer operational constraints
            p_elz_max, p_elz_min = calculate_elz_constraints(elz)
            for bat in bat_range:  # bat is the installed bettery capacity
            ↪  (kW)
                for h2tank in h2tank_range:  # h2tank is the inst. h2tank
                ↪  cap (kW)

                    # Reset simulation results and TAD for each system
                    ↪  configuration
                    simulation_results = []
                    TAD = np.zeros(t_sim) # total ammonia deficit (decimal
                    ↪  point)
                    total_TAD = 0

                    # Definitions and operational constraints
                    c_bat_max = bat  # max battery capacity (kWh)
                    c_bat_min = 0.2 * bat  # min battery capacity (kWh)
                    c_h2tank_max = h2tank  # max h2 tank capacity (kgH2)
                    c_h2tank_min = 0  # min h2 tank capacity (kgH2)

                    # Add a print statement here to track progress
                    print(f"Currently simulating: wt={wt}, pv={pv},
                    ↪  elz={elz}, bat={bat}, h2tank={h2tank}")

                    for t in range(t_sim):
                        # Calculate power generated
                        p_wt[t] = wt * wind_power_1kwp[t] # scaled up
                        ↪  power output from wt (kW)
                        p_pv[t] = pv * solar_power_1kwp[t] # scaled up
                        ↪  power output from pv (kW)
                        p_re[t] = p_wt[t] + p_pv[t]  # total renewable
                        ↪  power output (kW)
                        p_tot[t] = p_re[t] - p_asu_installed  # total
                        ↪  power output after asu demands (kW)

                        # Set initial state of charge for battery and h2
                        ↪  tank
                        if t == 0:
                            c_bat[t], c_h2tank[t] = c_bat_max,
                            ↪  c_h2tank_max
                        else:
```

```
        c_bat[t], c_h2tank[t] = c_bat[t-1],
        ↪  c_h2tank[t-1]

    # Case 1: not enough power to fully power asu (nor
    ↪  elz)
    if p_tot[t] < 0:
        power_deficit = abs(p_tot[t])
        m_h2_deficit = m_h2_asu_hour
        m_h2_elz[t], p_bat_in[t], p_elz[t],
        ↪  energy_curt[t], m_h2tank_in[t]  = (0,) * 5

        # Check if battery has enough charge to cover
        ↪  the deficit
        if (c_bat[t-1] - abs(power_deficit * dt)) >=
        ↪  c_bat_min and (c_h2tank[t-1] -
        ↪  (m_h2_deficit * dt)) >= c_h2tank_min:
            p_bat_out[t] = abs(power_deficit) # Power
            ↪  supplied by batteries to cover
            ↪  renewable deficit (kW)
            p_asu[t] = p_re[t] + p_bat_out[t] # Power
            ↪  consumed by the asu (kW)
            m_h2tank_out[t] = m_h2_deficit # H2 tank
            ↪  completely supplies H2 to asu
            ↪  (kgH2/h)
            m_h2_asu[t] = m_h2tank_out[t] # asu demand
            ↪  completely supplied by H2 tank
            ↪  (kgH2/h)

        else:
            # Not enough battery charge - system shuts
            ↪  down
            p_asu[t], p_bat_out[t], m_h2tank_out[t],
            ↪  m_h2_asu[t] = (0,) * 4


    # Case 2: Not enough excess power for h2 prod by
    ↪  elz, but enough to fully power asu
    elif (0 <= p_tot[t]) and (p_tot[t] < p_elz_min):
        power_available_for_bat = p_tot[t]
        m_h2_deficit = m_h2_asu_hour
        p_bat_out[t], p_elz[t], m_h2_elz[t],
        ↪  m_h2tank_in[t] = (0,) * 4

        if(c_h2tank[t-1] >= (m_h2_deficit*dt)):
            # Hydrogen tank supplies the ammonia
            ↪  demand
```

```
            m_h2tank_out[t] = m_h2_deficit
            m_h2_asu[t] = m_h2tank_out[t]

            # Excess power used to charge the
            ↪  batteries
            p_bat_in[t] = min(power_available_for_bat,
            ↪  (c_bat_max - c_bat[t-1]) / dt)

            # Power consumed by asu
            p_asu[t] = p_asu_installed

            # Set other outputs to zero
            p_elz[t] = 0

            # Calculate energy curtailment
            energy_curt[t] = max(p_tot[t] - p_asu[t] -
            ↪  p_bat_in[t], 0)

        else:
            # Not enough hydrogen tank capacity.
            ↪  System shuts down.
            # Set outputs to zero
            p_asu[t], p_bat_in[t], m_h2_asu[t],
            ↪  m_h2tank_out[t], energy_curt[t] = (0,)
            ↪  * 5


    # Case 3: Enough power for electrolyzers (and
    ↪  asu), but not enough to charge battery
    elif (p_elz_min <= p_tot[t]) and (p_tot[t] <=
    ↪  p_elz_max):

        # Calculate the available space in the H2
        ↪  tank
        available_h2tank_space = c_h2tank_max -
        ↪  c_h2tank[t-1]

        # Calculate the demand for H2 production based
        ↪  on ASU demand and available H2 tank space
        h2_demand = m_h2_asu_hour +
        ↪  (available_h2tank_space * dt)

        # The electrolyzers will produce enough H2 to
        ↪  cover the ASU demand and H2 tank demand,
        ↪  not exceeding max capacity
```

```
m_h2_elz[t] = min(h2_demand, (p_tot[t] /
↪  e_elz_h2), (p_elz_max / e_elz_h2))

# Power allocated to the electrolyzers
p_elz[t] = m_h2_elz[t] * (e_elz_h2 / dt)

# ASU is fully powered
p_asu[t] = p_asu_installed

# Calculate hydrogen deficit
m_h2_deficit = m_h2_asu_hour - m_h2_elz[t]

# Battery charges with excess power if it's
↪  not fully charged
power_available_for_bat = max(0, p_tot[t] -
↪  p_elz[t])
p_bat_in[t] = min(power_available_for_bat,
↪  (c_bat_max - c_bat[t-1]) / dt)
p_bat_out[t] = 0

# Calculate energy curtailment after
↪  accounting for battery charging
energy_curt[t] = max(0, p_tot[t] - p_elz[t] -
↪  p_bat_in[t])

if (m_h2_elz[t] < m_h2_asu_hour) and
↪  (c_h2tank[t-1] >= m_h2_deficit):
    # Electrolyzers and hydrogen tank supply
    ↪  hydrogen to ASU
    m_h2tank_out[t] = m_h2_deficit
    m_h2_asu[t] = m_h2tank_out[t] +
    ↪  m_h2_elz[t]
    m_h2tank_in[t] = 0

elif (m_h2_elz[t] < m_h2_asu_hour) and
↪  (c_h2tank[t-1] < m_h2_deficit):
    # Not enough H2 to support ASU operation:
    ↪  system shuts down.
    m_h2_asu[t], m_h2tank_out[t], p_asu[t] =
    ↪  (0,)*3
    m_h2tank_in[t] = min(m_h2_elz[t],
    ↪  available_h2tank_space)

elif m_h2_elz[t] == m_h2_asu_hour:
    # All H2 from elz supply ASU demand. No H2
    ↪  from tank needed
```

```
            m_h2_asu[t] = m_h2_elz[t]
            m_h2tank_out[t], m_h2tank_in[t]= (0,)*2

        else:
            # m_h2_elz[t] > m_h2_asu_hour
            m_h2_asu[t] = m_h2_asu_hour
            excess_h2 = m_h2_elz[t] - m_h2_asu[t]
            m_h2tank_out[t] = 0

            if c_h2tank[t-1] < c_h2tank_max:
                # Store the produced H2 in the H2 tank
                ↪  without exceeding its maximum
                ↪  capacity
                m_h2tank_in[t] = min(excess_h2,
                ↪  available_h2tank_space)
                energy_curt[t] = max((p_tot[t] -
                ↪  p_elz[t] - p_bat_in[t]), 0)

            else:
                # H2 tank is full, excess H2 is
                ↪  curtailed
                p_elz[t] = m_h2_asu_hour * (e_elz_h2 /
                ↪  dt)
                m_h2_elz[t] = m_h2_asu_hour
                energy_curt[t] = max((p_tot[t] -
                ↪  p_elz[t] - p_bat_in[t]), 0)
                m_h2tank_in[t] = 0


    # Case 4: surplus power that exceeds electrolyzer
    ↪  + ASU demands
    else: # when p_tot[t] > p_elz_max

        # Calculate the available space in the H2
        ↪  tank
        available_h2tank_space = c_h2tank_max -
        ↪  c_h2tank[t-1]

        # Calculate the demand for H2 production based
        ↪  on ASU demand and available H2 tank space
        h2_demand = m_h2_asu_hour +
        ↪  (available_h2tank_space * dt)

        # The electrolyzers will produce enough H2 to
        ↪  cover the ASU demand and H2 tank demand,
        ↪  not exceeding max capacity
```

```
m_h2_elz[t] = min(h2_demand, (p_tot[t] /
↪  e_elz_h2), (p_elz_max / e_elz_h2))

# Power allocated to the electrolyzers
p_elz[t] = m_h2_elz[t] * (e_elz_h2 / dt)

# ASU is fully powered
p_asu[t] = p_asu_installed

# Calculate hydrogen deficit
m_h2_deficit = m_h2_asu_hour - m_h2_elz[t]

# Battery charges with excess power if it's
↪  not fully charged
power_available_for_bat = max(0, p_tot[t] -
↪  p_elz[t])
p_bat_in[t] = min(power_available_for_bat,
↪  (c_bat_max - c_bat[t-1]) / dt)
p_bat_out[t] = 0

# Calculate energy curtailment after
↪  accounting for battery charging
energy_curt[t] = max(0, p_tot[t] - p_elz[t] -
↪  p_bat_in[t])

if (m_h2_elz[t] < m_h2_asu_hour) and
↪  (c_h2tank[t-1] >= m_h2_deficit):
    # Electrolyzers and hydrogen tank supply
    ↪  hydrogen to ASU
    m_h2tank_out[t] = m_h2_deficit
    m_h2_asu[t] = m_h2tank_out[t] +
    ↪  m_h2_elz[t]
    m_h2tank_in[t] = 0

elif (m_h2_elz[t] < m_h2_asu_hour) and
↪  (c_h2tank[t-1] < m_h2_deficit):
    # Not enough H2 to support ASU operation:
    ↪  system shuts down.
    m_h2_asu[t], m_h2tank_out[t], p_asu[t] =
    ↪  (0,)*3
    m_h2tank_in[t] = min(m_h2_elz[t],
    ↪  available_h2tank_space)

elif m_h2_elz[t] == m_h2_asu_hour:
    # All H2 from elz supply ASU demand. No H2
    ↪  from tank needed
```

```
            m_h2_asu[t] = m_h2_elz[t]
            m_h2tank_out[t], m_h2tank_in[t] = (0,)*2

        else:
            # m_h2_elz[t] > m_h2_asu_hour
            m_h2_asu[t] = m_h2_asu_hour
            excess_h2 = m_h2_elz[t] - m_h2_asu[t]
            m_h2tank_out[t] = 0

            if c_h2tank[t-1] < c_h2tank_max:
                # Store the produced H2 in the H2 tank
                ↪  without exceeding its maximum
                ↪  capacity
                m_h2tank_in[t] = min(excess_h2,
                ↪  available_h2tank_space)
                energy_curt[t] = max((p_tot[t] -
                ↪  p_elz[t] - p_bat_in[t]), 0)

            else:
                # H2 tank is full, excess H2 is
                ↪  curtailed
                p_elz[t] = m_h2_asu_hour * e_elz_h2
                m_h2_elz[t] = m_h2_asu_hour
                energy_curt[t] = max((p_tot[t] -
                ↪  p_elz[t] - p_bat_in[t]), 0)
                m_h2tank_in[t] = 0

    # Calculate TAD for this hour
    m_h2_diff = m_h2_asu_hour - (m_h2_elz[t] +
    ↪  m_h2tank_out[t])

    # Implement TAD value to list
    if m_h2_diff > 0:
        TAD[t] = 1
    else:
        TAD[t] = 0

    # Update state of charge for battery and h2tank
    if t > 0:
        c_bat[t] = max(c_bat_min, c_bat[t-1] +
        ↪  p_bat_in[t] * dt - p_bat_out[t] * dt)
        c_h2tank[t] = max(c_h2tank_min, (c_h2tank[t-1]
        ↪  + m_h2tank_in[t] * dt - m_h2tank_out[t] *
        ↪  dt))

    # Append simulation results to list
```

```
        simulation_results.append({'p_wt': p_wt[t],
        ↪  'p_pv': p_pv[t], 'p_re': p_re[t], 'p_tot':
        ↪  p_tot[t], 'p_asu': p_asu[t],
                                   'p_bat_in': p_bat_in[t],
                                   ↪  'p_bat_out':
                                   ↪  p_bat_out[t], 'p_elz':
                                   ↪  p_elz[t],
                                   'm_h2_elz': m_h2_elz[t],
                                   ↪  'm_h2_asu': m_h2_asu[t],
                                   ↪  'energy_curt':
                                   ↪  energy_curt[t],
                                   'm_h2tank_in':
                                   ↪  m_h2tank_in[t],
                                   ↪  'm_h2tank_out':
                                   ↪  m_h2tank_out[t],
                                   'c_bat': c_bat[t],
                                   ↪  'c_h2tank': c_h2tank[t],
                                   ↪  'TAD': TAD[t]})


    # This code block will store the final state of charge
    ↪  for c_bat and c_h2tank at t=8760
    # and sum up the values for all other variables
    ↪  throughout the year.
    yearly_simulation_results = {}

    for var in simulation_results[0]:
        if isinstance(simulation_results[0][var], (float,
        ↪  int)):
            if var in ['c_bat', 'c_h2tank']:
                yearly_simulation_results[var] =
                ↪  simulation_results[-1][var]  # Final
                ↪  state of charge at t=8760
            elif var == 'TAD':
                total_TAD = sum(res[var] for res in
                ↪  simulation_results)
                yearly_simulation_results[var] = total_TAD
            else:
                yearly_value = sum(res[var] for res in
                ↪  simulation_results)
                yearly_simulation_results[var] =
                ↪  yearly_value
        else:
            yearly_simulation_results[var] =
            ↪  simulation_results[0][var]
```

```
                print(f"Currently total TAD = {total_TAD}")

                if total_TAD <= TAD_threshold:
                    total_TAD = sum([result['TAD'] for result in
                    ↪  simulation_results])


                # Calculate TAD and check if it meets constraints
                if total_TAD <= TAD_threshold:
                    # Calculate capex and opex for this combination of
                    ↪  system component capacities
                    capex = calculate_capex(wt, pv, elz, bat, h2tank,
                    ↪  p_hb_installed, p_syngas_compression,
                    ↪  p_psa_installed)
                    opex = (calculate_opex(capex))

                    # Calculate LCOA for this combination of system
                    ↪  component capacities
                    lcoa = calculate_lcoa(capex, opex,
                    ↪  tonnes_nh3_prod_year_real)

                    if lcoa < min_lcoa:
                        min_lcoa = lcoa
                        best_config = {'wt': wt, 'pv': pv, 'elz': elz,
                                       'bat': bat, 'h2tank': h2tank}
                        best_results = yearly_simulation_results
                        best_hourly_results = simulation_results
                else: # when TAD exceeds max limit, next iteration
                    continue

""" End of the iterative optimization """
```

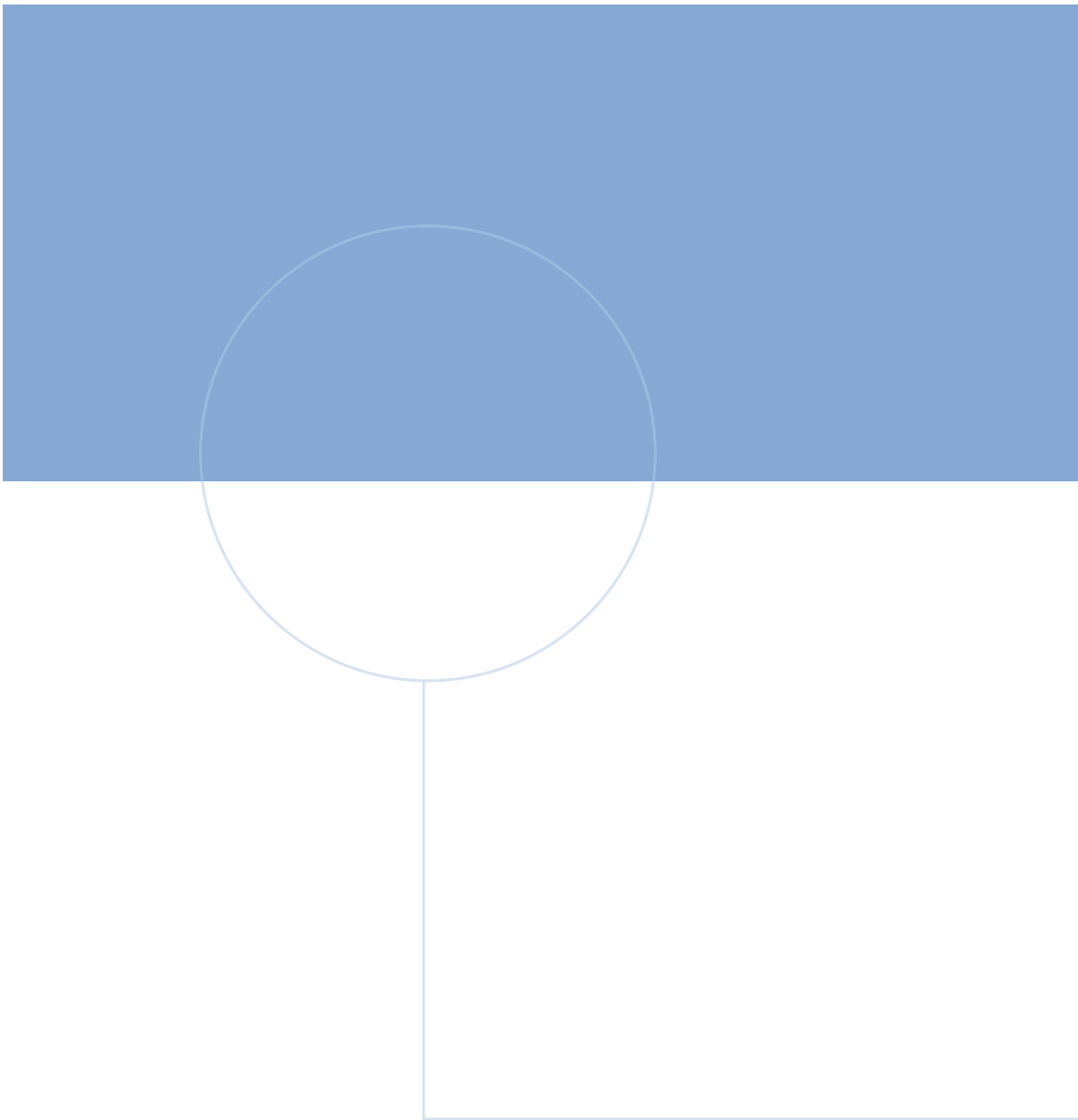

NTNU

Norwegian University of
Science and Technology